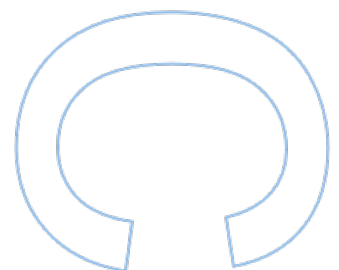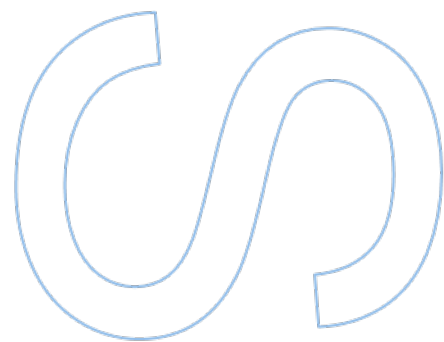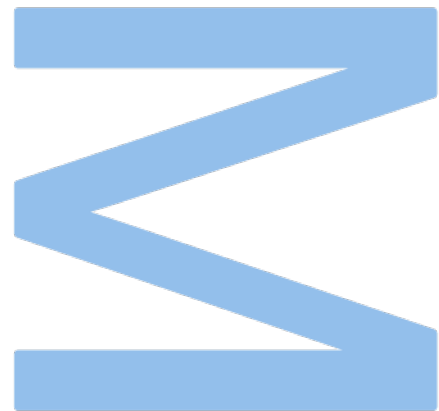# From Bloch Oscillations to Stationary Currents in Mesoscopic Systems
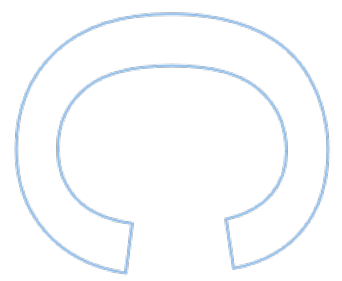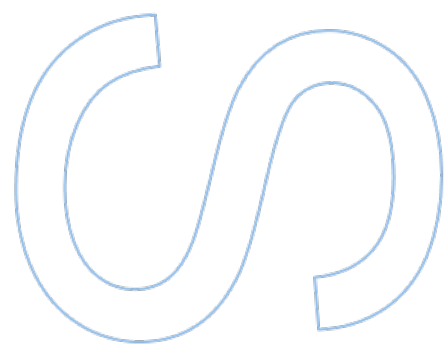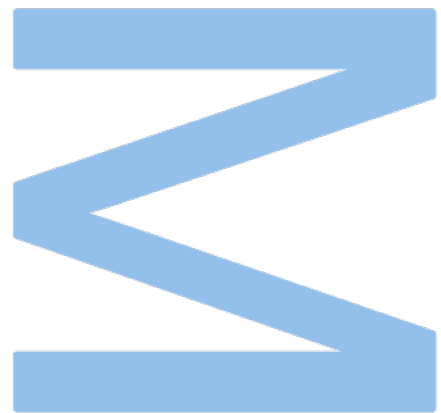
João Manuel Alendouro Oliveira Pinho
Mestrado em Física
Departamento de Física e Astronomia
2022

**Orientador**
João Manuel Viana Parente Lopes, FCUP

**Coorientador**
Bruno António Campos Amorim, U. Minho

# Declaração de Honra

Eu, João Manuel Alendouro Oliveira Pinho, inscrito no Mestrado em Física da Faculdade de Ciências da Universidade do Porto declaro, nos termos do disposto na alínea a) do artigo 14.º do Código Ético de Conduta Académica da U.Porto, que o conteúdo da presente dissertação reflete as perspetivas, o trabalho de investigação e as minhas interpretações no momento da sua entrega.

Ao entregar esta dissertação, declaro, ainda, que a mesma é resultado do meu próprio trabalho de investigação e contém contributos que não foram utilizados previamente noutros trabalhos apresentados a esta ou outra instituição.

Mais declaro que todas as referências a outros autores respeitam escrupulosamente as regras da atribuição, encontrando-se devidamente citadas no corpo do texto e identificadas na secção de referências bibliográficas. Não são divulgados na presente dissertação quaisquer conteúdos cuja reprodução esteja vedada por direitos de autor.

Tenho consciência de que a prática de plágio e auto-plágio constitui um ilícito académico.


João Manuel Alendouro Oliveira Pinho

Porto, 30 de Setembro de 2022

UNIVERSIDADE DO PORTO

FACULDADE DE CIÊNCIAS

MESTRADO EM FÍSICA

# From Bloch Oscillations to Stationary Currents in Mesoscopic Systems

João Manuel Alendouro Oliveira Pinho

*Supervisors*

Prof. Dr. João Manuel Viana Parente Lopes

Bruno António Campos Amorim

*A thesis submitted in fulfilment of the requirements*
*for the degree of Master of Science*

*at*

Departamento de Física e Astronomia

Porto, September of 2022

[This page was intentionally left blank]

*E pareciam campinas, vales tão estendidos*

*Pareciam mesmo os teus braços que me abraçam cingidos*

*Ou seria das silvas, do gengibre, do benjoim*

*Do cheiro daquela chuva dos cacimbos, enfim*

*Porque haveria de ter saudades tuas*

*Ao longo de um claro rio de água doce?*

**-Fausto Bordalo Dias**

[This page was intentionally left blank]

## Agradecimentos

Exprimir uma gratidão que, ao longo de cinco anos, fui devendo a colegas, amigos, família e professores numa página de texto é coisa impossível, e a devolução de tal dívida terá de ser um processo consideravelmente mais gradual. Posso, no entretanto, aproximar-me daquilo que sinto, o que farei, para todos os efeitos, na nossa lingua mãe - minha e de a quem este excerto é dirigido.

Ao meu orientador, Prof. João Viana Lopes, cujo infindos entusiasmo e disponibilidade me facultaram, acima de tudo, orgulho no conhecimento que adquiri e no trabalho que realizei. Por me transmitir não só conhecimento técnico, mas também pensamento crítico e criativo, fundamentais para o desenvolvimento científico. Por isto e pelo resto, obrigado.

Ao meu co-orientador, Prof. Bruno Amorim, agradeço sinceramente as questões incessantemente levantadas que me levaram a duvidar do que tinha já tomado como garantido, desenvolvendo em mim um processo de trabalho mais rigoroso.

Aos meus amigos: em primeiro lugar, David e Titi, que me acompanharam não só nos primeiros 3 anos de licenciatura, mas também nos restantes dois, cujas discussões foram fulcrais para o progresso no meu percurso académico e cuja companhia entornou na jornada as mais sinceras gargalhadas. Ao Carlos, César, Alex, André Miranda, Lemos, Chico, Ticas, Ana Cacho, Sanches, Nuno Tosta, Vitela, João Silva, Nico, Júlio, Diogo, Henrique, Raul, José Matos, Gonçalo Reboredo e Rui Peixoto, cujos momentos e alegria proporcionados não esquecerei.

Ao João Pires e Simão João, que de entre as palavras de orientação e ensino, encontrei também as de um amigo.

À minha mãe, ao meu pai, à minha irmã e a toda a minha família, pelo calor familiar que me fornecia a energia necessária para enfrentar mais uma semana. Aos meus amigos de Vizela, que contribuiram para este descanso, também vos estendo o meu agradecimento.

Ao Leonardo, cuja vivacidade e motivação brotou em mim a vontade de ser, como ele, focado e determinado. Contaste comigo para o que foi, conta agora para o que virá.

Por fim, à Maria. O teu apoio e amor incondicional ressoam em mim na mais bela emoção.É o meu maior prazer emprestar da tua bondade vibrante para fazer de mim melhor. Espero corresponder em ti aquilo que foste e és para mim.

[This page was intentionally left blank]

## Abstract

Cold electrons in crystals can have their quantum nature unveiled as an oscillatory behavior driven by uniform fields. Oscillating currents, referred to as Bloch Oscillations, are well-known to appear as transport regimes of electrons that move across periodic lattices in the presence of static electric fields. Moreover, the eigenstates of such a system (Wannier-Stark states) are well localized in a region of space inversely proportional to the electric field strength. These Bloch Oscillations can also occur on mesoscopic transport systems for high potential biases, clashing with the zero current predicted by the Landauer formula at long times. Conversely, a correspondence with the Landauer formula is expected for biases below a certain threshold. In this work, we seek to smoothly connect such oscillations to the steady-state, with and without disorder, by numerically time-evolving an initially thermalized mixed state using a Chebyshev method. In view of such goal, the current response to an electric bias in one- and two-dimensional tight-binding samples coupled to finite leads with open boundaries is analyzed. For high applied voltages, we observe an emergent oscillating current and a proper connection to the localization of the Wannier-Stark states of the potential ramp is drawn. Notwithstanding, this oscillations are seen to be a result of the existence of bound states inside the sample. To mitigate said states, the energy bounds of the propagating states in the leads is accounted for and controlled with the leads' hopping parameter. The proper choice of this parameter is then responsible for making of Bloch Oscillations a merely transient phenomenon which eventually relax towards a steady-state current given by the Landauer prediction, despite the time needed for this equilibration being much larger than that available to a simulation. Finally, the introduction of disorder in one- and two-dimensions is analyzed and, regardless of it not having much effect on the former, in bidimensional materials a Landauer current's growth from zero to a finite value is observed with the increasing of the disorder parameter, associated with a disorder-induced delocalization of the Wannier-Stark states, with a simple semi-classical intuition for such effect being provided.

[This page was intentionally left blank]

## Resumo

Eletrões frios em cristais podem ter a sua natureza quântica desvendada como um comportamento oscilatório impulsionado por campos uniformes. Correntes oscilantes são conhecidas por aparecerem como regimes de transporte em estado estacionário de eletrões que se movem através de redes periódicas na presença de campos elétricos estáticos. Para além disto, os estados próprios de tal sistema (estados de Wannier-Stark) estão bem localizados numa região do espaço inversamente proporcional à intensidade do campo elétrico. Estas oscilações de Bloch também são detetadas em sistemas de transporte mesoscópicos, como a configuração de Landauer sem partição, para fortes diferenças de potencial, colidindo com o valor de Landauer calculado para os parâmetros do sistema correspondente. Por outro lado, a correspondência com a fórmula de Landauer é esperada para pequenos potenciais. Neste trabalho, procuramos conectar subtilmente tais oscilações ao resultado de Landauer, com e sem desordem, através da evolução numérica de um estado misto inicialmente termalizado usando o método de Chebyshev. Em prol de tal objetivo, é analisada a resposta de corrente a uma perturbação elétrica em amostras uni e bidimensionais acopladas a terminais finitos com condições fronteira abertas. Para altas tensões, observamos uma corrente oscilante emergente e uma conexão adequada para a localização dos estados Wannier-Stark da rampa de potencial é concebida. Não obstante, essas oscilações são vistas como um artefato da existência de estados ligados dentro da amostra. Para mitigar esses estados, os limites de energia dos estados de propagação nos terminais são tidos em conta e controlados com o parâmetro de *hopping* dos terminais. A escolha adequada deste parâmetro é então responsável por tornar as oscilações de Bloch num fenômeno meramente transiente que eventualmente relaxa em para o valor de Landauer correspondente, apesar do tempo necessário para este equilíbrio ser muito maior do que o disponível para uma experiência. Por fim, analisa-se a introdução da desordem em uma e duas dimensões e, apesar de não ter muito efeito sobre a primeira, em materiais bidimensionais observa-se um crescimento da corrente de Landauer de zero a um valor finito com o aumento da parâmetro de desordem , associado a uma deslocalização induzida por desordem dos estados de Wannier-Stark, e é fornecida uma intuição semi-clássica simplista para tal efeito.

[This page was intentionally left blank]

# Contents

# List of Figures

[This page was intentionally left blank]

# 1. Introduction

It is of common knowledge that, within a classical framework, an application of a constant electric potential difference through a sample originates a constant current response, to which the term direct current (DC) response has been keyed. The relation between current and potential is often formulated by means of equations such as Ohm's Law, where another extensive quantity $R$ representing the resistance of the material to the electric current flow, and denominated resistance, is present. The reciprocal of such quantity is referred as conductance $G$ and, in such a classical framework, it scales with the dimensions of the sample as

$$G = g\frac{A}{L}, \tag{1.1}$$

where $L$ and $A$ are the length and the cross sectional area of the sample, respectively, and $g$ a well defined intensive property of the material, called conductivity. However, diminishing the size and temperature of the sample may unveil different behaviors from what is classically expected. The emergence of these novel phenomena is understood to be due to the quantum, wave-like features of the charge carriers. The actual observation of such effects requires the wavefunctions of the particles to remain coherent for long enough times and lengths. The catch is that coherence is progressively lost in time and space due to interactions of the carriers between each other and with the underlying lattice vibrations. Notwithstanding, if the length scale of this coherence loss is much larger than the characteristic length scale of the quantum problem at hand, the observation of this quantum effects is still feasible [1]. Among these are Anderson localization [2], mesoscopic transport [3,4] and Bloch Oscillations [5], each of which I will now proceed to briefly review.

Disorder might be more generically defined as imperfections on an otherwise periodic lattice. These imperfections may vary morphologically from one another: impurities, vacancies and even lattice deformations are all different types of disorder. These lattice defects can scatter the electronic propagating states associated with the underlying pristine lattice. In the absence of disorder, the eigenstates of a periodic lattice are known to obey Bloch's theorem [6], which has the consequence of their wave-function being periodic and therefore extending throughout the entire lattice. States like these are called extended sates. The presence of disorder, however, enables scattering between equienergetically Bloch states and thus destructive interference phenomena between these states emerge, which can lead to the localization of the eigenstates.

In 1958, Philip Anderson proposed a model to study such effects [2]. The model was com-

prised of a tight binding lattice with random on-site energies sampled from an uniform distribution in the interval $[-W/2, W/2]$, where $W$ is the disorder strength. He sought to mimic scattering and destructive interference by means of this random on-site energies. He found that, for sufficiently strong disorder, the system undergoes a transition from metallic to insulator due to the eigenstates becoming localized in space [2]. It was later found that for 1D systems, this transition happens for an infinitesimally small disorder strength [7]. Higher dimensions, however, proved to be a much harder beast to tackle. This led to the development of a one parameter scalling theory, which showed that, in two dimensions, any degree of disorder also localizes the wave-functions, and only in three dimensions do we get a transition for finite disorder strength [8,9]. Throughout this work, we will restrain ourselves to one and two dimensions.

As I have mentioned, the interference phenomenon will result in a decaying amplitude in space for the new eigenstates. The decayment, howbeit, is of a particular form, it being an exponential law of the form [2]

$$\Psi(r) \sim e^{-r/\xi_A}, \tag{1.2}$$

where $\xi_A$ is defined as the localization length. Analytical studies show that, for quasi-1D systems, the localization length of such electronic states is given by [10–12]

$$\xi_A \sim N\ell, \tag{1.3}$$

with $\ell$ being the mean free path and $N$ the number of conducting channels. For purely 1D wires, the computation of the mean free path may be performed, boiling the above equation down to

$$\xi_A \sim W^{-2}. \tag{1.4}$$

These results have been backed numerically by the powerful transfer matrix method [13]. Anderson localization transitions were already extensively studied, and very good reviews can be found in [14,15], and a more recent and broad review is found in Ref. [16].

Mesoscopic transport is another case where a quantum description is needed for an accurate modeling. It consists on the obtainance of transport quantities of samples at the mesoscopic scale, which in turn is defined as an intermediate scale separating the microscopic and the macroscopic. More specifically, it aims to study transport through samples smaller than the dephasing length $\ell_\phi$ of the problem, i. e., where wave coherence is maintained throughout the entire carrier transportation along the sample [1]. Such devices ergo range from the nanoscale to the micrometer, and the transport quantities cease to be intrinsic to the type of the material and begin depending on the geometrical shape and disorder configuration as well. This shape and disorder dependency renders intrinsic properties like conductivity ill-defined. In such

transport setups, a formalism created by Landauer [17] and later enhanced by Büttiker [18] was put forward to describe the steady-state current flowing through a device connected to two particle reservoirs, which will be henceforth referred to as leads. This formalism has had wide success, with the first instances of it being ballistic transport [19], quantized conductance [20, 21], quantum point contacts [22] and cold-atom systems [23, 24]. This non-equilibrium steady state dynamics may also be obtained by time-evolving a system subject to a certain perturbation, for which purpose many different methods have been devised [25–29]. However, transient phenomenon has not received as much attention until more recent years, where it was studied more extensively in samples attached to infinite [30–37] and finite leads [38–40], and a good amount of effort will be spent at describing transient regimes in this thesis.

Lastly, Bloch Oscillations (BO's) are, as the name suggests, a coherent oscillation of a particle's average position and velocity when subject to a periodic potential and a constant electric field, as per this Hamiltonian.

$$H = H_0 + eEx = \frac{p^2}{2M} + V(x) + eEx, \quad V(x + d) = V(x). \tag{1.5}$$

One would classically expect a particle subject to a constant electric field to move uniformly accelerated through space, but the introduction of a periodic potential actually subverts this picture, with the particle performing an oscillatory motion instead. We will soon see that although this behavior is present either in the semi-classical limit or in a purely quantum problem, the nature of this phenomenon is the same, as it arises, in essence, from the consideration that a particle is described by wave-like properties and that the normal modes of a periodic Hamiltonian obey Bloch's theorem [6].

The ultimate goal of this thesis is to study the emergence of BO's in a one and two-dimensional mesoscopic device with an applied uniform and static electric field connected to two leads, with and without Anderson disorder, and measure their effect in the transport quantities of a particular setup. Previous work on this model has shown, for the one-dimensional case, that for small electric fields, the current relaxes to the predicted Landauer value [41]. However, for sufficiently potential biases, we arrive at a stage where the current oscillates ad infinitum [5], clashing with the Landauer formula, which predicts a constant current response. Throughout this work, we will be seeking to reconcile these two results, as well as uncover, in one- and two-dimensional samples, the effect of Anderson disorder to BO's in this setup. To achieve this, given that Bloch Oscillations are a dynamical phenomenon, the Landauer formula wont suffice and we will need to evolve a certain system in time. For this purpose, we employ a time-evolution scheme with finite leads [41] based on the Chebyshev time-evolution operator expansion [42] for numerical enhancement.

This document is structured as follows: Chapter 2 is dedicated to Bloch Oscillations and their properties in one-dimensional finite and infinite systems and, particularly, the proper-

ties of the eigenstates of the infinite system are extracted. Chapter 3 aims to describe the appearance of BO's in a one-dimensional two-terminal mesoscopic device, with a thorough characterization of the clean sample as well as the study of the disorder's effect on the former. Chapter 4 does the same to a two-dimensional two-terminal mesoscopic device, this time with a much stronger focus on the disordered case. Finally, chapter 5 will conclude and briefly describe future work.

# 2. Bloch Oscillations

## 2.1. Semi-Classical Description

Bloch Oscillations were first predicted by Felix Bloch and Clarence Zenner in their seminal papers [6, 43] as a consequence of the semi-classical Band Theory equations. To understand the nature of these oscillations, we must also delve into how these semi-classical equations come about. In what follows, we will merely motivate the set of semi-classical equations of motion [44] and the reader interested in a rigorous and fulfilling proof is urged to check reference [45].

As mentioned in the introductory chapter, these equations of motion are a consequence of the wave-like nature of electrons, particularly Bloch's Theorem, stating that the solutions for the Schrödinger equation in a periodic potential take the form of a plane wave modulated by a periodic function [6]

$$\psi_k (\mathbf{r}) = e^{i\mathbf{k}\cdot\mathbf{r}} u(\mathbf{r}), \tag{2.1}$$

where $u(\mathbf{r})$ is a periodic function with the same periodicity as the periodic potential. Let us then consider an Hamiltonian diagonalizable by such waves

$$H_0 |\psi_{\mathbf{k}}\rangle = \varepsilon(\mathbf{k}) |\psi_{\mathbf{k}}\rangle. \tag{2.2}$$

Taking the mean velocity $v(k) = \frac{\hbar}{m} \langle\psi_{\mathbf{k}}| \hat{\mathbf{p}} |\psi_{\mathbf{k}}\rangle$ of a Bloch wave originates the equation

$$v(k) = \frac{1}{\hbar} \frac{d\varepsilon(\mathbf{k})}{d\mathbf{k}}. \tag{2.3}$$

This can be traced back as the familiar assertions that the group velocity of a wave-packet is given by $\partial\omega/\partial\mathbf{k}$. This equation then tells us how the mean velocity of a particle is obtained assuming we know the dispersion relation $\varepsilon(\mathbf{k})$. Adding an electric field will generate an equation of motion for the quasi-momentum $\mathbf{k}$. The Hamiltonian will now look like

$$H = H_0 + \phi(\mathbf{x}), \tag{2.4}$$

such that $-\nabla\phi = e\mathbf{E}$, where $\mathbf{E}$ is the electric field and $e$ is the charge of the particle. The motivation to obtain the second semi-classical equation is done by arguing that, since energy must be conserved, the wave-packet must move in a way such that the energy introduced by

the potential $\phi(\mathbf{x}(t))$ from instant $t$ to $t + dt$ into the system must correspond to the variation of $\varepsilon(\mathbf{k}(t))$ in the same interval. By denoting the variation of $\phi(\mathbf{x}(t))$ and $\varepsilon(\mathbf{k}(t))$ in this interval as $d\phi(\mathbf{x}(t))$ and $d\varepsilon(\mathbf{k}(t))$ respectively, this translates to saying

$$d\varepsilon(\mathbf{k}(t)) - d\phi(\mathbf{x}(t)) = 0. \tag{2.5}$$

Dividing by $dt$ and taking the limit $dt \to 0$ gives us

$$\frac{d}{dt}\varepsilon(\mathbf{k}(t)) - \frac{d}{dt}\phi(\mathbf{x}(t)) = 0. \tag{2.6}$$

which gives rise to the equation

$$\frac{d\varepsilon(\mathbf{k})}{d\mathbf{k}} \cdot \dot{\mathbf{k}} - \nabla\phi(\mathbf{x}) \cdot \dot{\mathbf{x}} = 0. \tag{2.7}$$

Having already identified $\dot{\mathbf{x}} = \frac{1}{\hbar}\frac{d\varepsilon(\mathbf{k})}{d\mathbf{k}}$, the equation above is only satisfied if

$$\hbar\dot{\mathbf{k}} = -e\mathbf{E}, \tag{2.8}$$

thus obtaining a close set of differential equations that describe the average motion of a particle in a periodic potential and a constant and uniform electric field, which in one dimension are simply written as

$$\hbar\frac{dk}{dt} = -eE, \tag{2.9}$$

$$v(k) = \frac{1}{\hbar}\frac{d\varepsilon}{dk}. \tag{2.10}$$

It is worth noticing that, coming from its definition in equation 2.1, $ka$ is defined modulo $2\pi$ with $a$ being the lattice constant, and we may choose in which interval to define this variable, which we will choose to be $ka \in [-\pi, \pi]$. If one chooses a tight binding system, for example, with a dispersion relation of

$$\varepsilon(k) = -2w\cos ka, \tag{2.11}$$

the solution of these equations yields, by defining $k_0 \equiv k(0)$,

$$k(t) = \frac{k_0 - eEt}{\hbar}, \tag{2.12}$$

$$v(t) = 2w\frac{a}{\hbar}\sin\left(\frac{a}{\hbar}(k_0 - eEt)\right), \tag{2.13}$$

(a) First Brillouin Zone

(b) Evolution of the average position $x$ of a particle subjected to a constant and uniform electric potential.
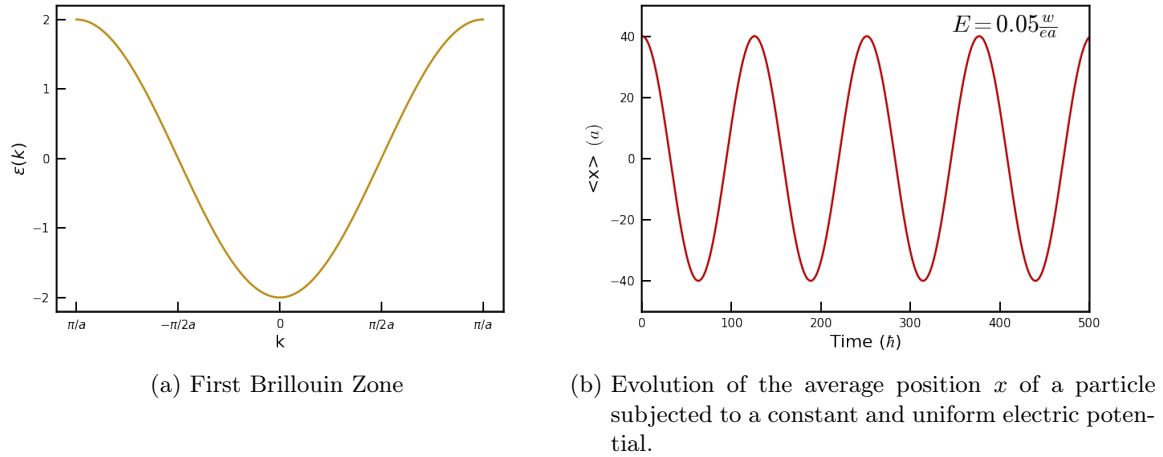
Figure 2.1.: Semi-Classical evolution of a particle in an 1D Tight Binding chain

which, when integrating the second equation, results in an oscillation of the particle in space:

$$x(t) = x_0 + \frac{2w}{\hbar e E} \cos\left(\frac{a}{\hbar}\left(k_0 - eEt\right)\right). \tag{2.14}$$

This dynamic is due to the Bragg reflection occurring at the edge of the Brillouin Zone: as seen, the dynamics of the system are such that a particle will traverse the First Brillouin Zone with an uniform motion, and when it reaches the edge, it will pop out the other side. When this happens, the group velocity changes continuously from a positive to a negative value, causing the oscillation in space seen in figure 2.1b. These oscillations in space are characterized by the period

$$T_{BO} = \frac{2\pi\hbar}{eaE}, \tag{2.15}$$

which is inversely proportional to the electric field. The amplitude of the oscillation

$$A_{BO} = \frac{2w}{\hbar e E}, \tag{2.16}$$

is itself inversely proportional to the electric field, which means that the region to which the particle is confined decreases with the electric field.

## 2.2. Quantum-Mechanical Description

Even though the oscillation of a particle in space might not be easily viewed when we are talking about extended states, Bloch Oscillations still exist as a coherent dynamic between the particles of a mixed state and can be spotted via oscillations in the current whose period scales with the electric field the same way as those of the semi-classical space oscillations do.

To demonstrate this, let us begin by writing out the Hamiltonian of a one dimensional tight binding ring with periodic boundary conditions

$$\hat{H}_0 = -w \sum_{i=0}^{L-1} \left( \hat{c}_{i+1}^\dagger \hat{c}_i + \hat{c}_i^\dagger \hat{c}_{i+1} \right), \tag{2.17}$$

where we conventionally say that $i = L$ is to be understood as $i = 0$ as to satisfy periodic boundary conditions. This system can be perturbed by the introduction of a flux $\phi(t)$ through the loop, giving rise to a time-dependent Hamiltonian

$$\hat{H}(t) = -w \sum_{i=0}^{L-1} \left( e^{i2\pi \frac{\phi}{\phi_0 L}} \hat{c}_{i+1}^\dagger \hat{c}_i + e^{-i2\pi \frac{\phi}{\phi_0 L}} \hat{c}_i^\dagger c_{i+1} \right), \tag{2.18}$$

where the phase factors arise via the Peierls substitution [46], $\phi_0 = h/e$ is the quanta of magnetic flux and $\phi$ the flux inside the ring that can be related with the electric field by the relation

$$\phi(t) = \int_0^L dx A(t) = -ELat, \tag{2.19}$$

where $a$ is the lattice parameter and $A$ is the vector potential which is chosen as $\mathbf{A}(t) = -Et\hat{\mathbf{e}}_x$. This basically follows from the Third Maxwell Equation

$$\int_C \mathbf{E} \cdot d\ell = -\int_A \left( \frac{\partial \mathbf{B}}{\partial t} \right) \cdot d\mathbf{S}, \tag{2.20}$$

with $d\mathbf{S}$ denoting the differential vector element of surface area $\mathbf{S}$, normal to surface $C$. The initial Hamiltonian is easily diagonalizable with Bloch states due to translational symmetry

$$
\begin{aligned}
\hat{c}_n &= \sum_k \frac{e^{-ikn}}{\sqrt{L}} \hat{c}_k \\
\hat{c}_n^\dagger &= \sum_k \frac{e^{ikn}}{\sqrt{L}} \hat{c}_k^\dagger
\end{aligned}
, k \in \left\{ -\frac{\pi}{2a}, \frac{\pi}{La} \left( -\frac{L}{2} + 1 \right), \ldots, \frac{\pi}{La} \left( \frac{L}{2} - 1 \right) \right\}. \tag{2.21}
$$

Writing the time-evolution Hamiltonian in this basis entails

$$
\begin{aligned}
\hat{H}(t) &= -w \sum_k \left( e^{i\left( 2\pi \frac{\phi(t)}{\phi_0 L} + ka \right)} + e^{-i\left( 2\pi \frac{\phi(t)}{\phi_0 L} + ka \right)} \right) \hat{c}_k^\dagger \hat{c}_k \\
&= -2w \sum_k \cos \left( 2\pi \frac{\phi(t)}{\phi_0 L} + ka \right) \hat{c}_k^\dagger \hat{c}_k. \tag{2.22}
\end{aligned}
$$

Note that, because we are in a system with periodic boundary conditions, the position operator

$$\hat{X} = \sum_n n c_n^\dagger c_n \tag{2.23}$$

is ill-defined at the borders, since the difference between the last and initial position should be 1 and is, instead, $L$. Therefore, we call for a different definition of the current operator

$$\hat{j}(t) = -\frac{\delta \hat{H}}{\delta A} = -\frac{e}{aL} \sum_k v_{k(t)}(t) \hat{c}_k^\dagger \hat{c}_k, \tag{2.24}$$

with

$$v_{k(t)} = \frac{2wa}{\hbar} \sin(k(t)a) \tag{2.25}$$

and

$$k(t) = k + 2\pi \frac{\phi(t)}{L\phi_0}. \tag{2.26}$$

The attentive reader might have noticed the familiar form of the equations above. In fact, it reflects the behavior described by the semi-classical equations (equations 2.9 and 2.10). The time evolution of the density matrix is simply

$$\begin{aligned}
\frac{d\rho_{kk'}(t)}{dt} &= \frac{i}{\hbar}[\hat{H}(t), \hat{\rho}(t)]_{kk'} \\
&= \frac{i}{\hbar}[\hat{H}(t)\hat{\rho}(t)]_{kk'} - [\hat{\rho}(t)\hat{H}(t)]_{kk'}.
\end{aligned} \tag{2.27}$$

The fact that the Hamiltonian is diagonal in this basis allows us to write

$$\begin{aligned}
\frac{d\rho_{kk'}(t)}{dt} &= \frac{i}{\hbar}\hat{H}_{kk}(t)\hat{\rho}_{kk'}(t) - \hat{\rho}(t)_{kk'}\hat{H}_{k'k'}(t) \\
&= \frac{i}{\hbar}\left(\hat{H}_{kk}(t) - \hat{H}_{k'k'}(t)\right)\hat{\rho}_{kk'}(t) \\
&= -2w\frac{i}{\hbar}\left(\cos\left(2\pi\frac{\phi(t)}{\phi_0 L} + ka\right) - \cos\left(2\pi\frac{\phi(t)}{\phi_0 L} + k'a\right)\right)\hat{\rho}_{kk'}(t).
\end{aligned} \tag{2.28}$$

Let us then start with a thermalized state at $t = 0$

$$\rho_{kk'}(0) = f(\varepsilon_k)\,\delta_{kk'}, \tag{2.29}$$

where $f(\varepsilon_k)$ is the Fermi-Dirac distribution (equation A.46). Time evolution then generates

$$\rho_{kk'}(t) = \begin{cases} 0 & k \neq k' \\ \rho_k(0) & k = k' \end{cases} \tag{2.30}$$

and, more importantly, the average current in such a state is

$$\langle j \rangle (t) = \mathrm{Tr}\left( \hat{\rho} j(t) \right) = -\frac{2we}{\hbar} \sum_k f(\varepsilon_k) \sin\left( 2\pi \frac{\phi(t)}{\phi_0 L} + ka \right) \tag{2.31}$$

$$= -\frac{2we}{\hbar} \left( \sin\left( 2\pi \frac{\phi(t)}{\phi_0 L} \right) \sum_k f(\varepsilon_k) \cos(ka) + \cos\left( 2\pi \frac{\phi(t)}{\phi_0 L} \right) \sum_k f(\varepsilon_k) \sin(ka) \right). \tag{2.32}$$

The fact that the Hamiltonian displays time inversion symmetry results in a symmetric dispersion relation, which in turn yields $f(\varepsilon_k) = f(\varepsilon_{-k})$. This implies that the second term is zero since the sine function is anti-symmetric. This finally yields

$$j(t) = -\frac{2we}{\hbar} \sin\left( 2\pi \frac{\phi(t)}{\phi_0 L} \right) \sum_k f(\varepsilon_k) \cos(ka)$$

$$= \frac{e}{\hbar} \sin\left( 2\pi \frac{\phi(t)}{\phi_0 L} \right) \sum_k f(\varepsilon_k)\varepsilon_k. \tag{2.33}$$

This final result is the product of perturbing the initial thermalized state with a uniform electric field, generating non-equilibrium oscillatory dynamics in the measured current. It is to be noticed that the argument of the sine function

$$2\pi \frac{\phi(t)}{\phi_0 L} = -\frac{eEat}{\hbar}, \tag{2.34}$$

meaning the period of this oscillations is $T_{BO} = \frac{\hbar}{eEa}$, the same as that of the Bloch Oscillations, allowing us to identify this current oscillations as such.

The local current operator, which describes the current through a single bond $n \to n+1$, is defined as

$$\hat{J}_n = -we\frac{i}{\hbar}\left( -e^{i2\pi\frac{\phi(t)}{\phi_0 L}} c^\dagger_{n+1} c_n + e^{-i2\pi\frac{\phi(t)}{\phi_0 L}} c^\dagger_n c_{n+1} \right). \tag{2.35}$$

Calculating the evolution of its average gives us

$$\mathrm{Tr}\left( \hat{\rho} \hat{J}_n(t) \right) = -we\frac{i}{\hbar} \sum_k f(\varepsilon_k)\left( -e^{i2\pi\frac{\phi(t)}{\phi_0 L}} e^{-ika} + e^{-i2\pi\frac{\phi(t)}{\phi_0 L}} e^{ika} \right)$$

$$= -we\frac{2}{\hbar} \sum_k f(\varepsilon_k) \sin\left( 2\pi \frac{\phi(t)}{\phi_0 L} - ka \right), \tag{2.36}$$

which displays the same oscillations, as it should, given the system is uniform. We have formulated the time evolution of a 1D periodic chain subject to a constant and uniform electric field within the so called velocity gauge, where the electric field is described in terms of a time-

dependent vector potential.

### 2.2.1. Wannier-Stark states

A static electric field may also be described as a scalar potential added to the on-site energies of the Hamiltonian. Therefore, BO's also appear in an infinite chain subject to a electric potential ramp added to the on-site energies, recasting the Hamiltonian into a time-independent one. The advantage of formulating such problem is that it allows for an intuition built upon the eigenstates of the full Hamiltonian, which actually proved fundamental in our understanding of the mesoscopic transport setup studied in chapters 3 and 4 (for more details, see [47–49]). To do so, we begin by writing this Hamiltonian in its first quantization

$$H = -w \sum_{n=-\infty}^{+\infty} \left( |n\rangle\langle n+1| + |n+1\rangle\langle n| \right) + aeE \sum_{n=-\infty}^{+\infty} n|n\rangle\langle n|, \tag{2.37}$$

where $e$ is the electric charge of the particle. We can once again express this Hamiltonian in the Bloch basis, which we will be denoting by

$$|k\rangle = \sum_{n=-\infty}^{+\infty} |n\rangle\langle n \mid k\rangle = \sqrt{\frac{a}{2\pi}} \sum_{n=-\infty}^{+\infty} |n\rangle \mathrm{e}^{inka}, \tag{2.38}$$

this time having in mind that this momentum basis is continuous since we have an infinite system, giving rise to the identities

$$\sum_{n=-\infty}^{+\infty} \langle k' \mid n+1 \rangle \langle n \mid k \rangle = \mathrm{e}^{-ik'a} \frac{a}{2\pi} \sum_{n=-\infty}^{+\infty} \mathrm{e}^{in(k-k')a} = \delta\left(k'-k\right) \mathrm{e}^{-ika}, \tag{2.39}$$

$$\sum_{n=-\infty}^{+\infty} n \langle k' \mid n \rangle \langle n \mid k \rangle = \frac{a}{2\pi} \sum_{n=-\infty}^{+\infty} n \mathrm{e}^{in(k-k')a} = \delta\left(k'-k\right) \frac{\mathrm{i}}{a} \frac{\mathrm{d}}{\mathrm{d}k}, \tag{2.40}$$

which we will use to write the Hamiltonian like

$$H = \int_{-\pi/a}^{\pi/a} \int_{-\pi/a}^{\pi/a} dk dk' \, |k\rangle \langle k'| \, \delta\left(k'-k\right) \left( -w\mathrm{e}^{-ika} - w\mathrm{e}^{ika} + ieE \frac{\mathrm{d}}{\mathrm{d}k} \right) \tag{2.41}$$

$$= \int_{-\pi/a}^{\pi/a} dk \, |k\rangle \langle k| \left( -2w\cos\left(ka\right) + ieE \frac{\mathrm{d}}{\mathrm{d}k} \right). \tag{2.42}$$

The eigenstates of the problem are then given by the Schrödinger equation

$$-2w\cos\left(ka\right)\Psi_m(k) + ieE \frac{\mathrm{d}}{\mathrm{d}k}\Psi_m(k) = \mathcal{E}_m\Psi_m(k), \tag{2.43}$$

with the periodic condition

$$\Psi(k + 2\pi/a) = \Psi(k). \tag{2.44}$$

Writing the equation like

$$\frac{\mathrm{d}}{\mathrm{d}k}\Psi_m(k) = \frac{\mathcal{E}_m}{ieE}\Psi_m(k) + \frac{2w}{ieE}\cos(ka)\,\Psi_m(k), \tag{2.45}$$

it is clear that the function

$$\Psi_m(k) = A\exp\left[-i\left(\frac{\mathcal{E}_m}{eE}k + \frac{2w}{aeE}\sin(ka)\right)\right] \tag{2.46}$$

satisfies the differential equation. The boundary condition 2.44 then allows us to discover the eigenenergies

$$\exp\left[-i\left(\frac{\mathcal{E}_m}{eE}k + \frac{2w}{aeE}\sin(ka)\right)\right]\exp\left[-i\left(\frac{\mathcal{E}_m}{eE}\frac{2\pi}{a}\right)\right] = \exp\left[-i\left(\frac{\mathcal{E}_m}{eE}k + \frac{2w}{aeE}\sin(ka)\right)\right]. \tag{2.47}$$

To satisfy the equality above, the eigenenergies must then be determined as

$$\mathcal{E}_m = aeEm\,,\ \ m \in \mathbb{Z}, \tag{2.48}$$

meaning the eigenenergies of the system are separated by multiples, or "steps", of $aeE$, forming the so called Wannier-Stark "ladder". Finally, the normalization condition then yields

$$A = \sqrt{\frac{a}{2\pi}}. \tag{2.49}$$

The eigenstates, which are known as Wannier-Stark states, are then, in the momentum space, given by

$$\Psi_m(k) = \sqrt{\frac{a}{2\pi}}\exp\left[-i\left(amk + \frac{2w}{aeE}\sin(ka)\right)\right]. \tag{2.50}$$

Having performed this diagonalization, the time-evolution operator in momentum space is given as

$$U_{k'k}(t) = \left\langle k'|U(t)|k\right\rangle = \sum_m \left\langle k' \mid \Psi_m\right\rangle \mathrm{e}^{-i\mathcal{E}_m t/\hbar}\left\langle \Psi_m \mid k\right\rangle \tag{2.51}$$

$$= \frac{a}{2\pi}\mathrm{e}^{-i\gamma[\sin k'd - \sin kd]}\sum_m \mathrm{e}^{-im(k'-k+eEt/\hbar)a} \tag{2.52}$$

$$= \mathrm{e}^{-i\gamma[\sin k'a - \sin ka]}\delta\left(k' - k + eEt/\hbar\right). \tag{2.53}$$

Once again, the semi-classical acceleration theorem 2.10 has emerged from yet another consideration of a different gauge

$$k' = k_t = k - eEt/\hbar. \tag{2.54}$$

We may now verify the appearance of coherent oscillations in the current for an initially fixed thermalized system, with an initial density matrix

$$\rho\left(0\right)_{kk'} = f\left(\varepsilon_k\right)\delta\left(k - k'\right). \tag{2.55}$$

The definition of the current operator is this time made easy, since this time the position operator

$$\hat{X} = a\sum_{n=-\infty}^{+\infty} n\left|n\right\rangle\left\langle n\right| \tag{2.56}$$

is well defined, and the current operator is then obtained by the Heisenberg equation

$$\hat{J} = e\hat{V} = e\frac{i}{\hbar}\left[\hat{H}, \hat{X}\right] \tag{2.57}$$

$$= e\frac{iaw}{\hbar}\sum_{n=-\infty}^{+\infty}\left|n+1\right\rangle\left\langle n\right| - \left|n\right\rangle\left\langle n+1\right| \tag{2.58}$$

$$= 2\frac{eaw}{\hbar}\sum_{k}\sin\left(ka\right)\left|k\right\rangle\left\langle k\right|. \tag{2.59}$$

The evolution of the averaged current is then

$$\left\langle\hat{J}\right\rangle(t) = \text{Tr}\left(\rho\left(0\right)J\left(t\right)\right) = \int_{-\pi/a}^{\pi/a}\int_{-\pi/a}^{\pi/a} dk dk' \rho_{kk}\left(0\right)U_{kk'}\left(t\right)J_{k'}U_{k'k}\left(-t\right) \tag{2.60}$$

$$= 2\frac{eaw}{\hbar}\int_{-\pi/a}^{\pi/a} dk f(\varepsilon_k)\sin\left(\left(k + eE\frac{t}{\hbar}\right)a\right) \tag{2.61}$$

$$= \frac{ea}{\hbar}\sin\left(-eEa\frac{t}{\hbar}\right)\int_{-\pi/a}^{\pi/a} dk f(\varepsilon_k)\varepsilon_k, \tag{2.62}$$

where we have used the same symmetry argument as in the previous subsection in step 2 to step 3. The oscillations are thus the same as in equation 2.33 with the visible promotion of the sum to in k-space to an integral over the entire FBZ.

Wannier-Stark states will prove more useful in the Wannier basis. To unveil their properties

in real space, we must perform a Fourier transformation, which yields

$$\Psi_m(n) = \langle n \mid \Psi_m \rangle = \int_{-\pi/a}^{\pi/a} dk \, ak \langle n \mid k \rangle \langle k \mid \Psi_m \rangle = \frac{a}{2\pi} \int_{-\pi/a}^{\pi/a} dk e^{i[(n-m)ka - \gamma \sin(ka)]}$$

$$= \frac{1}{2\pi} \int_{-\pi}^{\pi} du e^{i[(n-m)u - \gamma \sin u]}. \tag{2.63}$$

A Bessel function of the first kind of argument $\gamma$ and order $n$ is denoted as $J_n(\gamma)$ and has an integral representation of the form [50]

$$J_n(\gamma) = \frac{1}{2\pi} \int_{-\pi}^{\pi} e^{i(nu - \gamma \sin u)} du, \tag{2.64}$$

leading us to identify this eigenstates as

$$\Psi_m(n) = J_{n-m}(\gamma), \tag{2.65}$$

which we may write in the Wannier basis, yielding the so called Wannier-Stark states [49,51]

$$|\Psi_m\rangle = \sum_l J_{l-m}\left(2w/eEa\right)|l\rangle. \tag{2.66}$$

We can extract some useful properties from this space representation of the eigenstates from general properties of Bessel functions [50]. Particularly, we know that $J_{l-m}(\gamma)$ is mainly localized in the interval $|l - m| < \gamma$ and, outside this interval, decays exponentially as $J_n(\gamma) \sim \gamma^n$. This allows us to define a localization length as

$$\xi_{WS} = \frac{2w}{eEa}, \tag{2.67}$$

which as we can see in Figure 2.2 (red dashed line in the right panel) actually describes the states localization fairly well. We can also see that there is a Wannier-Stark state centered around each Wannier site. The symmetry property of Bessel functions [50]

$$J_{-n}(\gamma) = (-1)^n J_n(\gamma) \tag{2.68}$$

tells us the squared modulus of the state is symmetric around its center.
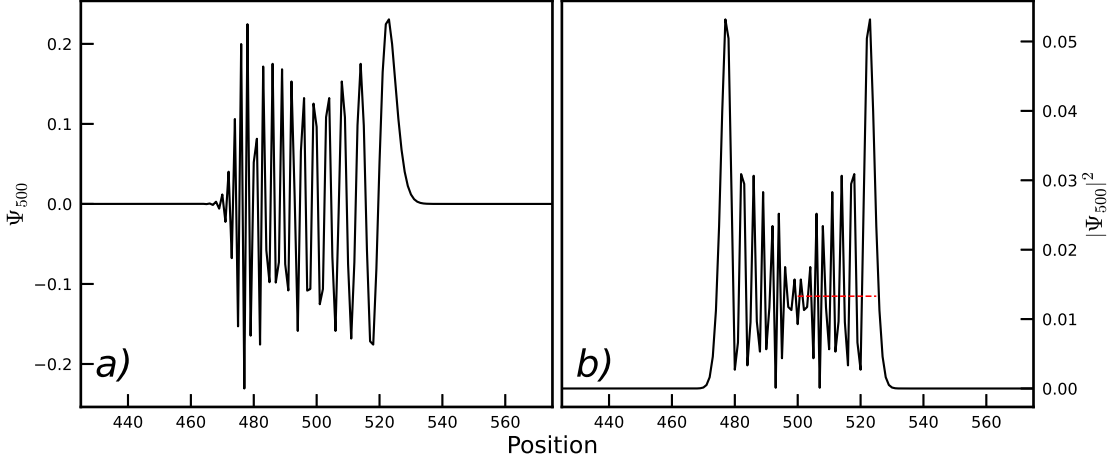
Figure 2.2.: Wannier-Stark state and its modulus squared, respectively, centered around site 500, for a system of size $L = 1024$ and $E = 0.08$ (in units of $a$ and $w/ea$ respectively).

The orthogonality and completeness of the Wannier-Stark states is guaranteed by the addition theorem of Bessel functions [49]

$$\sum_{k=-\infty}^{+\infty} J_k(z) J_{k+p}(z) \exp(\mathrm{i}k\alpha) = J_p(2z\sin(\alpha/2))\exp(\mathrm{i}p(\pi - \alpha)/2), \tag{2.69}$$

with $\alpha = 0$ as input. Such proof is a straightforward task, however, we need to make use of the following results regarding Bessel functions of the first kind [50]:

$$J_\nu(0) = 0, \ |\nu| > 0, \tag{2.70}$$

$$J_\nu(0) = 1, \ \nu = 0. \tag{2.71}$$

Using equation 2.69 with $\alpha = 0$ gives us

$$\sum_{k=-\infty}^{+\infty} J_k(z) J_{k-p}(z) = J_{-p}(0)\exp(-\mathrm{i}p\pi/2) = \langle \Psi_l \mid \Psi_{l-p} \rangle. \tag{2.72}$$

Using the relations above allows us to get

$$\langle \Psi_l \mid \Psi_{l-p} \rangle = 0, \ p \neq 0, \tag{2.73}$$

$$\langle \Psi_l \mid \Psi_l \rangle = 1, \tag{2.74}$$

Which is sufficient to prove the orthogonality and completeness of the Wannier-Stark states.

## 2.3. Time-Evolution of Gaussian Wave-packets in a 1-band system

Before proceeding to the discussion of this oscillations in a mesoscopic system, it will be crucial to develop an intuition on the evolution of Gaussian wave-packets in systems with an applied electric field. For Gaussian wave-packets sufficiently localized in both real and reciprocal space, their evolution will be governed by the semi-classical equations. Therefore, it will provide us with a good simulation of semi-classical behavior in a purely quantum system, which will serve us later as useful intuition in chapters 3 and 4. We will be retracing the calculations done in references [48, 49, 51].

### 2.3.1. Spatial Propagator

We define the spatial propagator as

$$K_{l,l'}(t) = \langle l| e^{-iHt/\hbar} |l'\rangle. \tag{2.75}$$

We may introduce the set of Wannier-Stark states and use 2.69 to obtain [49, 51]

$$
\begin{aligned}
K_{l,l'}(t) &= \sum_{m=-\infty}^{\infty} \langle l \mid \Psi_m \rangle \langle \Psi_m \mid l' \rangle \exp\left(-i\mathcal{E}_m t/\hbar\right) \\
&= \sum_{m=-\infty}^{\infty} J_{l-m}\left(2w/eEa\right) \sum_{l} J_{l'-m}\left(2w/eEa\right) \exp\left(-iaeEmt/\hbar\right).
\end{aligned} \tag{2.76}
$$

By applying the addition theorem 2.69 to equation 2.76 (which is only possible due to the energetically equidistant spectrum of the Wannier-Stark states), one arrives at the expression

$$K_{l,l'}(t) = J_{l-l'}\left(\frac{4w}{eEa}\sin\left(\frac{aeEt}{2\hbar}\right)\right)\exp\left(i\left(l-l'\right)\left(\frac{\pi - aeEt/\hbar}{2}\right) - il'\frac{aeE}{\hbar}t\right).$$

The obtained result is very telling on the dynamics of the system: the final equation shows that the spatial propagator is periodic in time with the Bloch period $T_{OB} = 2\pi\hbar/eaE$ and consequently any wave-packet will realize a periodic motion.

### Wave-Packet Dynamics

We may then use the result previously obtained to our advantage in order to regain semi-classical motion by considering the evolution of a Gaussian wave-packet with initial momentum $k_0$ [48, 49]

$$\psi_l(0) = \left(\frac{a^2}{2\pi\sigma^2}\right)^{1/4}\exp\left(-\frac{l^2 a^2}{4\sigma^2} + ik_0 la\right). \tag{2.77}$$

The evolution of this coefficients is given by

$$\psi_l(t) = \sum_{l'} K_{l,l'}(t)\psi_{l'}(0). \tag{2.78}$$

We can Fourier transform the above formula and use the generating function for the Bessel functions of the first kind [50]

$$\exp[iz\sin(\varphi)] = \sum_{k=-\infty}^{+\infty} \exp(ik\varphi)J_k(z) \tag{2.79}$$

to obtain the more convenient relation

$$
\begin{aligned}
\hat{\psi}(k,t) &= \sum_{l,l'} \exp(-ikla)K_{l,l'}(t)\psi_{l'}(0) \\
&= \exp\left[i\frac{4w}{eaE}\sin\left(\frac{eaEt}{2\hbar}\right)\cos\left(ka + \frac{eaEt}{2\hbar}\right)\right] \\
&\quad \times \sum_{l'} \exp\left(-i\left(k + eEat/\hbar\right)l'\right)\psi_{l'}(0).
\end{aligned}
\tag{2.80}
$$

Let us assume that $\sigma/a \gg 1$ so that the spatial localization of the initial wave-packet is sufficiently weak to allow us to approximate this summation by an integral and arrive at

$$
\begin{aligned}
\hat{\psi}(k,t) &\approx \left(\frac{8\pi\sigma^2}{a^2}\right)^{1/4} \exp\left[i\frac{4w}{eaE}\sin\left(\frac{eaEt}{2\hbar}\right)\cos\left(ka + \frac{eaEt}{2\hbar}\right)\right] \\
&\quad \times \exp\left(-2\sigma^2\left(k - k_0 + \frac{eEt}{\hbar}\right)^2\right).
\end{aligned}
\tag{2.81}
$$

At this point we can make contact with a familiar notion: The resulting wave-packet evolution in the reciprocal space is itself a periodic function modulated by a Gaussian whose mean is moving uniformly with velocity $eE/\hbar$. This observation is congruent with the first semi-classical equation 2.9. Though it may seem we have lost the periodicity of the motion equation 2.81, we need not forget that $k$ is only defined modulo $2\pi/a$, restoring the temporal periodicity in the equation above. But we can go even further by casting the evolution of the wave-packet in real space

$$\psi_l(t) = \frac{a}{2\pi} \int_{-\pi/a}^{\pi/a} dk\, \hat{\psi}(k,t) \exp(ikla). \tag{2.82}$$

The assumption that $a/\sigma \gg 1$ will once again come in handy, since it means that the momentum distribution function $\hat{\psi}(k,t)$ is sharply localized around $k(t) \equiv k_0 - \frac{eEt}{\hbar}$ in the reciprocal

space. This is good enough a reason to expand $\cos\left(ka + \frac{eaEt}{2\hbar}\right)$ around $k(t)$

$$\cos\left(ka + \frac{eaEt}{2\hbar}\right) \approx \cos\left(ak_0 - \frac{eaEt}{2\hbar}\right) - a\sin\left(ak_0 - \frac{eaEt}{2\hbar}\right)(k - k(t)). \qquad (2.83)$$

The computation needed to arrive at the final result is omitted for the sake of brevity, and the curious reader is referred to the appendix C for a more detailed derivation. With this said, we arrive at [49]

$$\psi_l(t) \approx \left(\frac{a^2}{2\pi\sigma^2}\right)^{1/4} \exp\left(i\left(k_0 - eE\frac{t}{\hbar}\right)la - i\Phi(t) - \frac{a^2}{4\sigma^2}(l - \bar{l}(t))^2\right), \qquad (2.84)$$

with

$$\Phi(t) = \frac{2w}{eEa}\left[\sin\left(k_0 a - eEa\frac{t}{\hbar}\right) - \sin(k_0 a)\right], \qquad (2.85)$$

and

$$\bar{l}(t) = \frac{2w}{eEa}\left[\cos\left(k_0 a - eEa\frac{t}{\hbar}\right) - \cos(k_0 a)\right]. \qquad (2.86)$$

The last equation tells us the center of the gaussian in space is oscillating with an amplitude and period inversely proportional to the electric field, as the semi-classical equations had foreseen. In fact, not only do they have the same functional dependence on $E$, they are exactly the same, and we can therefore confidently say that we reobtained the semi-classical behavior of Bloch Oscillations.

### 2.3.2. Numeric Simulation on a Finite Chain with Open Boundaries

Even though it might seem intuitive that a Gaussian wave-packet should behave the same in an open chain as it does in an infinite system as long as it does not reach the boundaries, it is still instructive to see this numerically to make sure the boundary conditions do not meaningfully alter the dynamics. The Hamiltonian for a 1D tight binding chain with an uniform and constant electric field is

$$H = -w\sum_{n=0}^{N-2}(|n\rangle\langle n+1| + |n+1\rangle\langle n|) + aeE\sum_{n=0}^{N-1}n|n\rangle\langle n|. \qquad (2.87)$$

An analytical study of the eigenstates of such a system has been performed in [52] with the conclusion that the eigenstates and eigenvalues at the center of the finite system are essentially Wannier-Stark states by calculating the corresponding eigenvalues for a given chain size N and see their fast convergence to the Wannier-Stark energy ladder with $N \to \infty$. In fact, the eigenstates between the two only differ meaningfully if the area described by the Wannier-Stark

localization length reaches the edge of the system.
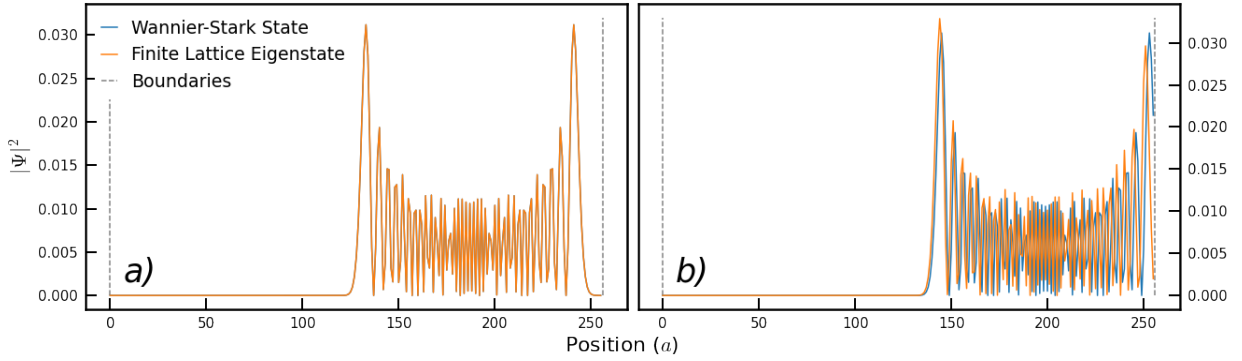


Figure 2.3.: Comparison between exact Wannier-Stark states and eigenstates of a finite system at the edge, for $L = 256$ and $E = 0.035$, in units of $a$ and $w/ea$, respectively. We can see that these only differ when the state is no longer fully localized inside the system.

We performed a time-evolution of a Gaussian wave-packet in such a system by expanding the time evolution operator in Chebyshev Polynomials with the method described in A.1.7 and obtained satisfying results, with the wave-packet performing an oscillatory motion with the amplitude and frequency predicted in the previous subsections (Fig. 2.4).
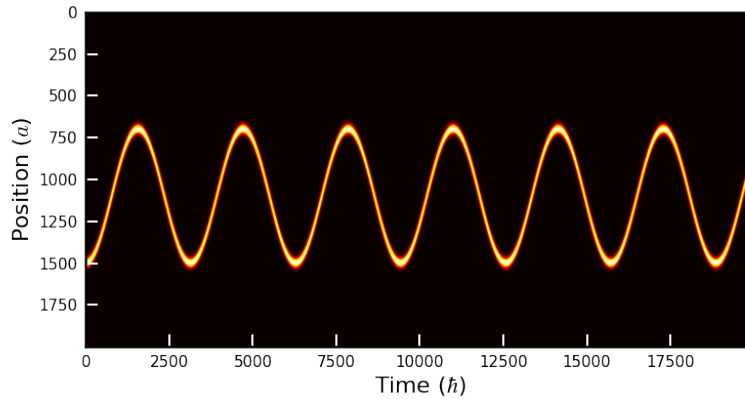


Figure 2.4.: Evolution of a Gaussian wave-packet of variance $\sigma = 20a$ initially centered at $\bar{l}_0 = 1500a$ in an 1D finite tight binding Hamiltonian subject to a constant and uniform electric field $E = 0.005w/ea$.

# 3. Bloch Oscillations in One-Dimensional Two-Terminal Mesoscopic Devices

In what follows, we will be aiming at studying the emergence of Bloch Oscillations in two-terminal mesoscopic systems: the case where the sample has no disorder will be studied thoroughly to characterize the appearance of this oscillations in terms of the different parameters of the system. They will appear both as an infinite oscillatory current response to a dc potential and as a transient regime relaxing to a constant current response. The dependence of this two different realizations of BO's on the system's parameters is something we shall discuss in the following subsections.

Furthermore, the effect of Anderson disorder in the average current inside and outside a sample with an applied constant electric field is also analyzed. Because of the many possible types of disorder, it is difficult to classify any encountered disorder-induced effect as universal. The most immediate intuition is that there will be some kind of interplay between the different localization lengths introduced by the electric field ($\xi_{WS}$) and disorder ($\xi_A$), but as for what actually happens it is not clear at all. Fortunately, we will later see that this effects are backed by a simplistic semi-classical view on particles being scattered in the First Brillouin Zone, keeping us optimistic on the possibility of generalizing this results to other types of disorder.

## 3.1. The Model

The Hamiltonian of the model follows the usual one dimensional tight binding scheme

$$H\left(t\right) = H_{CC}\left(t\right) + \sum_{\alpha=L,R}\left(H_{\alpha}\left(t\right) + H_{C\alpha}\left(t\right)\right), \tag{3.1}$$

where $H_{CC}$ stands for the central sample's Hamiltonian, $H_{L(R)}$ is the Hamiltonian for the left (right) lead and $H_{CL(R)}$ is the coupling term between the left (right) lead and the central sample. This coupling terms will from now on be included in the respective lead's Hamiltonian for simplicity. We will throughout this work only be working with clean leads. For simplicity, we will work in units of $\hbar = e = a = 1$, with $e$ and $a$ being the particle's charge and the lattice

parameter, respectively. The expansion of this matrices in the Wannier basis then yields

$$
H_{\text{CC}}(t) = \sum_{n=-(L-1)/2}^{(L-1)/2} (v_n(t) + \xi_n) c_n^\dagger c_n - w \sum_{n=-(L-3)/2}^{(L-3)/2} \left( c_{n+1}^\dagger c_n + \text{ h.c. } \right),
$$

$$
H_{\text{L}}(t) = \sum_{n=-\infty}^{-(L+1)/2} v_n(t) c_n^\dagger c_n - w_l \left( c_{n+1}^\dagger c_n + \text{ h.c. } \right), \tag{3.2}
$$

$$
H_{\text{R}}(t) = \sum_{n=(L+1)/2}^{+\infty} v_n(t) c_n^\dagger c_n - w_l \left( c_{n+1}^\dagger c_n + \text{ h.c. } \right),
$$

where $L$ is the size of the sample, $w$ is the hopping parameter inside the sample, $w_l$ is both the leads' hopping and the hopping term connecting the leads to the sample and $\xi_n$ is the disordered potential that we will eventually add to study the disordered case. To develop the non-equilibrium dynamics, we employ the partition-free approach [53, 54]: the sample is initially already connected to, and in thermal equilibrium with the leads, with no potential applied, meaning

$$
v_n(t < 0) = 0, \forall n, \tag{3.3}
$$

And the initial mixed state is thus

$$
\rho(t < 0) = \sum_k f(\varepsilon_k) |\psi_k\rangle \langle \psi_k| \tag{3.4}
$$

with $|\psi_k\rangle$ being the eigenstates eigenstates of the initial Hamiltonian, $\varepsilon_k$ their energy and $f(\varepsilon_k)$ the Fermi-Dirac distribution. At $t = 0$, the system is perturbed with an electric potential bias along the entire system. The actual shape of this potential, however, is the fundamental part of this work: the potential in the leads is constant and symmetric but in the sample it's a ramp, guaranteeing we only have a non-zero electric field applied inside the sample:

$$
v_n(t > 0) = \begin{cases} nE, & -\frac{L-1}{2} \leq n \leq \frac{L-1}{2}, \\ -\frac{\Delta V}{2}, & n < -\frac{L-1}{2}, \\ \frac{\Delta V}{2}, & \frac{L-1}{2} < n, \end{cases} \tag{3.5}
$$

With $E$ being the electric field. This field is crucial given it is the mechanism responsible for BO's in an infinite lattice, as we will see in the following section.

The detection of BO's will then consist of measuring the average local current through a specific bond

$$
\left\langle \hat{J}_n \right\rangle (t) = \text{Tr} \left( \rho(0) \hat{J}_n(t) \right), \tag{3.6}
$$
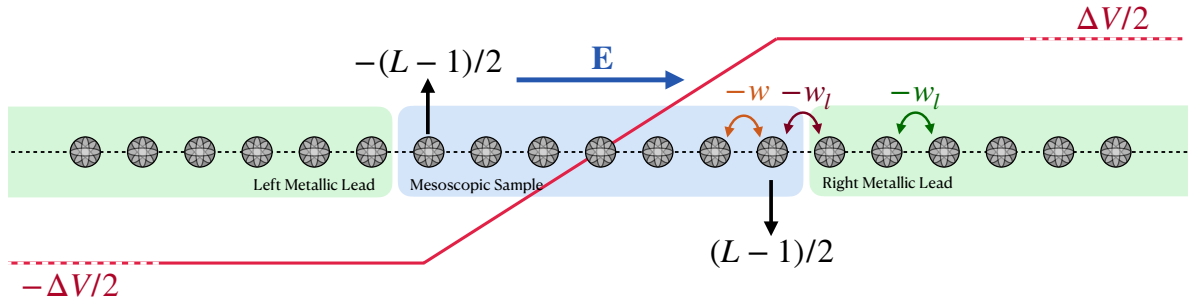
Figure 3.1.: Model used for the of non equilibrium transport in 1 dimension.

with

$$\hat{J}_n = \frac{w}{i\hbar} \left( c_{n+1}^\dagger c_n - c_n^\dagger c_{n+1} \right). \tag{3.7}$$

Such computation can be made very numerically efficient by truncating the leads to a finite size and implementing an expansion of the time-evolution operator in Chebyshev polynomials [42], with the tradeoff that an eventual reflexion at the boundaries of the leads will contaminate the results [41] (See Appendix A.1 for details). In the remainder of this document, the leads are made sufficiently large to avoid this reflexion in the time intervals considered. As for the disorder type, we employ the usual Anderson disorder and add random on-site energies in the sample's sites drawn from the uniform distribution. In other words, the probability density function of each on-site energy will be given by

$$p\left(\xi_n\right) = \begin{cases} 1/W, & \varepsilon_n \in \frac{W}{2}\left[-1, 1\right] \\ 0 & \text{otherwise} \end{cases}. \tag{3.8}$$

Finally, the results from such time evolution will be compared to the Landauer formula [17] for the current:

$$I_{L \to R} = \frac{e}{2\pi\hbar} \int d\varepsilon \left( f_L \left( \varepsilon - \frac{\Delta V}{2} \right) - f_R \left( \varepsilon + \frac{\Delta V}{2} \right) \right) T\left(\varepsilon\right), \tag{3.9}$$

Where $T\left(\varepsilon\right)$ is the inter-lead transmission coefficient, which is numerically calculated using the Kwant python package [55]. A full derivation of this coefficient as well as of the Landauer formula can be found in appendix B.

## 3.2. Homogeneous hoppings ($w_l = w$) for a Clean System

To first introduce Bloch Oscillations in the mesoscopic transport context, we will begin with the simplest case by setting the leads' hopping parameter equal to that of the central sample, that is, $w = w_l$, and setting $W = 0$ to study a clean sample. This choice of $w_l$ will have consequences we will later see, but for now this helps to understand a particular mechanism,
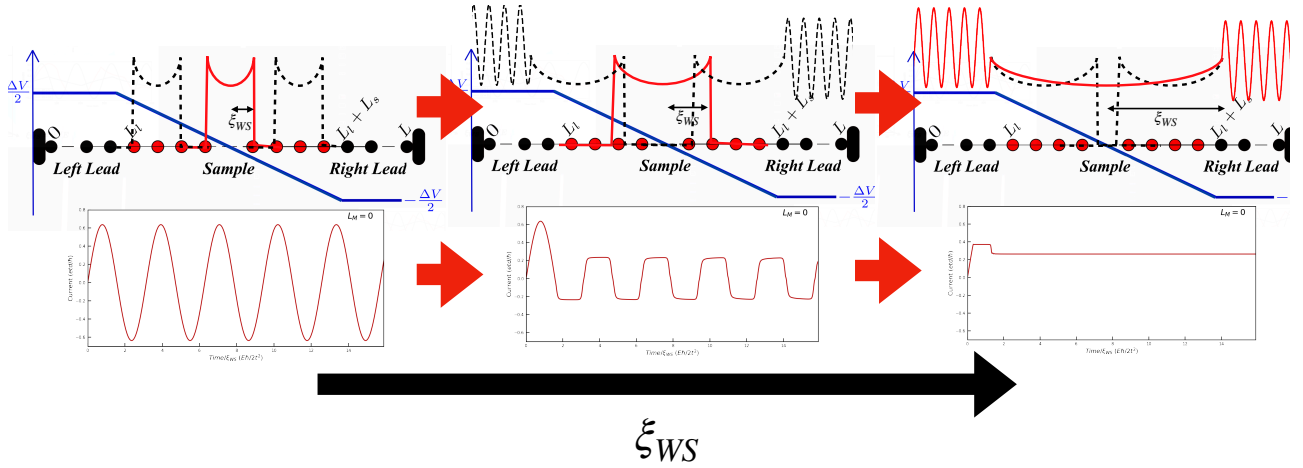
Figure 3.2.: Depictions of Wannier-Stark states inside the sample as we increase their localization length, with the corresponding current response shown below.

the localization of the Wannier-Stark states inside the sample, and the emergence of the Bloch Oscillations instead of the Landauer steady current prediction.

### 3.2.1. Bloch Oscillation's Existence Condition

We being this subsection by depicting the eigenstates of a sample connected to leads for different electric fields. This states are shown in figure 3.2, where the central-most state is depicted in red and two more states are depicted in a lack dashed line. In subsection 2.2.1 we discussed the eigenstates of an infinite lattice subject to a static and uniform electric field. These eigenstates are called Wannier-Stark states. Such states are very well localized in space and described by the localization length given in equation 2.67. We have also seen that the eigenstates of a finite lattice are very similar to said Wannier-Stark states as long as the region where they are predominantly non-zero is not touching the boundary of the system. Analogously, the eigenstates of the two-terminal device will be approximately Wannier-Stark states inside the sample coupled to propagating states in the leads, provided that the area where the Wannier-Stark state is significantly non-zero is far from the edge of the sample. This means that the average local current at the center of the sample with a sufficiently strong electric field (i.e, well localized Wannier-Stark states) will behave very similar to that of the infinite system, since the Wannier-Stark states that contribute to this current are well localized, thus originating Bloch Oscillations in the local current.(Left panel of figure 3.2). As we decrease the electric field, the states begin to extend, leading to more and more of them to effectively deform and "escape" the sample. This will obviously have an impact on the oscillatory motion of the current, but since some states in the vicinity of the center are still completely localized, we will still be able to spot some oscillation (Central panel of figure 3.2). Once we get the last state, which is the central one, to be completely delocalized, we will no longer get BO's, and a constant, Landauer-valued current will take place instead (Right panel of figure 3.2). Based on this image, we can then obtain a condition for the existence of BO's

inside the sample, which is, simply put [5]:

$$\xi_{WS} \leq \frac{L}{2}, \tag{3.10}$$

where $L$ is the size of the central sample. We can expand the Wannier-Stark localization length with equation 2.67 and perform some algebra to cast the condition into a more conventional form

$$4w \leq \Delta V. \tag{3.11}$$

This way of expressing the condition in terms of the potential difference and the central hopping parameter will prove more useful for following considerations.

### 3.2.2. Bound States Inside the Sample

Condition 3.11 allows one to know the minimum potential bias needed for a given system to display BO's, either deformed or not, and it has already been seen in Ref [5]. However, in that same reference, this oscillations do not decay in time to a constant value: they oscillate infinitely, which is a direct confrontation to the Landauer prediction. Underneath the obtainance of the Landauer formula, however, is the assumption that the system does not exhibit any bound states, meaning every eigenstate of the full Hamiltonian is a propagating state inside both leads and not an evanescent one. In fact, if bound states exist inside the sample, given they cannot propagate outside the leads, they will prevent the system from achieving a steady-state dynamic flow and will be responsible for oscillations in the current instead [31, 56, 57]. To probe our system for bound states, it is useful to look at the problem in terms of its energetic bounds. Particularly, one is to look at the bandwidths of the leads to find a justification for the observed infinite BO's.
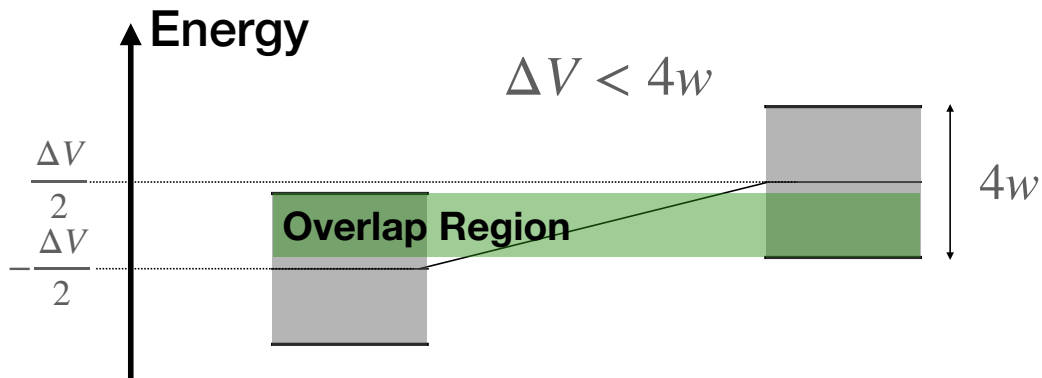


Figure 3.3.: Diagram of the energy bands of the leads for a system with $\Delta V < 4w$.

Let us draw out the electric bias and represent the energy bands of the leads as depicted in

figure 3.3, where the black lines limit the energy of the propagating states in the leads. For $\Delta V < 4w$, the width of the energy band of the leads, we will always have an overlap between the bands' leads, which means that by the energy conservation law, it is possible to couple propagating states in the left lead to those of the right lead. However, setting $\Delta V$ to be equal to this width will cause these bands to not overlap, meaning there won't be any coupling between leads and, consequently, no current, as seen in figure 3.4.
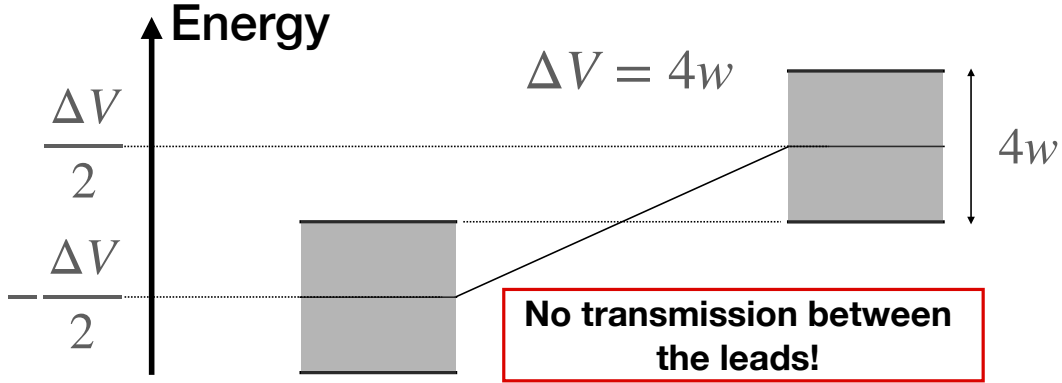


Figure 3.4.: Diagram of the energy bands of the leads for a system with $= \Delta V < 4w$.

It is now clear where the infinite BO's originate from: for potential biases stronger than $4w$, the gap between the top of the left lead's band and the bottom of the right lead's band is populated with states inside the sample that do not couple to the propagating states of the leads. These bound states will then originate an infinite oscillatory motion in the current. Coincidently, this limit for when bound states start being generated inside the sample is the same as the one found in the previous subsection (equation 3.11), where the eigenstates inside the sample begin to localize and become very similar to Wannier-Stark states. Therefore, the bound states generated are actually Wannier-Stark states, and thus the oscillations observed, albeit eventually deformed, will be Bloch Oscillations, whose period is given by the usual BO period (equation 2.15).

### 3.2.3. Numeric Results

The discussion performed up until now is corroborated by numerical evidence obtained from the time-evolution of the system using the partition-free approach: plotting the average local current evolution in the center of the sample for different Wannier-Stark localization lengths, it is clear that Bloch Oscillations emerge for sufficiently localized states and get deformed as we decrease the localization length (i.e increase the electric field), eventually ceasing and being replaced by a constant, steady-state current response congruent with the Landauer prediction for $\xi_{WS} = L/2$ (Figure 3.5.a)). It is worth noticing that the time in this figure has been rescaled for each curve by the respective $\xi_{WS}$, allowing the collapse of the oscillations in terms

of their periods. This is because both $\xi_{WS}$ and the period $T_{BO}$ of Bloch Oscillations are both inversely proportional to the electric field, and thus, by dividing the time by the localization length, one eliminates the dependency of the period on the electric field. This is a strong indication that the bound states generating this oscillations are indeed Wannier-Stark states, since the periods of the oscillations in figure 3.5.a) are all given by $T_{BO}$ for their respective electric field values.

Furthermore, the current inside one of the leads follows the same behavior , with the exception that we do not see the BO's and instead see the current decay to zero for $\xi_{WS} < L/2$ as expected, since in this regime the leads' bands do not overlap, preventing the coupling between their propagating states and, therefore, the existence of any transmission (Figure 3.5.b)).
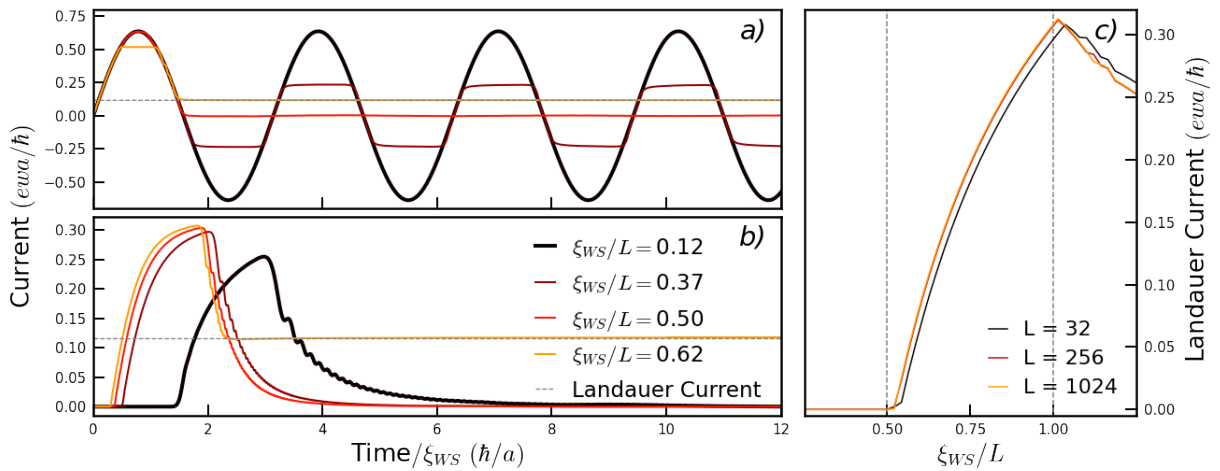


Figure 3.5.: a) and b) - Plots of the current time-evolution measured inside and outside a sample of size $L = 256$ (in units of $a$)and compared to their the Landauer values in dashed grey, respectively. c) - Landauer current as a function of the Wannier-Stark localization length divided by the size of the sample, for various sizes. The dashed grey lines depict the place where $\xi_{WS}/L = 1/2$ and $\xi_{WS}/L = 1$.

Finally, all of this can be summarized by plotting the total inter-lead transmission (to which we have labeled Landauer Current) as a function of $\xi_{WS}/L$ and see that, in fact, it is zero until we reach $\xi_{WS}/L = 1/2$, in which point we get an increase in the total transmission. It is also interesting to notice that the total current increases with the decrease of the electric field between $\xi_{WS}/L = 1/2$ and $\xi_{WS}/L = 1$, which is already not expected from a purely classical point of view. Such behavior is due to more and more Wannier-Stark states getting completely delocalized, meaning they strongly couple to both left and right propagating states, which increases transmission. After every single state is completely delocalized, which happens for $\xi_{WS}/L = 1$, we regain the usual behavior of current diminishing with the decrease of the electric field.

## 3.3. Inhomogeneous hoppings ($w_l > w$)

In the previous subsection, we have seen that BO's arise as persistent oscillations in a mesoscopic two-terminal device for sufficiently strong potential biases because of the bound states generated inside the sample. However, it is also shown in references [31, 56, 57] that, by guaranteeing there are no bound states in the system, a steady state exists, at which point the Landauer formula should accurately describe the attained steady-state current. Naturally, the question arises: is it possible to get inter-lead transmission and Bloch Oscillations at the same time? We will delve deeper in such affairs by now increasing $w_l > w$ arbitrarily as to control the width of their energy bands.

### 3.3.1. Mitigation of Bound states by Broadening the Leads' Energy Bands

As seen in the right depiction of figure 3.6, we can maintain $\Delta V = 4w$ to have Wannier-Stark states localized inside the sample. Increasing $w_l$ promotes the overlap between the bands, thus granting transmission and Bloch Oscillations in one setting. This will guarantee that the previously detected bound states will now couple to propagating states in the leads and the oscillations will cease oscillating infinitely and will have to be eventually replaced by a steady-state current described by the Landauer formula.
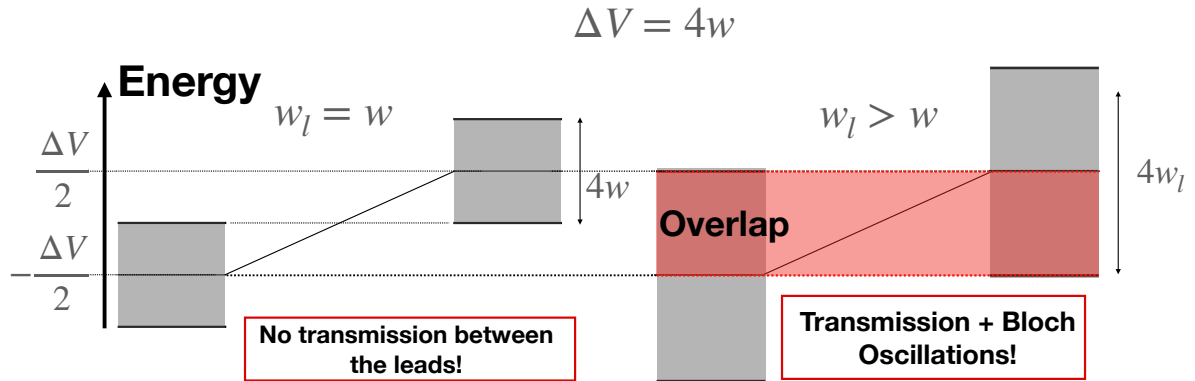


Figure 3.6.: Diagrams of the energy bands of the leads for a system with $\Delta V = 4w$. On the left, a system where the leads' hopping parameter $w_l$ equals that of the central sample $w$, resulting in no inter-lead transmission. On the right, whilst keeping $\Delta V = 4w$ , a system with $w_l > w$ such that there is overlap between the leads.

We complement our analysis using the Kwant package [55] to obtain information about total current transmission between the leads. To do this, we simply plot the transmission coefficient as a function of the energy, for different lead hoppings. The results clearly indicate that transmission is possible only for $w_l > \Delta V/4$, in accordance with the general image of the leads' bandwidths we have built so far. In the transmission regime, for a sufficiently strong electric field, lorentzian-shaped peaks around the energies of the Wannier-Stark states emerge
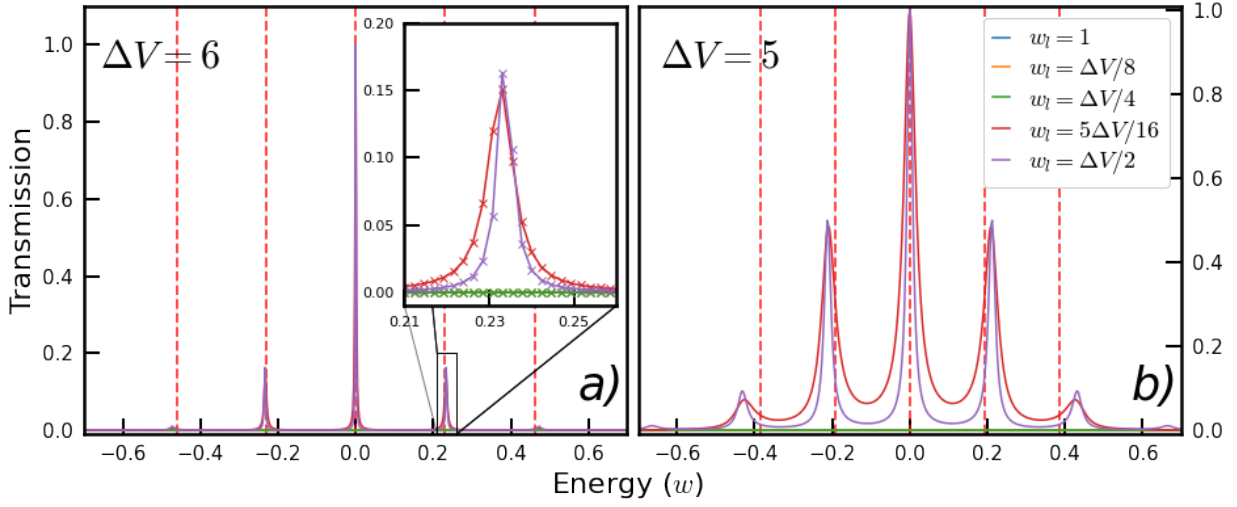
Figure 3.7.: Transmission coefficient curves as function of energy for a 1D chain of size L=25 (in units of $a$) and different lead hoppings for a) dV = 6 and b) dV = 5 (in units of $w$). The broadening of the peaks with the decreasing of the potential difference is clear.

out of the null flat curve that was in place for $w_l < dV/4$ (Fig 3.7.a)), with their widths being larger with the decreasing of the electric field (Fig 3.7.b)).

As we shall see in the next subsection, the width of a peak can be associated with a time uncertainty, which can in turn be interpreted as an estimation for the relaxation time of the whole system's eigenstate at the given energy. Ergo, stronger electrical fields will reduce the coupling between the Wannier-Stark states and the reservoirs, leading to thinner transmission peaks and, consequentially, larger relaxation times. It is not unreasonable, therefore, to conceive of a setup with a length and an electric field that, even though the Landauer calculation for the transmission is non-zero, the time to detect a non-zero current in the laboratory would be virtually infinite. The obtained evolution with a proper choice of $w_l$ that mitigates this bound states is shown in figure 3.8. It is now clear that BO's are a transient regime that decay towards a steady-state current given by the Landauer formula, as expected.
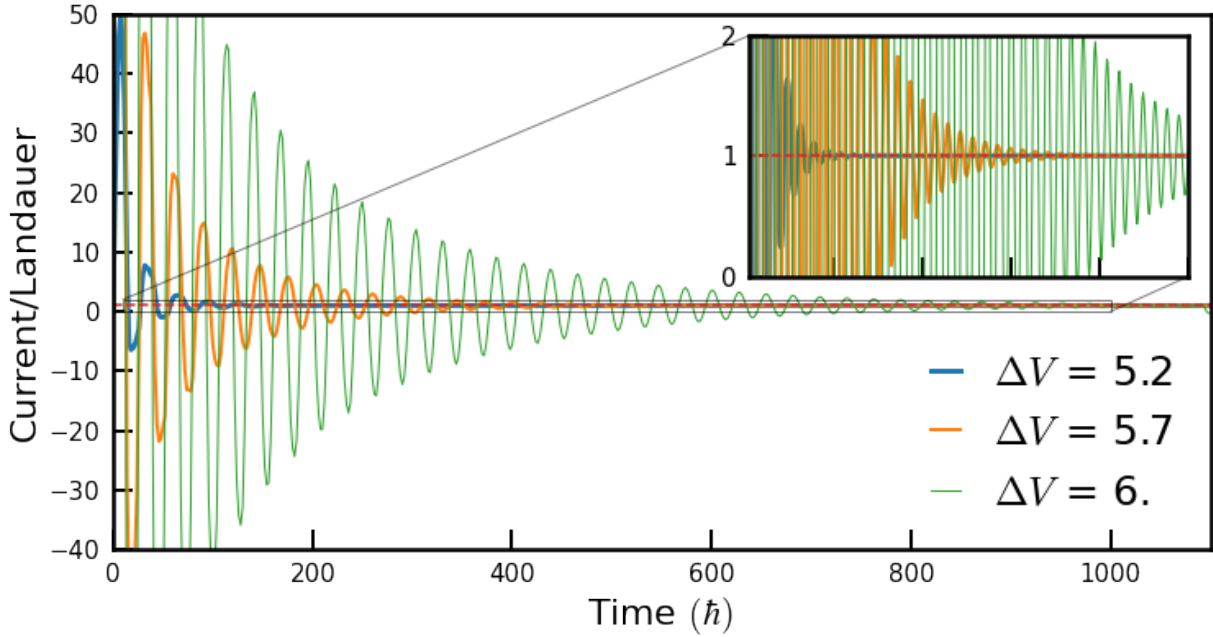
Figure 3.8.: Average current evolutions divided by their respective Landauer prediction for a system os size $L = 25$ (in units of $a$) and $w_l = (1/4 + 1/16)\,\Delta V$, for different potential biases in units of the central hopping $w$. It is clear that, with this choice of $w_l$, we have BO's decaying to a steady-state current given by the Landauer formula, shown clearly in the inset plot.

We can further notice in figure 3.7 that the highest peak clocks in at zero energy, which corresponds to the transmission associated to the central Wannier-Stark state in the sample, and these peaks decrease in value with the distance of the Wannier-Stark states to the central sample's site. Indeed, the central state has a transmission coefficient of 1 independently of the size of the sample, whereas the other peaks decrease with the increasing of the sample's size, as per figures 3.7.a) and 3.7.b), respectively. Such effect is due to the spatial symmetry of the Bessel function given in equation 2.68.
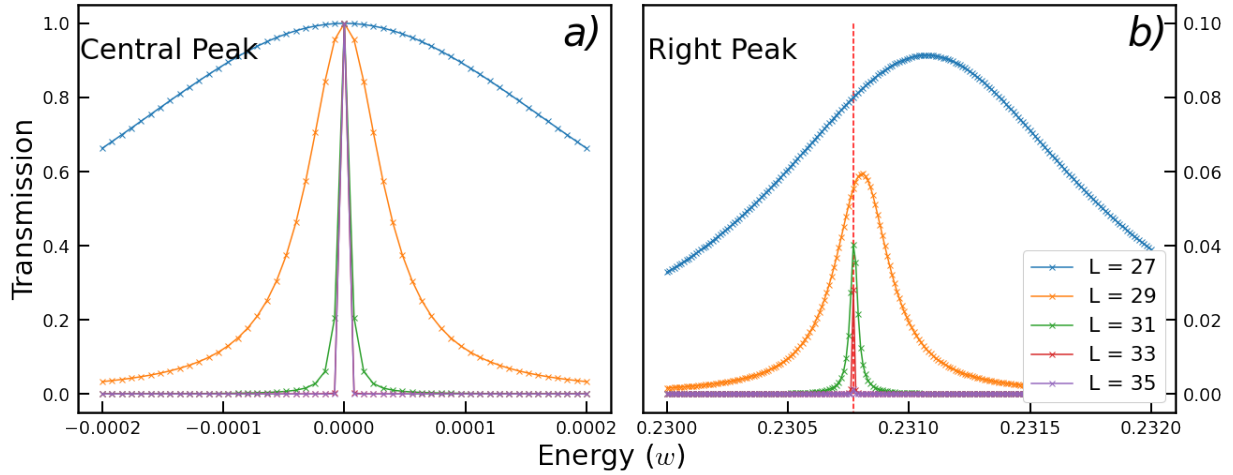
Figure 3.9.: Transmission coefficient curves as function of energy for a 1D chain different sizes centered around for a) zero energy and b) $= E$. While the second peak decreases with the increasing of the size, the central one has transmission one at energy zero for any size.

### 3.3.2. Relating the Lorentzian's Width to Wannier-Stark Half-Life Times

We have vaguely stated in the previous subsection that the width of the Lorentzian peaks may be associated with the characteristic decaying times of the Wannier-Stark states inside the sample. In the following subsection, we will proceed to motivate that claim as well as obtain the scaling of these decaying times with the potential bias as a power law. The purpose for this study is to be able to later characterize the time of the transient regimes of the current.

#### 3.3.2.1. Analytical Expression for Decaying Times with First Order Perturbation Theory

For this subsection, we will be working with the self-energy introduced by the leads in the central sample's Green function. For the derivation of this self-energy, the reader is urged to the appendix B.6. From now on, we will be denoting operators which are solely written in the central sample's Wannier basis as bold.

As we previously noted, the decay of BOs with time is inextricably linked to the fact that, if $w_l$ is allowed to exceed $\Delta V/4$, the central sample has a finite transmission. Therefore, our theory starts off from a study of the central sample's quantum transmittance, $T(\varepsilon)$, in the strong bias regime. As first shown by Caroli *et al.* [29], this quantity can be expressed using a Green's functions formalism, as follows:

$$T(\varepsilon) = \text{Tr}\left[\mathbf{G}_{CC}^{\dagger}(\varepsilon)\mathbf{\Gamma}_R(\varepsilon)\mathbf{G}_{CC}(\varepsilon)\mathbf{\Gamma}_L(\varepsilon)\right], \tag{3.12}$$

where $\mathrm{Tr}\left[\cdots\right]$ is a trace over the central sample's Hilbert space, $\mathbf{\Gamma}_\alpha(\varepsilon) = -2\mathrm{Im}\mathbf{\Sigma}_\alpha$ is the level-width function associated with lead $\alpha$, $\mathbf{\Sigma}_\alpha$ is the self-energy of lead $\alpha$ and $\mathbf{G}_{CC}(\varepsilon)$ is the Green function of the central sample connected to the leads. The latter is defined as the solution of

$$[\varepsilon\mathbf{I} - \mathbf{H}_{CC} - \mathbf{\Sigma}_L\left(\varepsilon\right) - \mathbf{\Sigma}_R\left(\varepsilon\right)]\mathbf{G}_{CC}\left(\varepsilon\right) = \mathbf{I}. \tag{3.13}$$

At this point, it is important to remember that the eigenstates of $\mathbf{H}_{CC}$ will be very similar to the exact Wannier-Stark states (as long as they are not to close to the boundaries) and we will henceforth be taking this states to be described by equation 2.66. Let us define $V_\alpha$ as the on-site energy of the corresponding lead $\alpha$. In our particular case, this will be $V_L = -\Delta V/2$ and $V_R = \Delta V/2$. Then, the one dimensional tight binding semi-infinite leads actually have a fairly simple analytical expression for the self-energy in the Wannier basis [58]

$$\mathbf{\Sigma}_\alpha = \begin{cases} \frac{1}{2}\left(\varepsilon - V_\alpha - i\beta_\alpha\right)|n_\alpha\rangle\langle n_\alpha|, & |\varepsilon - V_\alpha| \leq 2w_l \\ \frac{1}{2}\left(\varepsilon - V_\alpha - \mathrm{sgn}\left(\varepsilon - V_\alpha\right)\beta'_\alpha\right)|n_\alpha\rangle\langle n_\alpha|, & |\varepsilon - V_\alpha| > 2w_l \end{cases} \tag{3.14}$$

where $n_\alpha = -\frac{L-1}{2}\left(\frac{L-1}{2}\right)$ for the left (right) lead and

$$\beta_\alpha = \sqrt{4w_l^2 - \left(\varepsilon - V_\alpha\right)^2}, \tag{3.15}$$

$$\beta'_\alpha = \sqrt{\left(\varepsilon - V_\alpha\right)^2 - 4w_l^2}. \tag{3.16}$$

Hence, the level-width functions are, for $|\varepsilon - V_\alpha| \leq 2w_l$,

$$\mathbf{\Gamma}_L(\varepsilon) = \beta_L\left(\varepsilon\right)\left|-\frac{L-1}{2}\right\rangle\left\langle-\frac{L-1}{2}\right|, \tag{3.17}$$

$$\mathbf{\Gamma}_R(\varepsilon) = \beta_R\left(\varepsilon\right)\left|\frac{L-1}{2}\right\rangle\left\langle\frac{L-1}{2}\right|, \tag{3.18}$$

And zero otherwise. From now on, we will define $\mathbf{\Gamma}\left(\varepsilon\right) = \mathbf{\Gamma}_L\left(\varepsilon\right) + \mathbf{\Gamma}_R\left(\varepsilon\right)$. The sample's Green function is written as

$$\mathbf{G}_{CC}(\varepsilon) = (\varepsilon - \mathbf{H}_{CC} - \mathbf{\Sigma})^{-1}, \tag{3.19}$$

with $\mathbf{\Sigma} = \mathbf{\Sigma}_L + \mathbf{\Sigma}_R$. This Green function may be written in its eigenbasis, with the caveat that this matrix is now non-hermitian, meaning the right-eigenstates $\left|\Phi_n^R\right\rangle$ do not necessarily form a complete orthogonal set. We have to therefore consider the left-eigenstates $\left|\Phi_n^L\right\rangle$ as the dual basis for the former set, and now we can write

$$\mathbf{G}_{CC}(\varepsilon) = \sum_n \frac{1}{\varepsilon - \tilde{\varepsilon}_n - i\gamma_n}\left|\Phi_n^R\right\rangle\left\langle\Phi_n^L\right|, \tag{3.20}$$

with $\tilde{\varepsilon}_n = \mathrm{Re}\left\langle\Phi_n^L\right|\mathbf{H}_{CC} + \mathbf{\Sigma}\left|\Phi_n^R\right\rangle$ and $\gamma_n = \frac{1}{2}\left\langle\Phi_n^L\right|\mathbf{\Gamma}\left|\Phi_n^R\right\rangle$. The transmission function is can

thus be written as

$$
\begin{aligned}
T(\varepsilon) =& \beta_L \beta_R \left| \left\langle -\frac{L-1}{2} \left| \mathbf{G}_{CC}(\varepsilon) \right| \frac{L-1}{2} \right\rangle \right|^2 \\
=& \beta_L \beta_R \sum_n \frac{\left\langle -\frac{L-1}{2} \mid \Phi_n^R \right\rangle^2 \left\langle \Phi_n^L \mid \frac{L-1}{2} \right\rangle^2}{(\varepsilon - \tilde{\varepsilon}_n)^2 + \gamma_n^2} \\
&+ \beta_L \beta_R \sum_{\substack{n \\ m \neq n}} \frac{\left\langle -\frac{L-1}{2} \mid \Phi_n^R \right\rangle \left\langle \Phi_n^L \mid \frac{L-1}{2} \right\rangle}{\varepsilon - \tilde{\varepsilon}_n - i\gamma_n} \times \frac{\left\langle -\frac{L-1}{2} \mid \Phi_m^R \right\rangle \left\langle \Phi_m^L \mid \frac{L-1}{2} \right\rangle}{\varepsilon - \tilde{\varepsilon}_m + i\gamma_m}
\end{aligned}
\tag{3.21}
$$

After arriving at this exact expression, it is time to make some simplifying assumptions that will allow us to describe our regime of interest: the central Wannier Stark state of the sample is only weakly coupled to the leads. In spectral terms, this essentially means that the quantum transmittance function of the sample is made up of a set of sharp lorentzian-shaped peaks centered at around the exact Wannier-Stark energies. To describe this *weak coupling limit*, we must make two assumptions about the spectrum of the effective Hamiltonian:

1. The broadenings vary slowly across the spectrum around each peak, *i.e.*, $\gamma_n(\varepsilon) \simeq \gamma_n(\tilde{\varepsilon}_n)$,

2. These peaks are sufficiently far apart so that they do not overlap significantly, that is $\tilde{\varepsilon}_n - \tilde{\varepsilon}_m \geq \gamma_n$ for every $n \neq m$.

These two conditions guarantee that, for any value of $\varepsilon$, at least one of the factors in each term of the double summation is close to zero. Hence, the quantum transmittance is approximately given by a sum of lorentzian peaks (resonances), of the form

$$
T(\varepsilon) \simeq \beta_L(\varepsilon) \beta_R(\varepsilon) \sum_n \frac{\left\langle -\frac{L-1}{2} \mid \Phi_n^R \right\rangle^2 \left\langle \Phi_n^L \mid \frac{L-1}{2} \right\rangle^2}{(\varepsilon - \tilde{\varepsilon}_n)^2 + \gamma_n^2},
\tag{3.22}
$$

resulting in $\gamma_n$ being the Half Width at Half Maximum (HWHM) of the Lorentzian peaks. Note that this approximation does not require the leads' bandwidth to be much larger than that of the sample, as in the Wide Band Limit. It merely requires that each individual peaks' width is small enough to allow us to ignore the variation of $\gamma_n$ for each Lorentzian. As we shall see, this coefficients can be made arbitrarily small with the increasing of $\Delta V$.

The second approximation is based on the intuition that each lorentzian peak and width should approximately describe the energy and the decaying time of a Wannier-Stark state. This assumption entails that for every Wannier-Stark state $|\Psi_n\rangle$ there exists an eigenstate $|\Phi_n^R\rangle$ such that $\langle \Psi_m \mid \Phi_n^R \rangle \simeq C_n \delta_{mn}$, with $C_n$ being a complex number. This in turn allows

the Green function to be expandable in the Wannier-Stark basis as

$$\mathbf{G}_{CC}(\varepsilon) \simeq \sum_n \frac{\left\langle \Psi_n \mid \Phi_n^R \right\rangle \left\langle \Phi_n^L \mid \Psi_n \right\rangle}{\varepsilon - \varepsilon_n - \Delta_n - i\gamma_n} \left| \Psi_n \right\rangle \left\langle \Psi_n \right|, \tag{3.23}$$

with $\Delta_n$ being a small correction to the Wannier-Stark energy coming from $\Delta_n = \mathrm{Re} \left\langle \Phi_n^L \right| \mathbf{\Sigma} \left| \Phi_n^R \right\rangle$ . On the other hand, a straight-forward connection of these HWHM may be obtained by Fourier transforming the sample's Green function $\mathbf{G}_{CC}$, which entails

$$\mathbf{G}_{CC}(t > 0) \simeq \sum_n \mathcal{A}_n e^{-i(\varepsilon_n - \Delta_n)t/\hbar} e^{-\gamma_n t/\hbar} \left| \Psi_n \right\rangle \left\langle \Psi_n \right| \quad, \tag{3.24}$$

with $\mathcal{A}_n = \left\langle \Psi_n \mid \Phi_n^R \right\rangle \left\langle \Phi_n^L \mid \Psi_n \right\rangle$. This means that each $\gamma_n$ should describe the decaying rate of each Wannier Stark state $\left| \Psi_n \right\rangle$ inside the sample, i.e, it should describe the rate at which the corresponding Wannier-Stark state escapes the sample through the leads. To see that this is indeed the correct interpretation, we use the KPM time-evolution algorithm with the entire system (sample and the leads) described by the total Hamiltonian $H$ defined in equation 3.1. The initial state $\left| \bar{\Psi}_0 \right\rangle$ is then defined as a Wannier-Stark state inside the samples and zero in the leads. In other words:

$$\left\langle n \mid \bar{\Psi}_0 \right\rangle \equiv \begin{cases} J_n \left( 2w/eEa \right) \left| n \right\rangle, & |n| \leq (L-1)/2 \\ 0 & |n| > (L-1)/2 \end{cases} \tag{3.25}$$

and we calculate the time evolution of such state projected onto this same state, i.e,

$$\mathbf{G}_{00}(t) = \left\langle \bar{\Psi}_0 \right| e^{-iHt/\hbar} \left| \bar{\Psi}_0 \right\rangle. \tag{3.26}$$

The results confirm this time evolution's exponential decay with a characteristic time given by $\tau_0 = \hbar/\gamma_0$, with $\gamma_0$ being the HWHM coefficient obtained from the central Lorentzian in the transmission function, as shown in figures 3.10 a), b) and c). This in turn confirms that the Wannier-Stark state inside the sample escapes the sample with a rate described by $\gamma_0$. Furthermore, by Fourier transforming this function for long times originates a lorentzian with the width given by $\gamma_0$, as expected (3.10.d)).

We then sought to describe how this decaying times scale with the parameters of the system $\Delta V$, $L$ and $w_l$. An initial attempt to describe this would be to use first order perturbation theory to obtain the complex shift of the matrix $\mathbf{\Gamma}$ in the sample's Hamiltonian spectrum, which would yield

$$\left\langle \Phi_n^L \right| \mathbf{\Gamma} \left| \Phi_n^R \right\rangle \simeq \left\langle \Psi_n \right| \mathbf{\Gamma} \left| \Psi_n \right\rangle. \tag{3.27}$$

Unfortunately, we need not even finish the computation to see why this would ultimately
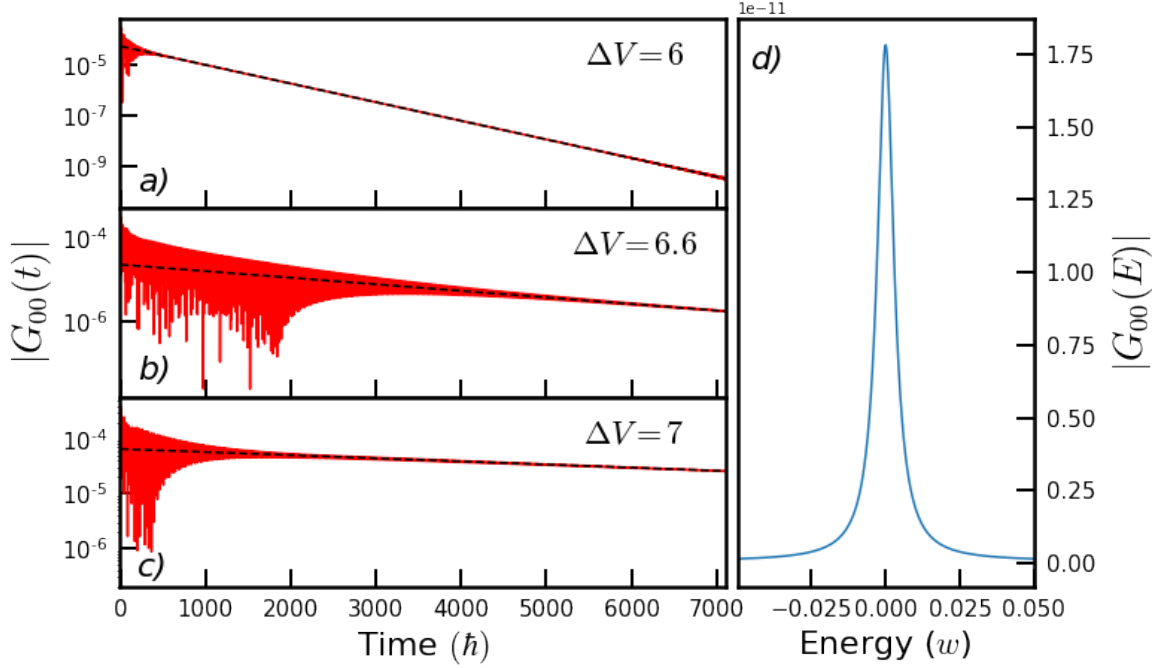
Figure 3.10.: a), b) and c) - $\mathbf{G}_{00}(t)$ evolution with time for different $\Delta V$ (in units of $w$) with a logarithmic scale in the y axis for a system of size $L = 25a$. The black dashed line is the exponential function $e^{-t/\tau_0}$ with $\tau_0$ being the characteristic decaying time for the corresponding system. d) - Fourier transform of $\mathbf{G}_{00}(t)$ for $\Delta V = 6w$, which originates a Lorentzian with width $\hbar/\tau_0$.

fail: In the RHS of the equation above, since $|\Psi_n\rangle$ has no dependence on $w_l$ whatsoever, the originated width from this computation would depend on $w_l$ as $\beta_\alpha(\varepsilon) = \sqrt{4w_l^2 - (\varepsilon - V_\alpha)^2}$, which increases with $w_l$. However, it is clear from figure 3.7 that the width should actually decrease with $w_l$. This discrepant behavior on the leads' hopping parameter is encoded in $|\Phi_n^L\rangle$ and $\langle\Phi_n^R|$ themselves, which have their tips in the spatial basis to be very dependent on the $\mathbf{\Gamma}$ matrix. Ergo, such strong dependence on $w_l$ cannot be mimicked by first order perturbation theory, or for any practical finite order for that matter. We may, however, circumvent this by assuming that the contribution of $|\Psi_n\rangle$ for the width's dependence on $\Delta V$ and $L$ should be the strongest out of all the states, and therefore we make the educated guess

$$\langle\Phi_n^L|\,\mathbf{\Gamma}\,|\Phi_n^R\rangle \simeq h_n(w_l, \Delta V, L)\,\langle\Psi_n|\,\mathbf{\Gamma}\,|\Psi_n\rangle, \tag{3.28}$$

where $h_n(w_l, \Delta V, L)$ are slow varying functions on $\Delta V$ and $L$ compared to $\langle\Psi_n|\,\Gamma\,|\Psi_n\rangle$ but may have a strong dependence on $w_l$. The scalar product of the WS-states with the level-width

function can be promptly calculated by using equation 2.66 and the symmetry property 2.68

$$\langle\Psi_n|\,\mathbf{\Gamma}\,|\Psi_n\rangle = (\beta_L\,(\tilde{\varepsilon}_n) + \beta_R\,(\tilde{\varepsilon}_n))\left(J^2_{\frac{L-1}{2}+n}\left(\frac{2w}{\Delta V}\,(L+1)\right) + J^2_{\frac{L-1}{2}-n}\left(\frac{2w}{\Delta V}\,(L+1)\right)\right)\,.$$

(3.29)

To get the asymptotic value of such function for stronger potential biases, it will be useful to express the Bessel functions of the first kind $J_\nu(z)$ in the limit $|\nu| > z$, which is [50]

$$J_\nu(z) \sim \frac{1}{\sqrt{2\pi\nu}}\left(\frac{\mathrm{e}z}{2\nu}\right)^\nu$$

(3.30)

With this, we obtain, if the state is well localized within the sample,

$$\langle\Psi_n|\,\mathbf{\Gamma}\,|\Psi_n\rangle \simeq (\beta_L\,(\tilde{\varepsilon}_n) + \beta_R\,(\tilde{\varepsilon}_n))\frac{1}{\pi}\left[\frac{1}{L-1+2n}\left(\frac{\mathrm{e}\frac{2w}{\Delta V}\,(L+1)}{L-1+2n}\right)^{L-1+2n}\right.$$
$$\left. + \frac{1}{L-1-2n}\left(\frac{\mathrm{e}\frac{2w}{\Delta V}\,(L+1)}{L-1-2n}\right)^{L-1-2n}\right].$$

(3.31)

We are now in place to calculate the coefficients $\gamma_0$, $\gamma_1$ and $\gamma_{-1}$ given by equation 3.28 for the central-most Wannier-stark states, $|\Psi_0\rangle$, $|\Psi_{-1}\rangle$ and $|\Psi_1\rangle$. These coefficients will of particular importance for the characterization of the transient time of the current in the next subsection. Firstly, for $|\Psi_0\rangle$ we have (for $\frac{L-1}{2} \gg \frac{2w}{dV}\,(L+1)$, which in this case is the same limit as the BO's existence condition $\Delta V \gg 4w$),

$$\langle\Psi_0|\,\mathbf{\Gamma}\,|\Psi_0\rangle \sim \frac{4\beta}{\pi\,(L-1)}\left(\frac{2we\,(L+1)}{\Delta V\,(L-1)}\right)^{L-1},$$

(3.32)

where $\beta \equiv \beta_L\,(0) = \beta_R\,(0) = \sqrt{4w_l^2 - \Delta V^2/4}$. One can then study the $h_0$ function numerically and obtain that $h_0\,(\alpha\Delta V, \Delta V, L) = C\,(\alpha)$, meaning that $h_0\,(w_l/\Delta V)$ will be solely a function of $w_l/\Delta V$. By plotting $h_0$ as a function of $w_l/\Delta V$ for different values of $\Delta V$ (Fig. 3.11 a)), one can actually conclude that

$$h_0\,(w_l/\Delta V) = A_0\left(\frac{w_l}{\Delta V}\right)^{-\nu},$$

(3.33)

where $\nu \simeq 2$. A small dependence of the amplitude coefficient $A$ on $\Delta V$ can be observed, but this will ultimately be negligible when compared to the power law dependence of the other term obtained in equation 3.32, and thus the amplitude assumes the value of $A \simeq 0.1514712$. Combining equations 3.32 and 3.33, one can then rebuild an expression for the decaying time

$\tau_0 = \frac{\hbar}{\gamma_0}$ as

$$\tau_0 \simeq \frac{2\hbar}{A_0} w_l^2 \frac{\pi (L-1) \left( \frac{(L-1)}{2we(L+1)} \right)^{L-1}}{\sqrt{\left( \frac{4w_l}{\Delta V} \right)^2 - 1}} (\Delta V)^{L-4}, \tag{3.34}$$

which for high enough $\Delta V$, scales with the potential bias as a power law of $L-4$. The validity of such analytical result is confirmed numerically by plotting this expression against the the HWHM of the central Lorentzian of the transmission function for various potential biases and system sizes, showing a good correspondence (Fig. 3.11.b)).
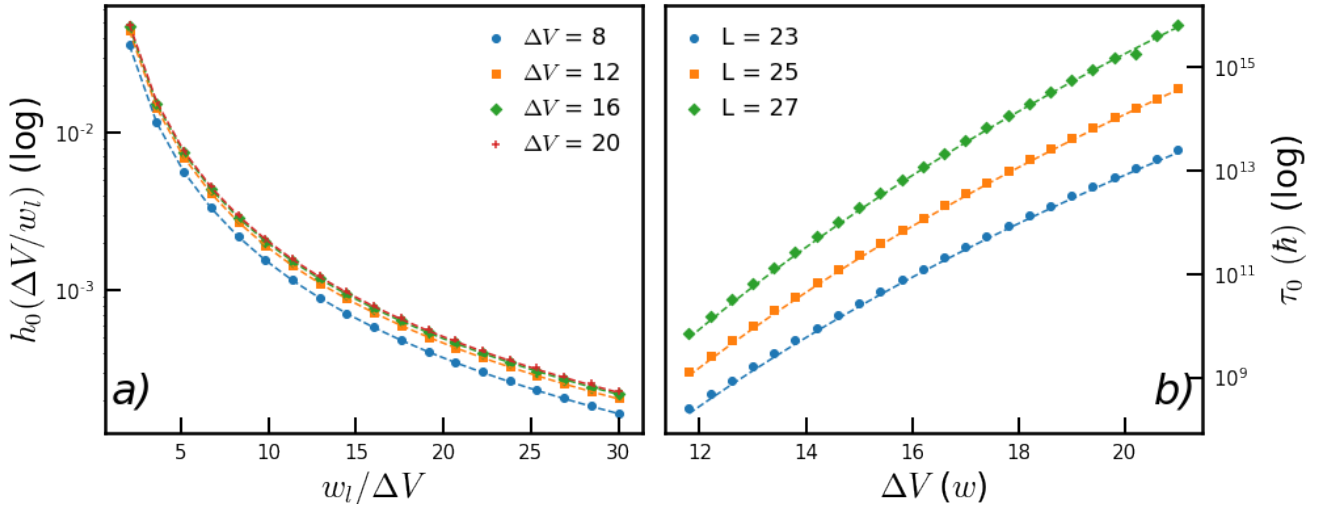


Figure 3.11.: a) - $h_0(\alpha)$ as a function of $w_l/\Delta V$ with $w_l = \alpha \Delta V$ for different values of $\Delta V$, with the dashed lines being curve fits of the form given in equation 3.33. b) - Inverted central Lorentzian's HWHM coefficients from the transmission functions (points) against the inverse of the analytical expression obtained via perturbation theory (dashed lines) as a function of $\Delta V$ for various system sizes, with $w_l = 2\Delta V$ and a system of size $L = 25a$.

Furthermore, it is now seen in this figure that $\tau_0$ varies over 6 orders of magnitude with $\Delta V$ spanning from 11.8 to 22, which completely annihilates the dependence of the amplitude coefficient $A$ on the potential bias seen in figure 3.11.a). Finally, the obtainance of larger times is capped only by machine error (which is of order of $10^{-16}$), making it impossible to probe for higher potential biases.

Analogously, we can calculate the decaying time of the Wannier-Stark states $|\Psi_{-1}\rangle$ and $|\Psi_1\rangle$.

Equation 3.29 for these states then yields a slightly more cumbersome expression:

$$
\begin{aligned}
\langle \Psi_1 | \, \boldsymbol{\Gamma} \, | \Psi_1 \rangle &= \langle \Psi_{-1} | \, \boldsymbol{\Gamma} \, | \Psi_{-1} \rangle \\
&\simeq \frac{(\beta_L(\varepsilon_1) + \beta_R(\varepsilon_1))}{\pi} \left[ \frac{1}{L+1} \left( e \frac{2w}{\Delta V} \right)^{L+1} + \right. \\
&\left. \qquad\qquad + \frac{1}{L-3} \left( \frac{e \frac{2w}{\Delta V}(L+1)}{L-3} \right)^{L-3} \right].
\end{aligned}
\tag{3.35}
$$

In a similar manner, numerically analyzing the function $h_1(t_l, \Delta V, L)$ originates identical results to the previous function $h_0(t_l, \Delta V, L)$, i.e,

$$
h_1(w_l/\Delta V) \simeq A_1 \left( \frac{w_l}{\Delta V} \right)^{-2},
\tag{3.36}
$$

shown in figure 3.12 a). The main difference from the previous function $h_0$ is that, this time, the explicit dependence on $\Delta V$ is larger, albeit still small when compared to the dependence of equation 3.35 on $\Delta V$. This is, nevertheless, expected, since these states are more strongly coupled to the leads than $|\Psi_0\rangle$, and thus the approximation is valid for higher values of $\Delta V$. $\tau_1$ is then obtained as

$$
\begin{aligned}
\frac{2\hbar}{\tau_1} &\simeq A_1 \left( \frac{w_l}{\Delta V} \right)^{-2} (\beta_L(\varepsilon_1) + \beta_R(\varepsilon_1)) \frac{1}{\pi} \left[ \frac{1}{L+1} \left( e \frac{2w}{\Delta V} \right)^{L+1} \right. \\
&\left. \qquad\qquad + \frac{1}{L-3} \left( \frac{e \frac{2w}{\Delta V}(L+1)}{L-3} \right)^{L-3} \right].
\end{aligned}
\tag{3.37}
$$

And thus $\tau_1$ scales with $\Delta V$, for large enough $L$, as

$$
\tau_1 \simeq \frac{1}{A_1} \frac{w_l^2 4\hbar\pi(L-3) \left( \frac{L-3}{2we(L+1)} \right)^{L-3}}{\sqrt{\left( \frac{4w_l}{\Delta V} \right)^2 - 1}} (\Delta V)^{L-7}
$$

The comparison of such times with those obtained from the Lorentzian peaks are, now for the state $|\Psi_1\rangle$, represented in figure 3.12 b), showing a good correspondence once again.
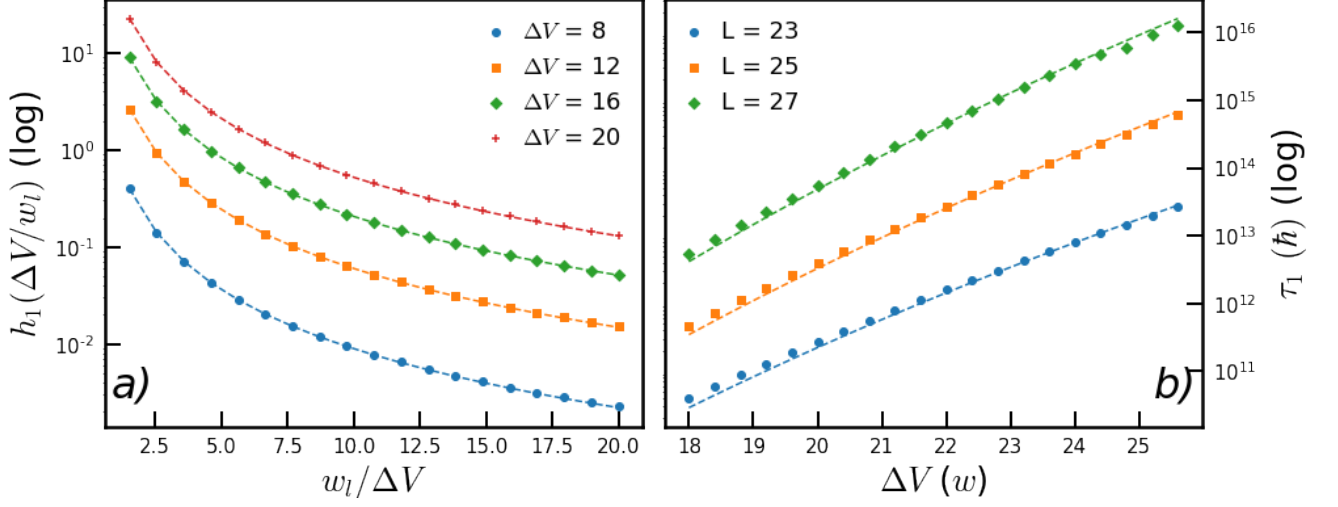
Figure 3.12.: a) - $h_1(\alpha)$ as a function of $w_l/\Delta V$ with $w_l = \alpha \Delta V$ for different values of $\Delta V$, with the dashed lines being curve fits of the form given in equation 3.36. b) - Inverted central Lorentzian's HWHM coefficients for the peak centered around $\varepsilon = aeE$ (points) against the inverse of the analytical expression obtained via perturbation theory (dashed lines) as a function of $\Delta V$ for various system sizes, with $w_l = 2\Delta V$ and a system of size $L = 25$.

### 3.3.3. Transient BO's in the Current

We now have everything we need to characterize the transient regime of the central average current evolution for $\Delta V > 4w$ and a proper choice of $w_l$ that mitigates the bound states inside the sample. We may use the sample's Green function $\mathbf{G}_{CC}(t)$ to obtain the contribution to the average current evolution through a specific bond from the states that are escaping the sample. It is worth to notice that this quantity cannot account for incoming states from the leads, and therefore will not describe the constant asymptotic Landauer prediction for the current $j(t \to +\infty)$. To this specific current we will call the *transient current*, and define it as $j_n^{Trans}(t) \equiv j_n(t) - j(t \to +\infty)$, where $j_n(t)$ is the average current evolution if we were accounting for incoming states of the leads. Such current can then be expressed as

$$j_n^{Trans}(t) = \text{Tr}\left[f(\mathbf{H}_{CC}^0)\mathbf{G}_{CC}(t)\hat{J}_n\mathbf{G}_{CC}^{\dagger}(t)\right], \tag{3.38}$$

where $\mathbf{H}_{CC}^0$ is the unperturbed Hamiltonian and $f(\mathbf{H}_{CC}^0)$ is the Fermi-Dirac distribution of the initially thermalized state

$$f(\mathbf{H}_{CC}^0) = \sum_k \frac{1}{e^{-\beta(\varepsilon_k - \mu)} + 1}|\psi_k\rangle\langle\psi_k|, \tag{3.39}$$

where $|\psi_k\rangle$ is the initial eigenbasis of $\mathbf{H}^0_{CC}$. Using the Wannier-Stark basis to perform the trace, this function will be responsible for the mixing of the different components of the two Green functions, coupling different exponentials with different decaying times. Assuming that the Wannier-Stark energies $\varepsilon_n$ are much larger than the energetic shift introduced by the leads $\tilde{\varepsilon}_n$ (which is a valid assumption for sufficiently large $\Delta V$), the transient current can thus be written as

$$j_n^{Trans}(t) \sim \sum_{nm} A_{nm} e^{-i(\varepsilon_n - \varepsilon_m)t} e^{-(1/\tau_n + 1/\tau_m)t}. \tag{3.40}$$

The dominating decaying time scale should therefore be $\tau_0/2$., since the central Wannier-Stark state is the least coupled to the leads. However, one should remember that Wannier-Stark states are real states, meaning the states themselves do not carry any current, i.e, $\langle \Psi_n | \hat{J}_n | \Psi_n \rangle = 0$. This leads to

$$A_{nn} = \langle \Psi_n | f\left(H^0_{CC}\right) | \Psi_n \rangle \langle \Psi_n | \hat{J}_n | \Psi_n \rangle = 0, \tag{3.41}$$

Therefore, we could never see a decayment of $\tau_0/2$ in the current, and the largest non-zero decaying time scale is given by $(1/\tau_0 + 1/\tau_1)^{-1} = \tau_0\tau_1/(\tau_0 + \tau_1)$.

By plotting the average central current time evolution for different potential biases with an appropriate choice of the leads' hopping parameter (in this case, $w_l = (1/4 + 1/16)\Delta V$), it is clear that Bloch Oscillations cease to be a permanent phenomenon and instead take part as a transient phase, decaying to the corresponding Landauer value (Fig 3.13.a)).
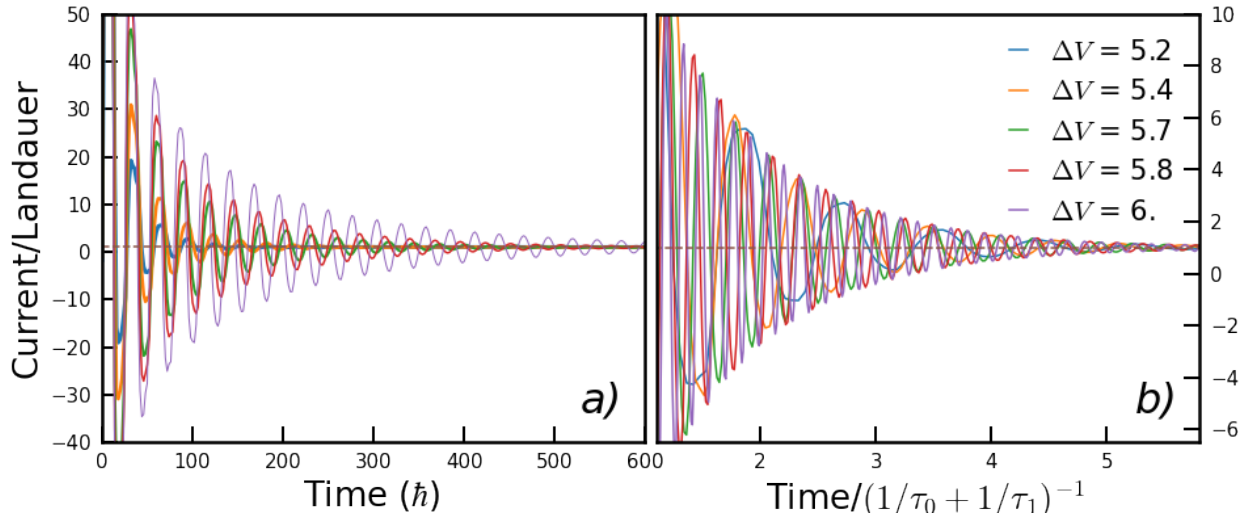


Figure 3.13.: a) Average current evolution divided by the respective Landauer value for different potential biases (in units of $w$) for a sample of size $L = 25a$. b) Same current evolutions with time scaled by the inverse of HWHM coefficients and amplitudes adjusted. The dashed brown line denotes Current/Landauer = 1.

Furthermore, by scaling the time by the respective $\tau_0\tau_1/(\tau_0 + \tau_1)$ value, it is possible to obtain a similar decaying behavior across the different curves (Fig 3.13.b)). It is to be noted that the BO's should not be expected to collapse to the same curve, because their frequency depends only on $\Delta V$ while the decaying time depends on both $\Delta V$ and $w_l$.
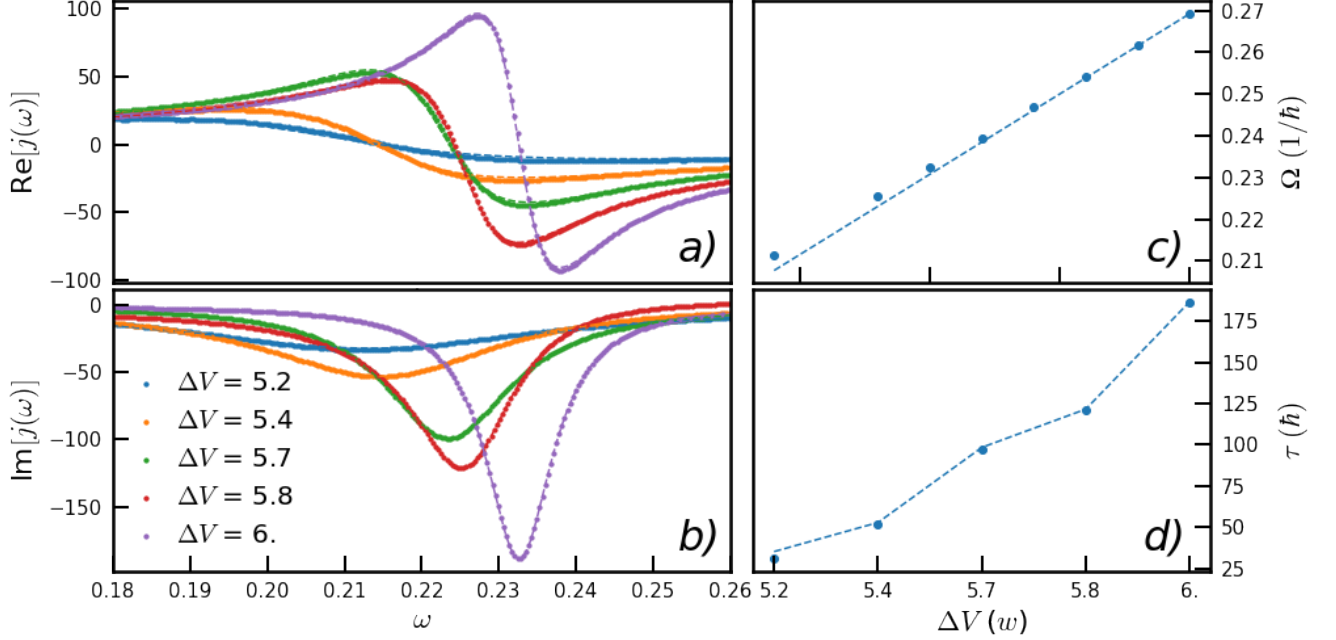


Figure 3.14.: a) Real and b) complex part of the Fourier transform of the current for different potential biases (in units of $w$) for a system of size $L = 25a$. The dashed lines are the corresponding fits of the functions in equations 3.43 and 3.44. c) $\Omega$ values obtain from the fit for different $\Delta V$ (blue points) compared to the BO's frequency for the corresponding $\Delta V$ (dashed blue line). d) $\tau$ values obtain from the fit for different $\Delta V$ (blue points) compared to the corresponding values of $\tau_0\tau_1/(\tau_0 + \tau_1)$ (dashed blue lines).

We would still like to further instill the notion that the observed oscillations are in fact Bloch Oscillations decaying exponentially and $\tau_0\tau_1/(\tau_0 + \tau_1)$ is indeed the dominating time scale of such decayment. If this is true, then for large times the average current should be a sinusoidal function with the frequency of the BO's modulated by an exponential, i.e.,

$$j_n(t \gg 0) \simeq A\cos(\Omega t + \phi)\,e^{-t/\tau} + j(t \to +\infty). \tag{3.42}$$

We can then remove the Landauer value from the current and try to fit such function to the current curves. Unfortunately, sinusoidal functions are known to be prone to many fitting

errors because of their periodic nature. A more sophisticated analysis may then be put forward by Fourier transforming the signal. It can be shown from a simple calculation that the real and complex components of the Fourier transform of the current are given by

$$\mathrm{Re}\left[j\left(\omega\right)\right] = A\tau \frac{\cos\phi + \tau\sin\phi\left(\omega - \Omega\right)}{1 + \tau^2\left(\omega - \Omega\right)^2} \tag{3.43}$$

$$\mathrm{Im}\left[j\left(\omega\right)\right] = A\tau \frac{\sin\phi - \tau\cos\phi\left(\omega - \Omega\right)}{1 + \tau^2\left(\omega - \Omega\right)^2}. \tag{3.44}$$

The result of fitting this expressions to the Fourier transform is shown in figure 3.14, where it is seen that the fits are actually quite good and increase for stronger potential biases.

From this fits, $\Omega$ may be extracted and compared to the BO's frequency $2\pi/T_{BO}$. As seen in figure 3.14 c), such $\Omega$'s are in accordance with the BO's frequency, allowing us to identify this oscillations as such.The $\tau$ coefficient may also be extracted, with it corresponding to the respective values of $\tau_0\tau_1/\left(\tau_0 + \tau_1\right)$ (Fig. 3.14 c)).

To see this more clearly, we plot the transient current for $\Delta V = 6.2w$ and the corresponding exponential enveloping function $\exp\left[-\left(1/\tau_0 + 1/\tau_1\right)t\right]$ in figure 3.15. In this figure, it is easily seen that such exponential function describes the decay of the transient current extremely well.
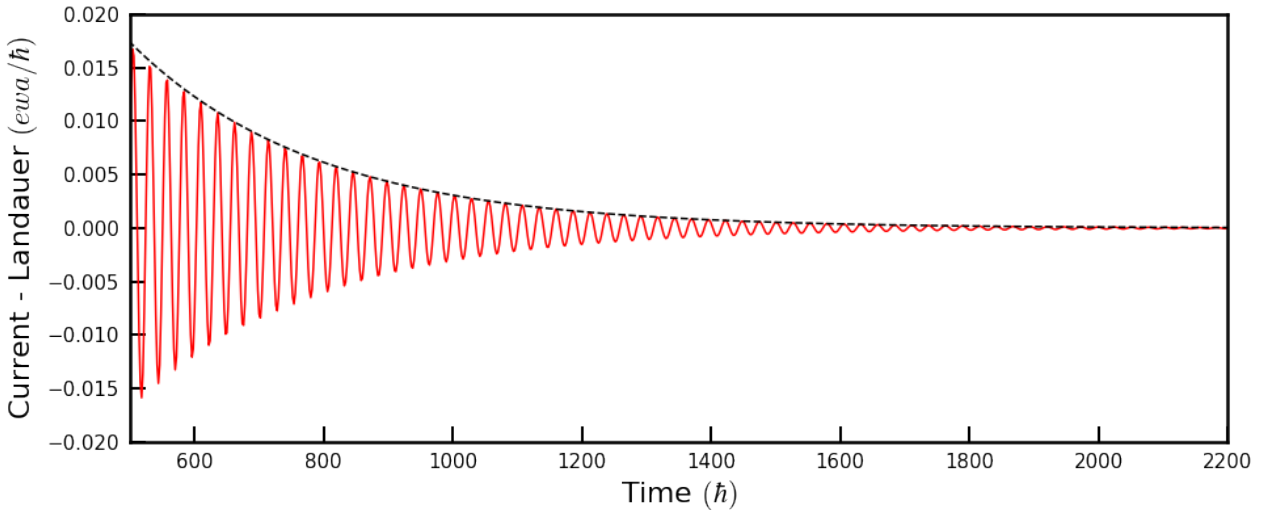


Figure 3.15.: Time evolution of the average current minus the Landauer prediction through the central bond of a sample of size $L = 25a$ with $\Delta V = 6.2w$ and $t_l = \left(1/4 + 1/16\right)\Delta V$. The envelope function $\exp\left[-\left(1/\tau_0 + 1/\tau_1\right)t\right]$ is represented with the dashed black curve, showing a perfect correspondence with the decaying of the transient current.

### 3.3.4. Phase Identification

As a compact way to summarize the results, we have constructed a phase diagram depicting the different states of the transport phenomenon.
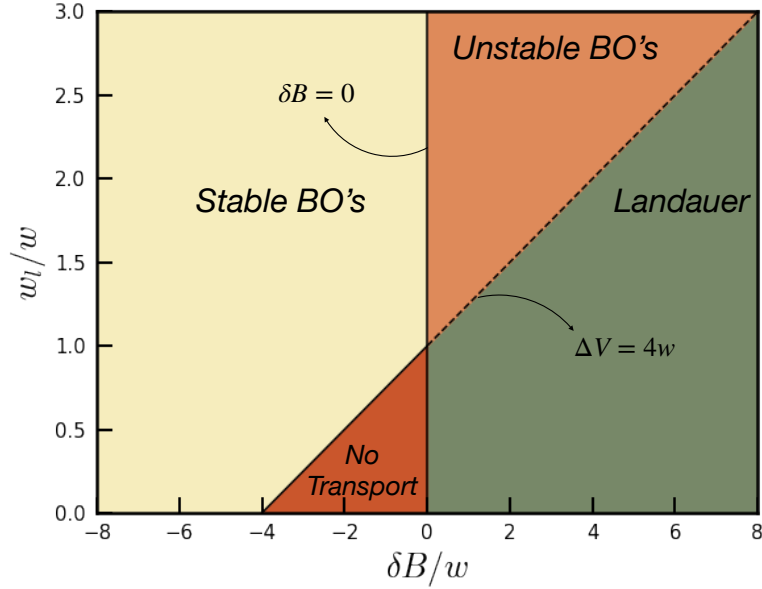


Figure 3.16.: Phase diagram in terms of the leads' hopping and lead overlap.

In this diagram, four different phases are then identifiable. "Stable" and "Unstable BO's" refer to Bloch Oscillations which occur infinitely or as a transient phenomenon respectively, whereas "Landauer" is a regime where no BO's are to be detected, i.e, all Wannier-Stark states are completely delocalized from the sample, and we get a constant current response instead. Finally, The "No Transport" phase refers to the phase where there is no overlap between leads and no Wannier-Stark states localized inside the sample. In this phase, because we still have bound states, we will have infinite oscillations in the current, but they will not correspond to BO's, since there is no Wannier-Stark state inside the sample. The diagram is drawn in terms of $w_l/w$ and $\delta B/w$, where $\delta B$ is the total overlap between the leads' bands, given by

$$\delta B = -\Delta V + 4w_l \tag{3.45}$$

The dashed line between the "Unstable BO's" and the "Landauer" phases denotes a continuous cross-over rather than a phase transition.

## 3.4. Disordered Samples

With this extensive characterization of the clean case performed, we are free to move on to the effect of disorder in a one-dimensional two-terminal mesoscopic device and, in particular,

its effect on the originated Bloch Oscillations and on the Landauer current. Because disorder is known for localizing states, we sought to see the effect of disorder on the already localized Wannier-Stark states, which should be telling on the dependency of the inter-lead current on the disorder parameter. Hence, it is absolutely instructive to explore the interplay between these two length scales.

### 3.4.1. State's Localization with Disorder

Firstly, let us discuss what happens to the Wannier Stark states of a one dimensional chain with an electric field when we introduce Anderson disorder with strength $W$. What we find by plotting the eigenstates of said system is that, up to a certain value of $W$, the disorder does not alter the extent of the Wannier-Stark states, i.e, their Wannier-Stark localization lengths (Figs. 3.17 a), b) and c)). At some point with the increasing $W$, the disorder will dominate the Hamiltonian's diagonal, which translates in the effect from the potential ramp becoming negligible. In this limit, the localization of the eigenstate will be dictated by disorder, which gets smaller with the increase of $W$ [2,16] (Fig.3.17 d)). This is the limit where the interference effects have a strong role in the localization of the eigenstates.
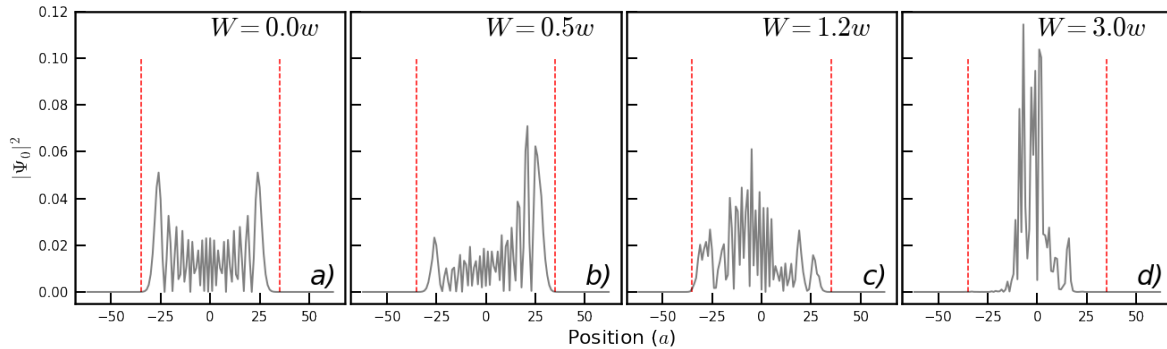


Figure 3.17.: Eigenstates of a 1D chain of length $L = 125a$ with potential bias of $\Delta V = 9w$ for disorder strengths of a) $W = 0$, b) $W = 0.5w$, c) $W = 1.2w$ and d) $W = 3w$. The red dashed lines delimit the space interval from $-35a$ to $35a$. As can be seen, this interval roughly corresponds to the length where the eigenstate is non-zero for a), b) and c), but it is much larger than the corresponding length for the state in figure $d$). This should happen for a sufficiently strong disorder, where the dominance of the disordered potential makes the eigenstates localized in a length scale that is in accordance to the Anderson theory for localization.

There are, therefore, two different regimes: The one where interference effects are negligible, and the localization of the states remains described by the Wannier-Stark localization length and unaltered by disorder, and the one where interference is important, where the localization of the eigenstates is dictated by disorder and therefore diminishes with the disorder strength.

Figure 3.18.: Time evolution of a Gaussian wave-packet of variance $\sigma = 20a$ initially centered at $\bar{l}_0 = 1000a$ in a one-dimensional tight-binding chain of size $L = 2000$ with $E = 0.01w/ea$ and a) a single impurity added to site $750a$ with on-site energy $1w$ (the blue dashed line denotes the impurity position) b) Anderson disorder with a disorder parameter $W = 0.5w$.

The crossover between these two different regimes therefore occurs when the Anderson localization length becomes of the same order of magnitude as the Wannier-stark localization length.

The fact that, in the former regime, the eigenstates remain with the same localization may actually be viewed semi-classically. We now evoke our intuition built on sections 2.3 for the evolution of Gaussian wave-packets in 1D lattices subject to an electric field to develop the following line of reason: In a 1D clean chain, a gaussian wave-packet will realize sinusoidal oscillations and confine itself to a region of space given by the Wannier-Stark localization length, $2w/E$. By introducing an impurity in its path, the conservation of energy allows merely two possibilities for the scattering of the electron - forward scattering and backscattering - both of which preserve the modulus of the momentum, $k$. The forward scattering will obviously maintain the dynamics of the Gaussian wave-packet, not leading to any change in the region of confinement. The backscattering is less obvious, but one can determine its effect by noting that the dynamics generated at a given point with velocity of $v$ or $-v$ are the same apart from a phase factor in its space-time diagram (Fig 3.18 a)). Thus, in 1D, the introduction of an impurity wont change the confinement region of the oscillation.

### 3.4.2. Numeric Results

The main observation to pay attention to is that in the BO's regime, the introduction of disorder kills off the oscillations to zero, as seen in figure 3.19. In the left panel of this figure, it is worth noticing that, although the disorder localization length is larger than the sample, the oscillations still decay to zero. To explain this effect, we need to keep in mind that BO's are a coherent dynamical phenomenon between the states, and the scattering provided by this disorder strength is sufficient to dephase the oscillations, killing them to zero [59].
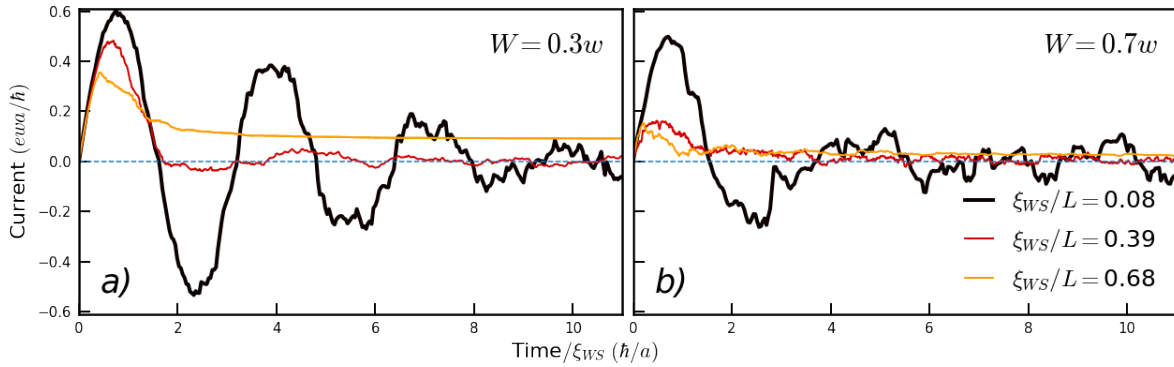
Figure 3.19.: Plots of the current time-evolution measured inside the sample for a sample of size $L = 256a$ and $\Delta V = 0$ with Left - $W = 0.3w$ and Right - $W = 0.7w$, with Anderson localization lengths of $533.13a$ and $97.76a$, respectively, for a single realization of disorder.

As is has been stated, for a proper choice of $w_l$ it is possible to obtain a non-zero asymptotic current predicted by the Landauer formula. We thus plot such asymptotic current as a function of the disorder parameter $W$ in figure 3.20.
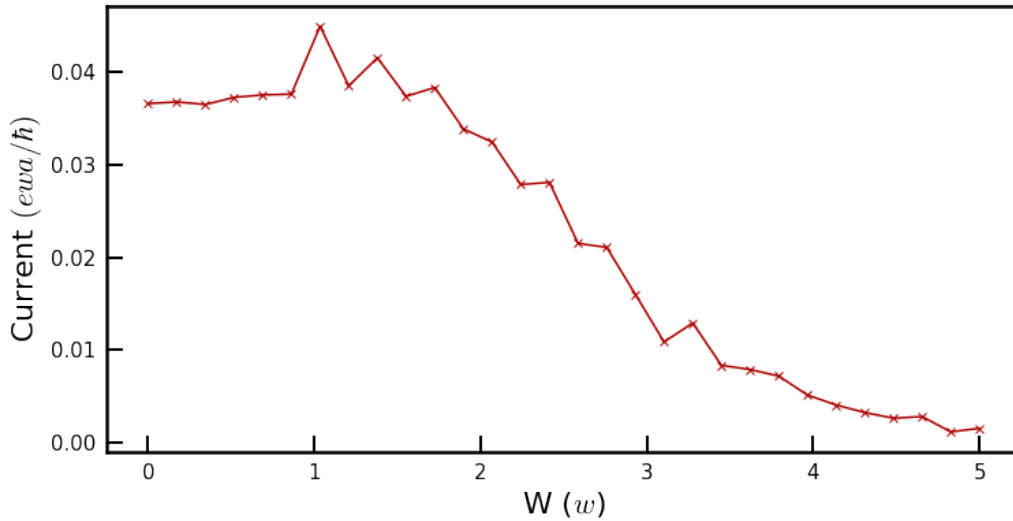


Figure 3.20.: Total Landauer current through the sample as a function of the disorder parameter averaged over 240 different realizations of disorder. Such a large averaging is needed because of the problematic resolution of the thin Wannier-Stark states, originating very big fluctuations at this current's scale. To see how the curve for a single realization of disorder looks like, the reader is referred to Appendix D.1 to figures D.1a and D.1b to see the curves for a single realization of disorder.

We can explain the results in terms of the localization of the eigenstates inside the sample.

In the weak disorder regime, the localization of the eigenstates will be similar to the Wannier-Stark localization length (see figure 3.17 a), b) and c)), and therefore the current should not get meaningfully altered, which explains the fairly constant regime of the plot up to $W \simeq 1w$. For strong enough disorder, however, the eigenstates will start to localize even further (figure 3.17 d)), which will lead to a decay of the current. Notice that the current is already extremely small, which will be worthy, as for this entire result in general, to keep in mind when we compare it to the 2D case.

# 4. Bloch Oscillations in Two-Dimensional Two-Terminal Mesoscopic Devices

As the title reveals, this chapter aims to study BO's in two-dimensional two terminal meso-scopic devices. The model will be similar to the previous case, with the difference that now the sample and the leads will be two-dimensional square lattices with a specific width (figure 4.1).
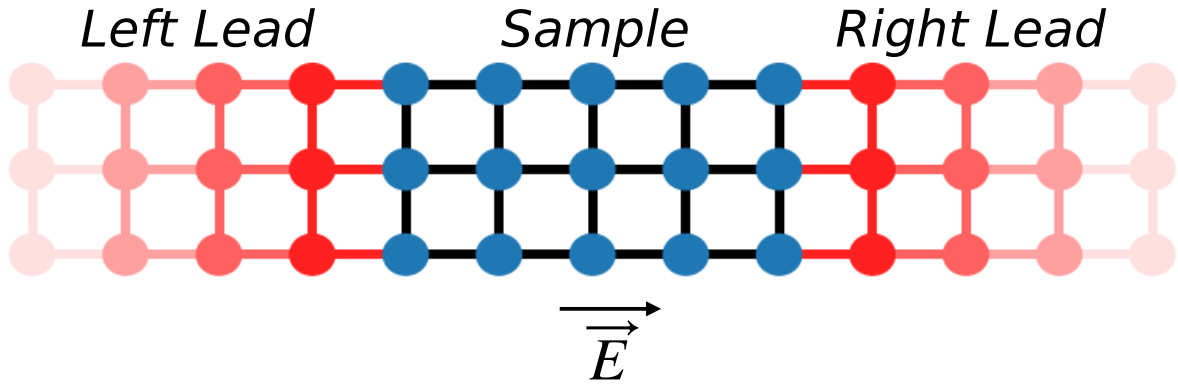


Figure 4.1.: Depiction of the model for the 2D case, where both the leads and the sample are a square lattice with the same width, where the electric field is non-zero only in the sample.

The two-dimensional clean sample will display the same behaviors as in the 1D case, with the difference being that the bandwidths of the leads are now different and dependent on the system's width, thus changing the condition for BO's existence and for the mitigation of the bound states. Regardless, we would still be studying infinite and transient BO's, which have already been studied in the previous chapter. This chapter will therefore be solely focused in studying the disordered case, which is where the interesting physics lies, and we will be doing this by studying the effect of disorder in the localization of the states and on the coupling of the conduction channels, which will pose much more interesting results than in the one-dimensional disordered sample.

## 4.1. State Localization with Disorder: An interesting Twist!

We will start by noticing something interesting: diagonalizing the Hamiltonian of a clean sample, we get states that are Wannier Stark states in the x direction and propagating states in the y direction as expected, since the problem is separable in both this axis. Plotting a density plot of such states in space reveals that they are indeed localized in the x direction with the usual Wannier Stark localization length. However, introducing disorder in the system actually has the opposite effect of the usual: it delocalizes the states, leading them to have a larger localization length. One can then hypothesize that for a certain disorder parameter fine tuned to the length of the sample, we might be able to completely delocalize the states inside the sample, obtaining a non-zero current response.
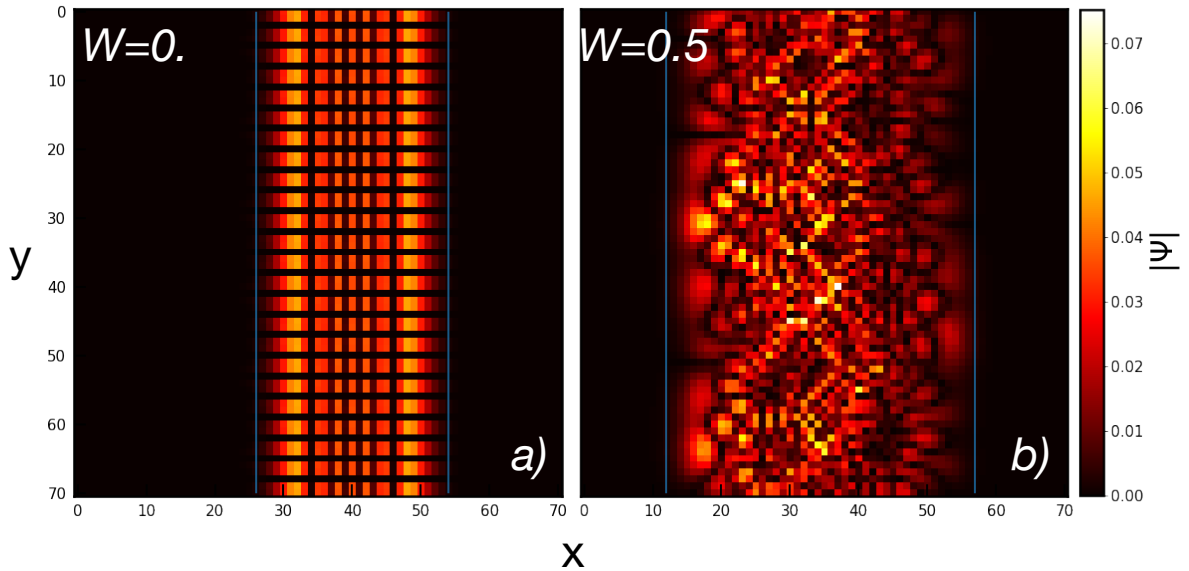


Figure 4.2.: Density plots of eigenstates of a 2D system with dimensions 71x71 for $E = 0.143$ (in units of $w/ea$) and for disorder parameters of a) $W = 0$ and b) $W = 0.5$ (in units of $w$). The blue lines delimit the spatial extent of the states.

To see how this comes about, we once again borrow the intuition built from gaussian wave-packet propagation to interpret this result. Contrarily to the 1D case, in a 2D tight-binding lattice the impurity has a different effect on the wave-packet: Because there are now other accessible $k_x$ values via energy and momentum conservation laws, the dynamic of the scattered electron in the $x$ direction will change accordingly. In particular, we can imagine an electron in a given position $\mathbf{x_a}$ with momentum $k_x > 0$ being scattered to $k_x = 0$, at which point the oscillatory motion will restart and the electron will be able to travel outside the original confinement region (Fig 4.3).
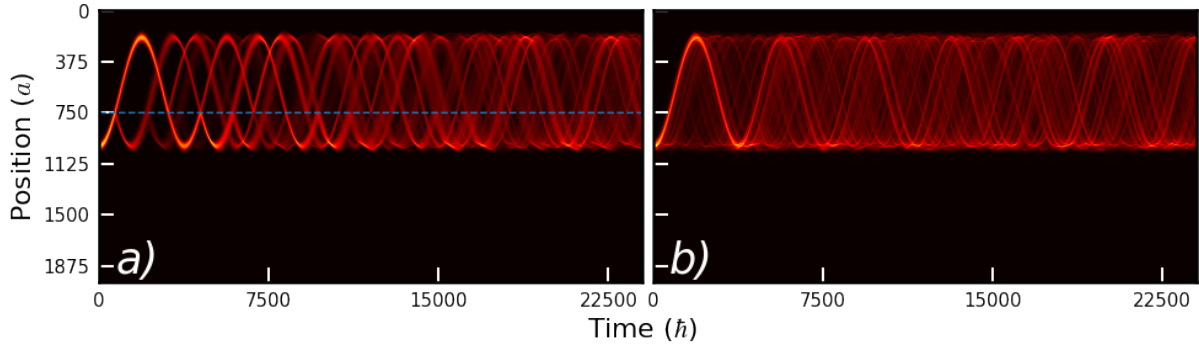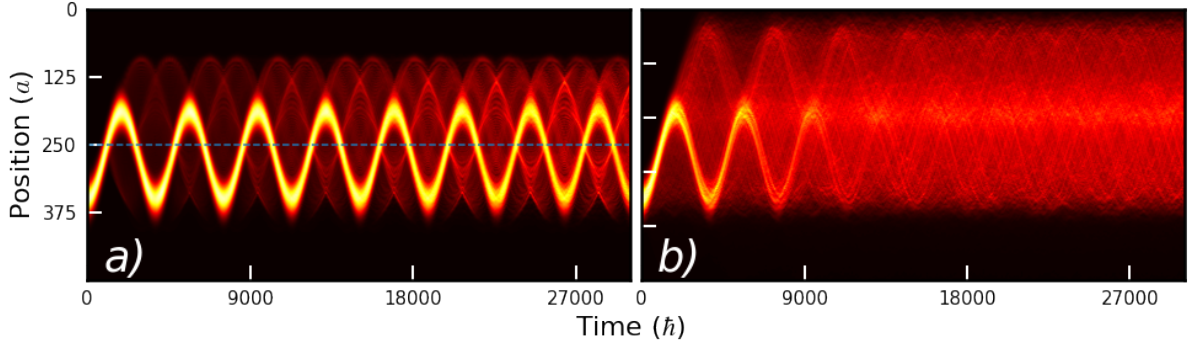
Figure 4.3.: Time evolution of a Gaussian wave-packet of variance $\sigma = 20a$ initially centered at $\bar{l}_0 = 250a$ in a two-dimensional tight-binding square lattice of length $L_x = 500a$ and $L_y = 40a$ with an applied electric field of $E = 0.05w/ea$ and a) a single impurity added to site $250a$ with on-site energy $2.5w$ (the blue dashed line denotes the impurity position) b) Anderson disorder with a disorder parameter $W = 1.2w$.

Given this picture, we can now suppose that the introduction of Anderson disorder, being spatially uncorrelated, will have similar effects on 1D and 2D tight binding lattices, that is, it will preserve the confinement region of a gaussian wave-packet in 1D and broaden this region in 2D. Furthermore, since we can reasonably assume that the eigenstates of such systems will still each be centered around each of the sites and confined to a certain spatial region on average, we are able to deduce that the eigenstates of the 2D system get enlarged by the introduction of Anderson disorder. However, as it has been stated in the one-dimensional case, this picture will not hold for sufficiently strong disorder, as interference effects will diminish the localization length. Nonetheless, the regime where the eigenstates get larger with disorder in a two-dimensional system will radically change the behavior of the Landauer current with the disorder parameter when compared to the one-dimensional system.

## 4.2. Coupling Different Conduction Channels via Disorder

Before moving on the the numeric results, another mechanic is at play that need to be taken into account for us to get the full picture. For a broad enough mesoscopic setup, the dispersion relation for the leads will be

$$\varepsilon(k_x, k_y) = -2w_l \cos k_x a - 2w_l \cos k_y a \tag{4.1}$$

The leads will then have an energy band spanning from $-4w_l$ to $4w_l$. To see the formation of Bloch Oscillations inside the sample, we need a potential ramp $\Delta V > 4w$ and to get overlap between the bands of the leads we need $\Delta V > 8w_l$, so for $w_l = w$ we have a regime where we could potentially have Bloch Oscillations inside the sample and transmission between the leads. However, because the translation symmetry in the y-direction is conserved throughout

the entire system in the absence of disorder, the y component of the momentum of an ingoing propagating state must match that of the outgoing state for them to couple. Therefore, for a clean sample, a propagating state in the left lead with, say, $k_y = 0$ will only couple to a propagating state in the right lead if this state also has $k_y = 0$, and with the momentum and energy conservation laws, this amounts precisely to the 1D case, where it is only possible to have transmission for $\Delta V < 4w_l$.
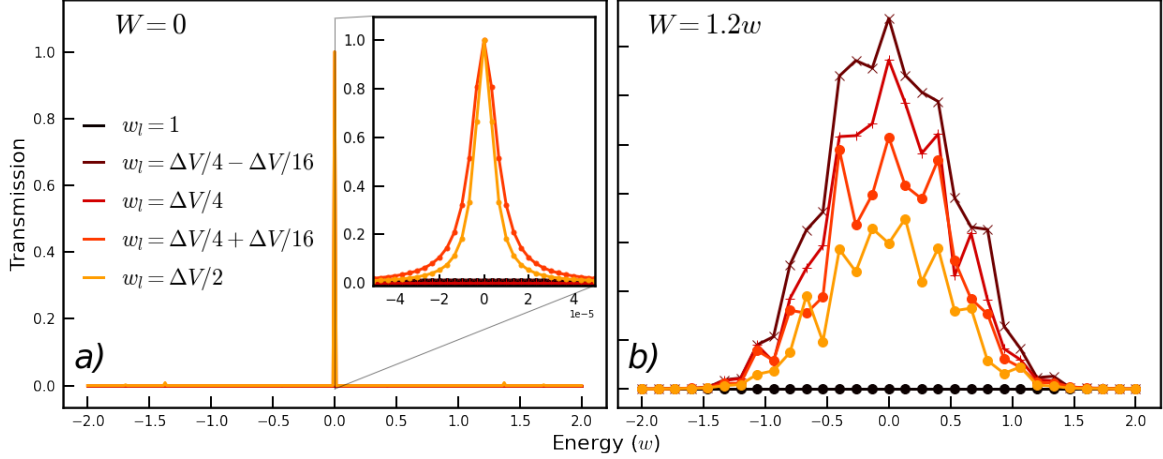


Figure 4.4.: a) Transmission as a function of energy in the clean system for different values of $w_l$ in units of $w$. System's width = 61, length = 25 (in units of $a$) and $\Delta V = 8.2$, such that $\xi_{WS} = 6.34$ (in units of $w$ and $a$, respectively). It is immediate to see that for values of $w_l < \Delta V/4$ there is no transmission between the leads, with the transmission acquiring non-zero values around $E = 0$ for $w_l > \Delta V/4$. b) Same system as a) but with a disorder parameter $W = 1.2$ (in units of $w$), where now we get non-zero transmission for $w_l > \Delta V/8$, meaning the effective bands are destroyed.

One can thus conceptualize this problem by means of two effective bands of the same width as the 1D leads' bands, and the propagating states in the leads will only couple if these bands overlap. Plotting the transmission coefficient as a function of energy (Fig.4.4.a)) does, forsooth, corroborate this hypothesis, as we see that for $w_l < \Delta V/4$ we get no transmission and for $w_l > \Delta V/4$ we get the usual peak around zero energy. The introduction of disorder in the sample breaks the y-translation symmetry, thus coupling propagating states with different $k_y$ and obtaining non-zero transmission for $w_l > \Delta V/8$.(Fig.4.4.b)

## 4.3. Numeric Results

Up until now, we have discussed two effects that can potentially induce an increase in current with the introduction of disorder, but we are still to confirm this is actually the case. Fortunately, both of this effects allow for a fine-tuning of a system where we can actually see

this increase: In figure 4.5, we measure the current in a single bond inside a 2D sample for no disorder (left panel) and disorder of strength $W = 0.5w$ (right panel), and what we end up observing is that, indeed, while for the former case we spot obvious Bloch Oscillations, which will induce a small Landauer current with very large relaxation times, in the latter we observe that, with a proper choice of the leads' hopping, these BO's decay elegantly to a non-zero, constant current plateau.
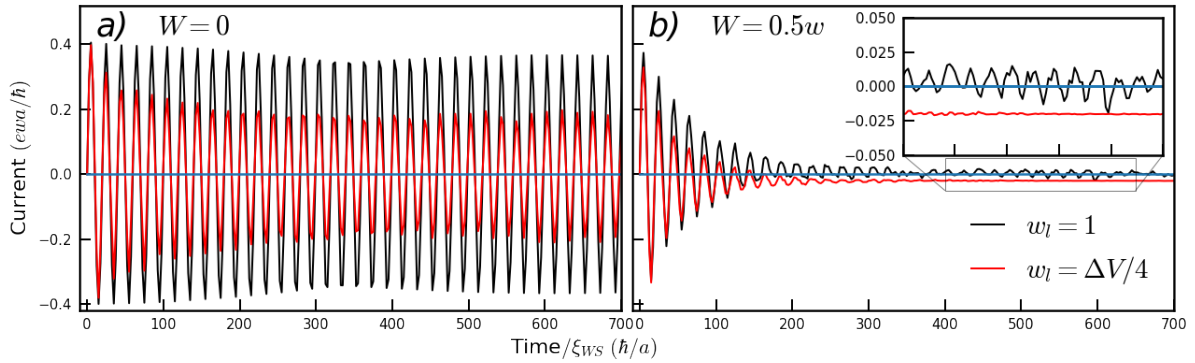


Figure 4.5.: Time evolution of the current for a single bond inside a 2D sample of length $L_x = 25$ and width $L_y = 61$ for a) $W = 0$ and b) $W = 0.5w$. The inset zooms in in a region closer to zero current to show that the red curve decays to a non-zero value while the black curve slightly oscillates around zero.

We have included two curves in each case to point out the importance of the increase of the leads' hopping: In the disordered sample, even though we have broad enough states to mitigate the oscillations to a non-zero constant current, we can not see this increased response for $w_l = w$, where instead we only observe the decay of the oscillations to zero. As for the clean sample, this augment on $w_l$ decreases the amplitude of the oscillations, which is expected once we understand that when we increase the bands' width, we allow for the former bound states that were contributing to the oscillation to escape, which diminished the amplitude of the current. Nevertheless, these are still identifiable as Bloch Oscillations because its the period the BO's period $T_{BO}$.

We can double down on these facts by plotting the current inside one bond of one of the leads for a clean sample and a disordered sample, shown in figure 4.6 a) and b) respectively. The inset in figure 4.6 b) zooms in in a region closer to zero current to show that the red curve ($w_l = \Delta V/4$) decays to a non-zero value while the black curve ($w_l = 1$) decays to zero, demonstrating once more the importance of the choice of $w_l$. Furthermore, the obtainance of a non-zero current response is only possible for a disordered sample, as in the clean sample (figure 4.6 a)) the currents for both $w_l = 1$ and $w_l = \Delta V/4$ decay to zero because the effects mentioned in subsections 4.1 and 4.2 are not present.

As a take home message, we compute the Landauer current of a system divided by the width
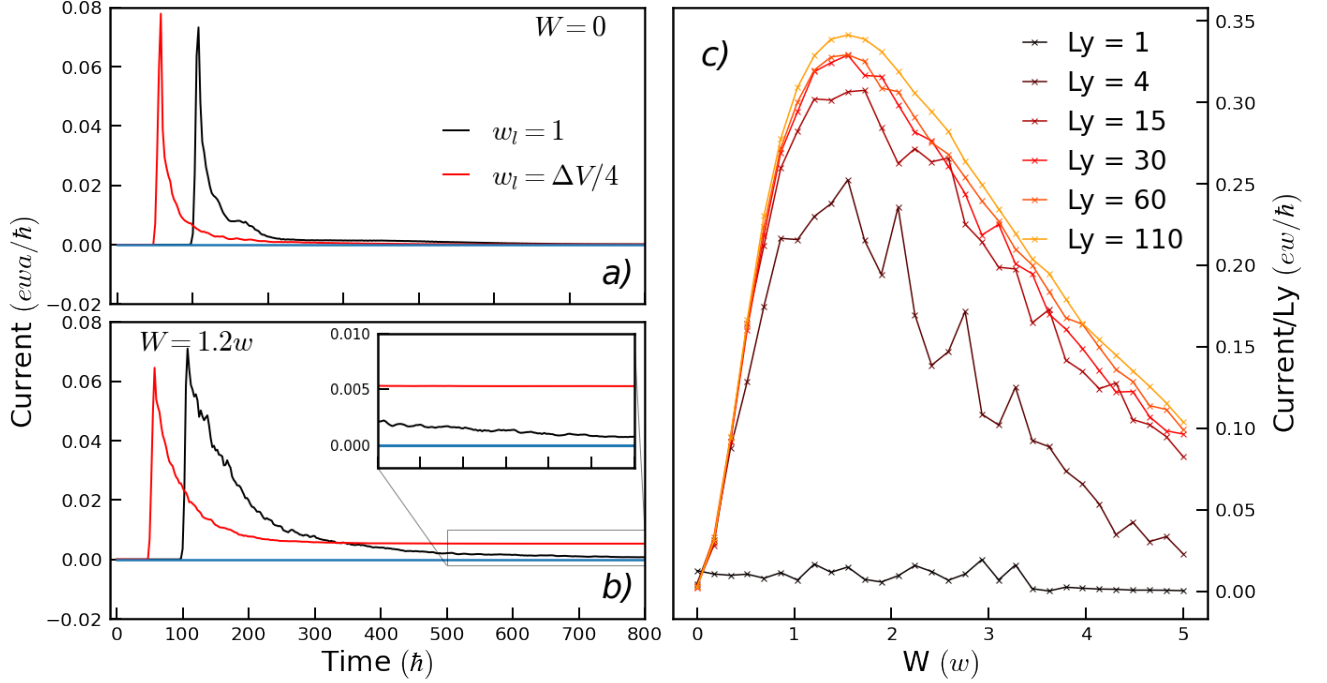
Figure 4.6.: Time evolution of the current for a single bond inside the right lead for a sample of length $L_x = 25a$ and width $L_y = 61a$ for a) $W = 0$ and b) $W = 1.2w$. c) Total Landauer current through the sample divided by the width on a sample of length $Lx = 25a$ and $\Delta V = 6w$ as a function of the disorder parameter for different widths and a single disorder realization.

of the sample as a function of the disorder parameter averaged over ten different realizations of disorder (Fig. 4.6 c)). The choice for this averaging is to characterize a mean behavior of the system with the disorder, however, the current curve for a single realization clearly has the same behavior as these ones. To view such curves, the reader is referred to the Appendix D.2 to figures D.2 a) and b). The results are promising: The currents go from virtually zero to a maximum value of an order of magnitude above its initial value, which is a more than clear indication that the effects described previously are in action. Furthermore, the current curves for $L_y \geqslant 15$ collapse to a single curve . This means the only effect that contributes for the increase of the current with the increase of $L_y$ is purely the addition of more transversal channels, and the current's functional dependence on the disorder parameter is essentially the same, which is an interesting result by itself. With everything we have discussed so far, we are now in a position to develop an interpretation of this figure: Up until $W \sim 1.7w$, the current increases rather rapidly, due to the delocalization of the Wannier-Stark states and the mixing of propagating states with different momentums in the y direction. Interestingly enough, all

of the curves peak at around the same value of $W$, and then decrease in the same way for large enough $L_y$. Conversely to the one-dimensional case, in a two-dimensional system we have two different length scales introduced by disorder: The Anderson localization length $\xi_A$ and the mean free path $\ell$. We cannot therefore conclude, as we did in the one-dimensional case, that the reason for the decay of the current is solely due to the interplay between the Wannier-Stark localization length and the Anderson localization length. Although a thorough examination on this front is lacking, it is still intuitive that such decay comes from the interference effects that are described by the Anderson localization length.

# 5. Conclusion and Outlook

Throughout this work, we sought to connect the Landauer constant current value to the observed oscillations for high potential biases. This was successfully done when considering a system without bound states, i.e, where the leads' energy bands are overlapping, and we have concluded that the oscillations will decay exponentially to a constant current given by the Landauer formula. These decaying oscillations in the transient regime were effectively identified as Bloch Oscillations. The exponential decaying time of this transient regime was characterized in terms of the escaping rates of the three central-most Wannier-Stark states. An analytical expression for such escaping rates was found, allowing one to obtain a power law scaling of these rates with the potential bias' strength.

We have further studied the behavior of the system with disorder, and found that in 1D, before interference effects start taking place inside the sample, disorder does not, on average, alter the localization length of the eigenstates. This is backed by a simplistic semi-classical view in terms of the evolution of gaussian wave-packets. When this interference effects start taking place, corresponding to the strong disorder limit, the localization length diminishes. This has obvious impact on the Landauer current, which decreases with disorder in this regime. For 2D, however, this picture gets subverted, as we are able, by increasing the disorder parameter $W$, to increase the inter-lead current from virtually zero to a finite value, and is mainly associated with the disorder-induced delocalization of the Wannier-Stark states. This interesting result is once again explained semi-classically by extending the same intuition built on one-dimensional materials to this case.

Although the results in this thesis were interesting and new, particularly when considering two dimensional disordered samples, we are all but finished: The transient Bloch Oscillations decaying with the escaping time scale of the center-most state is still to be seen. This may be attainable by increasing the leads' size and the time-evolution in the numerical simulation. As for the disordered case, it is mandatory to quantitatively define the increase in the extent of the Wannier-Stark states with disorder, and study how the Anderson localization length enters the equation. In order to do so, we need to find a good way to define the extent of the eigenstates so we can automatically compute it numerically. With that done, we could also study the effect with the rising of the temperature. It would also prove an interesting, although demanding problem if, instead of a classical electrical potential introduced phenomenologically in the Hamiltonian, we were to solve such transport setups with the Coulomb interaction term.

# A. Numeric Methods

## A.1. Kernel Polynomial Method

### A.1.1. Chebyshev Polynomials and the Recursion Relation

The Chebyshev polynomials is an orthogonal set of functions defined in the interval $]-1,1[$ and are defined as

$$T_n(x) = \cos(n \arccos(x)).\tag{A.1}$$

The first polynomials are then found to be

$$
\begin{aligned}
T_0(x) &= 1, \\
T_1(x) &= x, \\
T_2(x) &= 2x^2 - 1, \\
T_3(x) &= 4x^3 - 3x,
\end{aligned}
\tag{A.2}
$$

At first one might miss the utility of such functions given there are other polynomial basis with a much simpler analytical expression, however, this set presents an advantage since they can be recursively written in terms of previous polynomials like

$$T_{m+1}(x) = 2xT_m(x) - T_{m-1}(x),\tag{A.3}$$

which can be proven directly like

$$
\begin{aligned}
T_{n+1}(\cos(\theta)) + T_{n-1}(\cos(\theta)) &= \cos((n+1)\theta) + \cos((n-1)\theta) \\
&= \cos(n\theta)\cos(\theta) - \sin(n\theta)\sin(\theta) + \cos(n\theta)\cos(\theta) + \sin(n\theta)\sin(\theta) \\
&= 2\cos(n\theta)\cos(\theta) = 2\cos(\theta)T_n(\cos(\theta)).
\end{aligned}
\tag{A.4}
$$

Therefore, by explicitly calculating the first two polynomials, all others can be constructed from this recursive relation.

### A.1.2.  Orthogonality

The orthogonality relation is given in this case by

$$\int_{-1}^{1} \frac{dx}{\pi\sqrt{1-x^2}} T_n(x) T_m(x) = \frac{1+\delta_{n0}}{2} \delta_{nm}. \tag{A.5}$$

To prove this, let us formulate this integral in terms of their analytical form:

$$\int_{-1}^{1} \frac{dx}{\pi\sqrt{1-x^2}} \cos(n\arccos(x)) \cos(m\arccos(x)). \tag{A.6}$$

Let us now perform the variable substitution $x = \cos\theta$

$$\int_{\pi}^{0} \frac{1}{\pi\sin(\theta)} \cos(n\theta)\cos(m\theta)[-\sin(\theta)]d\theta = \frac{1}{\pi}\int_{0}^{\pi} \cos(n\theta)\cos(m\theta)d\theta = \frac{1+\delta_{n0}}{2}\delta_{nm}. \tag{A.7}$$

This orthogonality relation follows from the orthogonality of the Fourier series. The fact they are so closely related explains why the Chebyshev Polynomials actually inherit a lot of properties from the Fourier series. This orthogonality, as we will see, will allow for an easy expansion of any function into this polynomials.

### A.1.3.  Function Expansion

Because this is a completely orthogonal basis, we can describe any function $f(x)$ defined in the interval $]-1, 1[$ in terms of these Chebyshev polynomials and apply the Fourier trick to obtain the expansion coefficients. This expansion is then written as

$$f(x) = \sum_{n=0}^{\infty} a_n T_n(x) \tag{A.8}$$

Where the coefficients are found by making use of the orthogonally relation, hence giving

$$a_n = (1+\delta_{n0}) \int_{-1}^{1} \frac{dx}{\pi\sqrt{1-x^2}} T_n(x) f(x). \tag{A.9}$$

It will come in handy to define

$$f(x) = \sum_{n=0}^{\infty} \frac{2b_n}{\pi(1+\delta_{n0})} T_n(x) \tag{A.10}$$

purely to get rid of the multiplicative factor behind the integral

$$b_n = \int_{-1}^{1} \frac{dx}{\sqrt{1-x^2}} T_n(x) f(x). \tag{A.11}$$

For elucidative purposes only, we could also define

$$f(x) = \frac{1}{\sqrt{1-x^2}} \sum_{n=0}^{\infty} \frac{2c_n}{\pi\left(1+\delta_{n0}\right)} T_n(x) \tag{A.12}$$

which would eliminate the square root in the integral

$$c_n = \int_{-1}^{1} dx\, T_n(x) f(x), \tag{A.13}$$

but this will not be necessary.

This characteristic, together with the recursion relation, is highly useful for a fast writing of functions of operators.

### A.1.4.  Truncated Series

The need for calculating this summation numerically will eventually call for a truncation of the series, which can lead to some problems, specially around a point where the function, or at least its derivative, is discontinuous. For such functions, the approximated sum will result in appearance of oscillations around this points, denominated Gibb's Oscillations. To smooth these out, one can introduce additional coefficients $w_n$ as to better approximate the truncated series to the original function, meaning the expansion would assume the form

$$f(x) = \sum_{n=0}^{N} w_n \frac{2b_n}{\pi\left(1+\delta_{n0}\right)} T_n(x). \tag{A.14}$$

The form of these new coefficients $w_n$ can depend on the truncation degree $N$. We will not delve further into detail around these coefficients and will instead show the formula which works best, named Jackson Kernel, and given by

$$w_n^J = \frac{(N-n+1)\cos\frac{\pi n}{N+1} + \sin\frac{\pi n}{N+1} \cot\frac{\pi}{N+1}}{N+1}. \tag{A.15}$$

To illustrate the power of such coefficients, it is shown in figure A.1 an expansion of a square wave with and without these coefficients.

### A.1.5.  Writing Functions of Operators in terms of the Chebyshev Polynomials

Let us now move on to an Hermitian operator, living in a given Hilbert space of dimension L, $\hat{H}$. So we will be performing the change from a real variable to an operator

$$x \to \hat{H}. \tag{A.16}$$
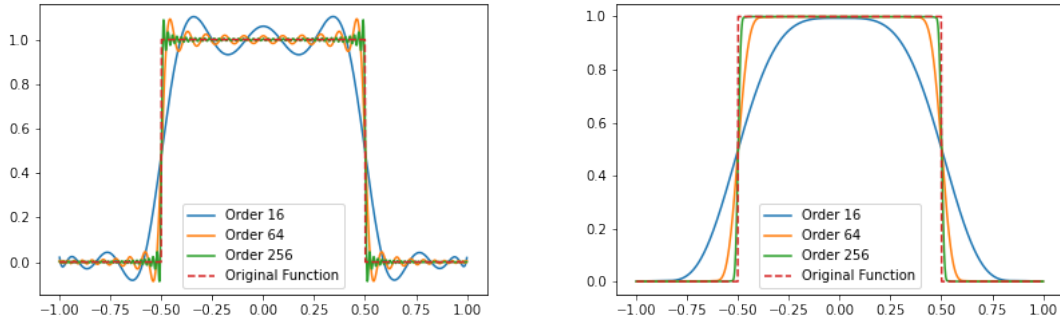
(a) Truncated Chebyshev expansions for a square wave without the Jackson Kernel

(b) Truncated Chebyshev expansions for a square wave with the Jackson Kernel

Figure A.1.: Truncated Chebyshev expansions at different orders of a square wave compared to the original function

A function with no singularities may always be expressed in terms of its Taylor expansion

$$f\left(x\right) = \sum_{n=0}^{\infty} a_n x^n. \tag{A.17}$$

A function of an operator is then defined through its Taylor expansion, i.e, using the coefficients obtained in the usual expansion to write

$$f\left(\hat{H}\right) = \sum_{n=0}^{\infty} a_n \hat{H}^n. \tag{A.18}$$

We are interested in expanding a certain function of this operator in terms of the Chebyshev polynomials. Luckily, since the function itself is only a function of the the operator alone, it is easy to see that the result will be diagonal in the eigenbasis of the operator, allowing us to write

$$f(\hat{H}) = \sum_{l=1}^{L} \sum_{n=0}^{\infty} \frac{2b_n}{\pi\left(1 + \delta_{n0}\right)} T_n(\varepsilon_l) \left|\varepsilon_l\right\rangle \left\langle\varepsilon_l\right|. \tag{A.19}$$

There is, however, an important caveat to be taken into account: Since the Chebyshev polynomials are only defined in the interval $]-1,1[$, the expansion above only converges if, in this case, $-1 < \varepsilon_l < 1$, for every $l$. Since this is not generically true, one has to rescale the spectrum to fit this interval and allow the expansion to converge. So, in truth, we will be expanding a different operator:

$$\hat{\tilde{H}} = \frac{\hat{H}}{\lambda}, \tag{A.20}$$

where $\lambda$ is chosen to make every eigenvalue obey $-1 < \tilde{\varepsilon}_l < 1$, as to make sure that the expansion is now well defined:

$$f(\hat{\tilde{H}}) = \sum_{l=1}^{L} \sum_{n=0}^{\infty} \frac{2b_n}{\pi \left(1 + \delta_{n0}\right)} T_n(\tilde{\varepsilon}_l) \left|\tilde{\varepsilon}_l\right\rangle \left\langle\tilde{\varepsilon}_l\right|. \tag{A.21}$$

It comes from the definition of a function of an operator that the coefficients $b_n$ are the same as those of the function of a real variable, and so are obtained in the usual form using equation A.11.

### A.1.6. Truncated Series of Operators

We are now in a place to consider the application of a function of an operator to a vector, or state, $\left|\Psi\right\rangle$. We will be promptly employing the Kernel Jackson to transform the expansion into a finite sum. In terms of the Chebyshev Polynomials, such an operation would be

$$f(\hat{\tilde{H}}) \left|\Psi\right\rangle = \sum_{l=1}^{L} \sum_{n=0}^{N} w_n^J \frac{2b_n}{\pi \left(1 + \delta_{n0}\right)} T_n(\tilde{\varepsilon}_l) \left|\tilde{\varepsilon}_l\right\rangle \left\langle\tilde{\varepsilon}_l \mid \Psi\right\rangle. \tag{A.22}$$

We have gained some computational advantage since the Chebyshev series might converge faster that the Taylor series, but this way we still need to diagonalize the operator $\hat{H}$ to obtain the corresponding eigenvectors and eigenvalues. However, we may notice that the Chebyshev Polynomials are themselves a function of the operator,

$$\sum_{l=1}^{L} T_n(\tilde{\varepsilon}_l) \left|\tilde{\varepsilon}_l\right\rangle \left\langle\tilde{\varepsilon}_l\right| = T_n(\hat{\tilde{H}}) \tag{A.23}$$

and the action of the function on a state its then written as

$$f(\hat{\tilde{H}}) \left|\Psi\right\rangle = \sum_{l=1}^{L} \sum_{n=0}^{N} w_n^J \frac{2b_n}{\pi \left(1 + \delta_{n0}\right)} T_n(\hat{\tilde{H}}) \left|\Psi\right\rangle. \tag{A.24}$$

The recursion relation is valid for operators as well

$$T_{m+1}(\hat{\tilde{H}}) = 2\hat{\tilde{H}} T_m(\hat{\tilde{H}}) - T_{m-1}(\hat{\tilde{H}}), \tag{A.25}$$

which can be proven by expanding the LHS in the eigenbasis of the operator

$$T_{m+1}(\hat{\tilde{H}}) = \sum_{l=1}^{L} T_{m+1}(\tilde{\varepsilon}_l) \, |\tilde{\varepsilon}_l\rangle \, \langle\tilde{\varepsilon}_l|$$

$$= \sum_{l=1}^{L} (2\tilde{\varepsilon}_l T_m(\tilde{\varepsilon}_l) - T_{m-1}(\tilde{\varepsilon}_l)) \, |\tilde{\varepsilon}_l\rangle \, \langle\tilde{\varepsilon}_l|$$

$$= 2\tilde{H} T_m(\hat{\tilde{H}}) - T_{m-1}(\hat{\tilde{H}}) \tag{A.26}$$

and using the already known recursion relation A.3 from the second to the third step.

Let us define

$$T_m(\hat{\tilde{H}}) \, |\Psi\rangle = |\Psi_m\rangle \,. \tag{A.27}$$

Then the expansion is

$$f(\hat{\tilde{H}}) \, |\Psi\rangle = \sum_{n=0}^{N} w_n^J \frac{2b_n}{\pi \, (1 + \delta_{n0})} \, |\Psi_n\rangle \,. \tag{A.28}$$

Then we can write

$$|\Psi_{m+1}\rangle = 2\hat{\tilde{H}} \, |\Psi_m\rangle - |\Psi_{m-1}\rangle \,. \tag{A.29}$$

Evoking the first two Chebyshev Polynomials written as functions of an operator:

$$T_0(\hat{\tilde{H}}) = 1, \tag{A.30}$$

$$T_1(\hat{\tilde{H}}) = \hat{\tilde{H}}, \tag{A.31}$$

Assuming we know how the operator $\hat{\tilde{H}}$ acts on state $|\Psi\rangle$, then $|\Psi_2\rangle$ is completely determined by making use of the recursion relation

$$|\Psi_2\rangle = 2\hat{\tilde{H}} \, |\Psi_1\rangle - T_0(\hat{\tilde{H}}) \, |\Psi_0\rangle$$

$$= 2\hat{\tilde{H}}\hat{\tilde{H}} \, |\Psi\rangle - |\Psi\rangle \,. \tag{A.32}$$

This means we may now retrieve each state $|\Psi_m\rangle$ iteratively and add their contributions to the expansion A.28. This algorithm can be exploited in numeric calculations, since we now do not have to diagonalize the operator $\hat{\tilde{H}}$ to find the action of the function. In particular, if the operator $\hat{\tilde{H}}$ is represented by a sparse matrix, its action upon a state can be explicitly written in a few lines of code, saving us a lot of memory from storing the whole matrix.

### A.1.7. Expansion of the Time-Evolution Operator

The expansion of the evolution operator $e^{-i\hat{H}t/\hbar}$ of a time independent Hamiltonian will be central for the algorithm we are aiming to build. It was first put forward in [42] by Tal Ezer to avoid Range-Kutta-like methods of evolving differential equations. If such an expansion is successful, we will be able to evolve large systems without ever diagonalizing the Hamiltonian. To do so, Let us first find out the coefficients for the expansion of the such a function by expanding its real variable form first:

$$e^{-ixt/\hbar} = \sum_{n=0}^{\infty} \frac{2b_n}{\pi\,(1+\delta_{n0})} T_n(x).$$
(A.33)

The coefficients are thus given by

$$b_n = \int_{-1}^{1} dx \frac{e^{-ixt/\hbar} T_n(x)}{\sqrt{1-x^2}}$$
$$= \int_{-1}^{1} dx \frac{e^{-ixt/\hbar} \cos(n\arccos(x))}{\sqrt{1-x^2}}.$$
(A.34)

Performing the change of variable $x = \cos\theta$ leads us to

$$b_n = \left( \int_0^{\pi} d\theta e^{it/\hbar\cos\theta} \cos(n\theta) \right)^* .$$
(A.35)

One integral representation of a Bessel function of the first kind is [50]

$$J_n(z) = \frac{i^{-n}}{\pi} \int_0^{\pi} dt e^{iz\cos(t)} \cos(nt)/; n \in \mathbb{N}^+,$$
(A.36)

which we can use to express the coefficients for $n > 0$ as

$$b_n = \pi \left( i^n J_n(\frac{t}{\hbar}) \right)^*$$
$$= \pi\,(-i)^n\, J_n(\frac{t}{\hbar}),\ \ n > 0.$$
(A.37)

For $n = 0$, the integral is simply

$$b_0 = \int_{-1}^{1} dx \frac{e^{-ixt/\hbar} T_0(x)}{\sqrt{1-x^2}}$$
$$= \int_0^{\pi} d\theta \cos\left(it/\hbar\cos\theta\right)$$
$$= \pi J_0(\frac{t}{\hbar}),$$
(A.38)
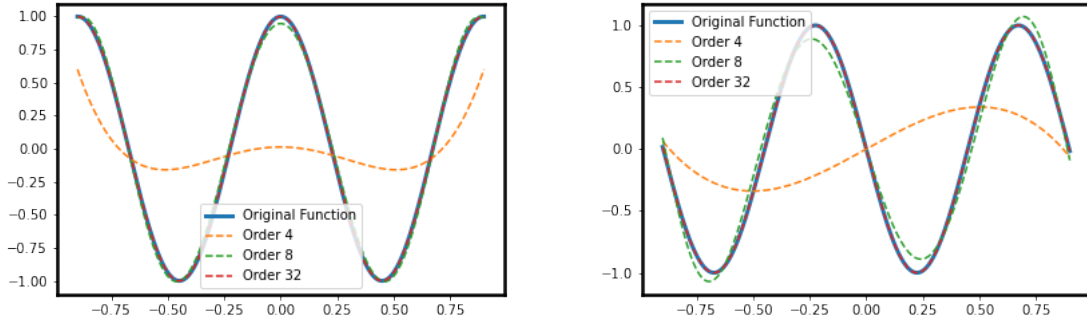
(a) Real part of the time-evolution function compared to its truncated expansions at different orders.

(b) Complex part of the time-evolution function compared to its truncated expansions at different orders.

Figure A.2.: Time-evolution operator compared to its truncated expansions at different orders.

where we have used the fact that $\frac{\sin(-ixt/\hbar)}{\sqrt{1-x^2}}$ is an odd function and have identified the last equation as such because of [50]

$$J_0(z) = \frac{1}{\pi} \int_0^\pi \cos(z \cos \theta) \mathrm{d}\theta \tag{A.39}$$

To extend this to expansion of the time evolution operator written as a function of the Hamiltonian, we must once more be careful enough to normalize the Hamiltonian by a factor $\lambda$ to make sure the series converges. This is equivalent as writing

$$\exp\left(-i\hat{H}\frac{t}{\hbar}\right) = \exp\left(-i\frac{\hat{H}}{\lambda}\lambda\frac{t}{\hbar}\right) = \exp\left(-i\hat{\tilde{H}}\lambda\frac{t}{\hbar}\right) \tag{A.40}$$

and the expansion will now look like

$$e^{-i\hat{H}t/\hbar} = \sum_{n=0}^{\infty} \frac{2(-i)^n J_n(\frac{\lambda t}{\hbar})}{(1+\delta_{n0})} T_n(\hat{\tilde{H}}). \tag{A.41}$$

I urge the reader to notice that the factor of normalization of the Hamiltonian is accounted for in the Bessel function, meaning the final operator we get is not affected by the normalization.

Of course, if we are to evolve times numerically, we will need to end the expansion at some point. Fortunately, because the time-evolution operator is a continuous function with continuous derivative, the Jackson Kernel wont be needed and the truncated Chebyshev series actually converges rather quickly with the number of polynomials, as seen in Figure A.2. Thus, to evolve a state over time, one merely needs to run the algorithm described in A.1.6 with the expansion of the time evolution operator and $t$ as the time wished for the system to evolve.

### A.1.8. Current Average Evolution with KPM

We will see in the next chapter that the detection of Bloch Oscillations in a system at non-equilibrium may be done by measuring oscillations in the current. In what follows, we will seek to develop an efficient algorithm to effectively measure the current average evolution in time with the ultimate goal of performing this measurement.

The model is described by a nearest neighbors tight-binding Hamiltonian with an initially thermalized state which is perturbed with an electric potential at time $t = 0$. The Hamiltonian will then have the generic form

$$\hat{H}\left(t > 0\right) = \underbrace{-t \sum_{n=0}^{N-2} |n+1\rangle \langle n| + |n\rangle \langle n+1| \sum_{n=0}^{N-1} \epsilon_n |n\rangle \langle n|}_{\hat{H}_0} + \underbrace{\sum_{n=0}^{N-1} \xi_n |n\rangle \langle n|}_{\hat{V}}, \tag{A.42}$$

where we have used open boundary conditions and $\xi_n$ are the onsite energies of the tight binding Hamiltonian. The calculation of the current operator has already been done in subsection 2.2.1 and thus the local current operator is written as

$$\hat{J}_n = -t \frac{i}{\hbar} \left( |n\rangle \langle n+1| - |n+1\rangle \langle n| \right). \tag{A.43}$$

The evolution of the average local current of a state described by a density matrix $\hat{\rho}$ is

$$\begin{aligned}
\langle j_n \rangle \left(t\right) &= \text{Tr} \left( \hat{\rho}(t) \hat{J}_n \right) \\
&= \text{Tr} \left( e^{i\hat{H}t/\hbar} \hat{\rho}(0) e^{-i\hat{H}t/\hbar} \hat{J}_n \right).
\end{aligned} \tag{A.44}$$

Let us then introduce the assumption that the initial state is thermalized with the initial Hamiltonian $\hat{H}_0$. This means that the density matrix can be written as

$$\hat{\rho}(0) = \sum_k f\left(\varepsilon_k, \beta, \mu\right) |k\rangle \langle k|, \tag{A.45}$$

where $f\left(\varepsilon_k, \beta, \mu\right)$ is the Fermi-Dirac function

$$f\left(\varepsilon_k, \beta, \mu\right) = \frac{1}{e^{\beta(\varepsilon - \mu)} + 1}, \tag{A.46}$$

and the states $|k\rangle$ are to be understood as the eigenstates of the initial Hamiltonian indexed by the quantum number $k$ and $\varepsilon_k$ their corresponding eigenenergies. This allows us to express the mean current value as

$$\langle j_n \rangle \left(t\right) = \text{Tr} \left( e^{i\hat{H}t/\hbar} \sum_k f\left(\varepsilon_k, \beta, \mu\right) |k\rangle \langle k| e^{-i\hat{H}t/\hbar} \hat{J}_n \right) \tag{A.47}$$

Realizing the trace in the eigenbasis of $\hat{H}_0$ would entail diagonalizing such matrix, which would, numerically speaking, be very costly as we increase the system's size. To avoid such a conundrum, we use the Wannier basis instead, and write the Fermi-Dirac function as a function of the initial Hamiltonian:

$$
\begin{aligned}
\langle j_n \rangle (t) &= \sum_{m=0}^{N-1} \langle m | e^{i\hat{H}t/\hbar} f\left(\hat{H}_0, \beta, \mu\right) e^{-i\hat{H}t/\hbar} \hat{J}_n |m\rangle \\
&= -t\frac{i}{\hbar} \langle n+1 | e^{i\hat{H}t/\hbar} f\left(\hat{H}_0, \beta, \mu\right) e^{-i\hat{H}t/\hbar} |n\rangle - \langle n | e^{i\hat{H}t/\hbar} f\left(\hat{H}_0, \beta, \mu\right) e^{-i\hat{H}t/\hbar} |n+1\rangle \\
&= -t\frac{i}{\hbar} \left( \langle n+1(t) | f\left(\hat{H}_0, \beta, \mu\right) |n(t)\rangle - \langle n(t) | f\left(\hat{H}_0, \beta, \mu\right) |n+1(t)\rangle \right) \\
&= 2t\frac{1}{\hbar} \mathrm{Im}\left( \langle n+1(t) | f\left(\hat{H}_0, \beta, \mu\right) |n(t)\rangle \right).
\end{aligned}
\tag{A.48}
$$

We have reduced the problem of the diagonalization of both Hamiltonians $\hat{H}_0$ and $\hat{H}$ to that of the time-evolution of two states $|n(t)\rangle$ and $|n+1(t)\rangle$ with initial conditions $|n(0)\rangle = |n\rangle$ and $|n+1(0)\rangle = |n+1\rangle$ , which can be performed with the already described method. Unfortunately, we are still left with a Fermi-Dirac function to deal with, but since it is a function of $\hat{H}_0$, we may once again expand it in the Chebyshev Polynomial basis:

$$
f\left(\hat{\tilde{H}}_0, \tilde{\beta}, \tilde{\mu}\right) = \sum_{n=0}^{M} w_n^J \frac{2b_n}{\pi(1+\delta_{n0})} T_n(\hat{\tilde{H}}_0),
\tag{A.49}
$$

where we have already attended for the Hamiltonian's spectrum to be normalized:

$$
f(\varepsilon, \beta, \mu) = \frac{1}{e^{\beta(\varepsilon-\mu)}+1} = \frac{1}{e^{\lambda\beta(\varepsilon/\lambda - \mu\lambda)}+1} = \frac{1}{e^{\tilde{\beta}(\tilde{\varepsilon}-\tilde{\mu})}+1} = f\left(\tilde{\varepsilon}, \tilde{\beta}, \tilde{\mu}\right),
\tag{A.50}
$$

with the changes

$$
\tilde{\beta} = \beta\lambda
\tag{A.51}
$$

$$
\tilde{\mu} = \mu/\lambda
\tag{A.52}
$$

$$
\tilde{\varepsilon} = \varepsilon/\lambda
\tag{A.53}
$$

We have also included the Jackson Kernel coefficients $w_n^J$ for a better approximation of the function due to the function approximating a step function for high $\beta$ values, which is computationally cumbersome because of Gibb's oscillations. The coefficients $b_n$ are obtain with the usual method at the start of the computation.

So the final algorithm is as follows:

1. Start with the initial states $|n(0)\rangle = |n\rangle$ and $|n+1(0)\rangle = |n+1\rangle$.

2. For each time evolution step $dt$, evolve the states $|n(t-dt)\rangle$ and $|n+1(t-dt)\rangle$ to $|n(t)\rangle$

and $|n + 1\,(t)\rangle$, respectively, with the operator $e^{-i\hat{H}t/\hbar}$.

3. Then, act with $f\left(\hat{\tilde{H}}_0, \tilde{\beta}, \tilde{\mu}\right)$ on $|n\,(t)\rangle$ via the Chebyshev recursion method and perform the scalar product $x = \langle n + 1\,(t)| \, f\left(\hat{H}_0, \beta, \mu\right) |n\,(t)\rangle$.

4. The result $2t\frac{1}{\hbar}\mathrm{Im}\,(x)$ will entail the average value of the local current $\langle j_n \rangle\,(t)$ at the bond $n \to n + 1$ at time $t$.

# B. Landauer Formula

The Landauer formula describes the total current that is transmitted through a sample connected to two semi-infinite leads in the steady-state regime. The main idea is that these leads will actually be acting as waveguides, and so the solution of a particular setup is described by the transmission and reflexion coefficients of each of these existing waves, recasting the usual transport problem into a scattering problem.
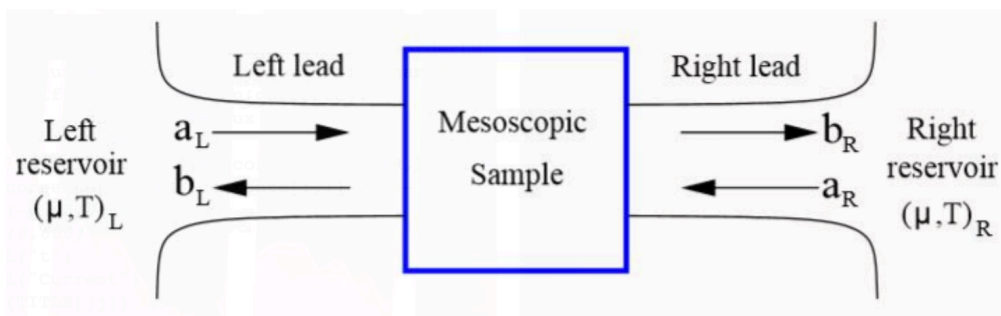
Figure B.1.: Depiction of the setup considered for the derivation of the Landauer formula.

The physical quantities of interest are therefore described in terms of this reflexion and transmission coefficients. In particular, the total current traversing the sample is given by the celebrated Landauer Formula, which is also written in terms of these coefficients [17, 60]:

$$I_{L \to R} = \frac{e}{2\pi\hbar} \int d\varepsilon \left( f_L \left( \varepsilon - \frac{\Delta V}{2} \right) - f_R \left( \varepsilon + \frac{\Delta V}{2} \right) \right) T(\varepsilon), \qquad \text{(B.1)}$$

where $T(\varepsilon)$ is the transmission coefficient at a certain energy $\varepsilon$ which already accounts for different conduction channels and $f_L(\varepsilon)$ and $f_R(\varepsilon)$ are the Fermi-Dirac distribution functions for the left and right leads, respectively. In this brief appendix, we will deduce the the Landauer formula for a generic two-dimensional system, as per references [61, 62].

## B.1. Scattering Matrix

For the generic 1D or 2D tight binding system made of a sample connected to two semi-infinite leads, we can write the Hamiltonian in terms of smaller matrices representing the

Hamiltonian of each of the the cross-sections of the system comprised by the unitary cells $\mathbf{h}_n$ and the coupling between these different smaller hamiltonians $\mathbf{v}_{n,n+1}$ (we will assume a nearest neighbor tight binding Hamiltonian is in place), forging the Hamiltonian onto the form

$$H = \begin{bmatrix} \ddots & \ddots & & & & & & \\ \ddots & \boldsymbol{h}_L & \boldsymbol{v}_L & & & & & \\ & \boldsymbol{v}_L^\dagger & \boldsymbol{h}_L & \boldsymbol{v}_{0,1} & & & & \\ & & \boldsymbol{v}_{1,0} & \boldsymbol{h}_1 & \ddots & & & \\ & & & \ddots & \ddots & \ddots & & \\ & & & & \ddots & \boldsymbol{h}_N & \boldsymbol{v}_{N,N+1} & \\ & & & & & \boldsymbol{v}_{N+1,N} & \boldsymbol{h}_R & \boldsymbol{v}_R \\ & & & & & & \boldsymbol{v}_R^\dagger & \boldsymbol{h}_R & \ddots \\ & & & & & & & \ddots & \ddots \end{bmatrix} \tag{B.2}$$

where $\boldsymbol{v}_L$ and $\boldsymbol{v}_R$ are the hoppings for the left and right leads which are made constant assuming the leads are translational invariant in the x direction. This in turn will generate an infinite set of identical equations for the eigenstates in each lead of the form

$$\boldsymbol{h}\Psi_n + \boldsymbol{v}\Psi_{n+1} + \boldsymbol{v}^\dagger\Psi_{n-1} = E\Psi_n, \tag{B.3}$$

which can be recast as a transfer matrix equation

$$\begin{bmatrix} \mathbf{0} & \mathbf{1} \\ -\boldsymbol{v}^\dagger & (E-\boldsymbol{h}) \end{bmatrix} \begin{bmatrix} \Psi_{n-1} \\ \Psi_n \end{bmatrix} = \begin{bmatrix} \mathbf{1} & \mathbf{0} \\ \mathbf{0} & \boldsymbol{v} \end{bmatrix} \begin{bmatrix} \Psi_n \\ \Psi_{n+1} \end{bmatrix}. \tag{B.4}$$

Meanwhile, because of the translation invariance in the leads, the eigenstates will also be eigenstates of the translation operator, meaning

$$T\Psi_n = \lambda\Psi_n. \tag{B.5}$$

On the other hand

$$T\Psi_n = \Psi_{n-1}, \tag{B.6}$$

giving

$$\Psi_{n-1} = \lambda\Psi_n. \tag{B.7}$$

The normalization condition forces $|\lambda| \leq 1$. States where $|\lambda| = 1$ are denominated propagating states and states with $|\lambda| < 1$ are called evanescent states and decay exponentially to zero with the distance from the sample. With this said, we can rewrite equation B.4 as a generalized

eigenvalue problem $(Ax = \lambda Bx)$

$$\begin{bmatrix} \mathbf{0} & \mathbf{1} \\ -\boldsymbol{v}^\dagger & (E - \boldsymbol{h}) \end{bmatrix} \begin{bmatrix} \Psi_{n-1} \\ \Psi_n \end{bmatrix} = \lambda \begin{bmatrix} \mathbf{1} & \mathbf{0} \\ \mathbf{0} & \boldsymbol{v} \end{bmatrix} \begin{bmatrix} \Psi_{n-1} \\ \Psi_n \end{bmatrix}. \tag{B.8}$$

The current operator is defined as

$$\frac{d\rho_n}{dt} = I_{n-1 \to n} - I_{n \to n+1}, \tag{B.9}$$

giving us

$$I_{n \to n+1} = \frac{i}{\hbar} \begin{bmatrix} \mathbf{0} & \boldsymbol{v}_{n,n+1} \\ -\boldsymbol{v}_{n+1,n} & \mathbf{0} \end{bmatrix}. \tag{B.10}$$

For propagating states, we have

$$\langle \Phi \left| I_{n \to n+1} \right| \boldsymbol{\Psi} \rangle = \frac{i}{\hbar} \left( \Phi_n^\dagger \boldsymbol{v}_{n,n+1} \Psi_{n+1} - \Phi_{n+1}^\dagger \boldsymbol{v}_{n+1,n} \Psi_n \right)$$

$$= \frac{i}{\hbar} \Phi_n^\dagger \left( \lambda_\Psi \boldsymbol{v}_{n,n+1} - \lambda_\Phi^* \boldsymbol{v}_{n+1,n} \right) \Psi_n. \tag{B.11}$$

## B.2. Orthogonality of Propagating States

Let us consider two propagating states obeying equation B.8 or, simply put,

$$\left( \lambda_\Psi \boldsymbol{v}_L + \lambda_\Psi^{-1} \boldsymbol{v}_L^\dagger \right) \Psi_n = (E - \boldsymbol{h}_L) \Psi_n, \tag{B.12}$$

$$\left( \lambda_\Phi \boldsymbol{v}_L + \lambda_\Phi^{-1} \boldsymbol{v}_L^\dagger \right) \Phi_n = (E - \boldsymbol{h}_L) \Phi_n. \tag{B.13}$$

By taking the hermitian conjugate of the second equation and act with $\Psi_n$ we get

$$\Phi_n^\dagger \left( \lambda_\Phi^* v_L^\dagger + (\lambda_\Phi^*)^{-1} v_L \right) \Psi_n = \Phi_n^\dagger (E - \boldsymbol{h}_L) \Psi_n = \Phi_n^\dagger \left( \lambda_\Psi v_L + \lambda_\Psi^{-1} v_L^\dagger \right) \Psi_n, \tag{B.14}$$

which can be written as

$$\left[ \lambda_\Phi^* - \lambda_\Psi^{-1} \right] \Phi_n^\dagger v_L^\dagger \Psi_n = \left[ \lambda_\Psi - (\lambda_\Phi^*)^{-1} \right] \Phi_n^\dagger v_L \Psi_n. \tag{B.15}$$

Multiplying by $\lambda_\Psi \lambda_\Phi^*$ and making use of the fact that $\lambda_\Psi \lambda_\Psi^* = \lambda_\Phi \lambda_\Phi^* = 1$, we arrive at

$$[\lambda_\Psi \lambda_\Phi^* - 1] \lambda_\Phi^* \Phi_n^\dagger \boldsymbol{v}_L^\dagger \Psi_n = [\lambda_\Psi \lambda_\Phi^* - 1] \lambda_\Psi \Phi_n^\dagger v_L \Psi_n, \tag{B.16}$$

which can be written as

$$[\lambda_\Psi \lambda_\Phi^* - 1] \Phi_n^\dagger \left( \lambda_\Psi v_L - \lambda_\Phi^* v_L^\dagger \right) \Psi_n = 0. \tag{B.17}$$

So, if $\lambda_\Psi \lambda_\Phi^* \neq 1$, we immediately obtain

$$\langle \Phi | I_{n \to n+1} | \Psi \rangle = \frac{i}{\hbar} \Phi_n^\dagger \left( \lambda_\Psi \boldsymbol{v}_L - \lambda_\Phi^* \boldsymbol{v}_L^\dagger \right) \Psi_n = 0. \tag{B.18}$$

Otherwise, if $\lambda_\Psi \lambda_\Phi^* \neq 1$, we can choose our states such that

$$\langle \Phi | I_{n \to n+1} | \Psi \rangle = \frac{i}{\hbar} \Phi_n^\dagger \left( \lambda_\Psi \boldsymbol{v}_L - \lambda_\Phi^* \boldsymbol{v}_L^\dagger \right) \Psi_n = v_\Psi \delta_{\Psi,\Phi}. \tag{B.19}$$

## B.3. Propagating States

It is important to note, nevertheless, that the propagating states have, in the general case, two degrees of freedom and therefore two distinct components for the momentum. In what follows, we will fix an energy for a state and use greek letters to index the different propagating states at that energy. With that said, an eigenstate propagating to the right can be expanded in the leads' propagating states in the following way:

$$|\Psi_{+,\alpha}(E)\rangle = \begin{cases} \left| \Psi_{L,+,\alpha}^+(E) \right\rangle + \sum_\beta r_{\beta\alpha}^{R \leftarrow L} |\Psi_{L,-,\beta}(E)\rangle & \text{, Left lead} \\ ? & \text{, Sample} \\ \sum_\gamma t_{\gamma\alpha}^{R \leftarrow L} |\Psi_{R,+,\gamma}(E)\rangle & \text{, Right lead} \end{cases} \tag{B.20}$$

Similarly, an eigenstate propagating to the left is

$$|\Psi_{-,\gamma}(E)\rangle = \begin{cases} \sum_\alpha t_{\alpha\gamma}^{L \leftarrow R} \left| \Psi_{L,\alpha}^-(E) \right\rangle & \text{, Left lead} \\ ? & \text{, Sample} \\ |\Psi_{R,-,\gamma}(E)\rangle + \sum_\delta r_{\delta\gamma}^{L \leftarrow R} \left| \Psi_{R,+,\delta}^+(E) \right\rangle & \text{, Right lead} \end{cases} \tag{B.21}$$

## B.4. Current Conservation

Writing out the current flowing in the right lead due to $|\Psi_{+,\alpha}(E)\rangle$ gives us

$$\begin{aligned} I_R^+(E,\alpha) &= \left\langle \Psi_\alpha^+(E) | I_{N+1 \to N+2} | \Psi_\alpha^+(E) \right\rangle \\ &= \sum_{\gamma,\delta} \left( t_{\delta\alpha}^{R \leftarrow L} \right)^* t_{\gamma\alpha}^{R \leftarrow L} \left\langle \Psi_{R,\delta}^+(E) | I_{N+1 \to N+2} | \Psi_{R,\gamma}^+(E) \right\rangle \\ &= \sum_{\gamma,\delta} \left( t_{\delta\alpha}^{R \leftarrow L} \right)^* t_{\gamma\alpha}^{R \leftarrow L} v_{\gamma,R} \delta_{\gamma,\delta} \\ &= \sum_\gamma v_{\gamma,R} \left| t_{\gamma\alpha}^{R \leftarrow L} \right|^2, \end{aligned} \tag{B.22}$$

with the current in the left lead due to the same state being

$$
\begin{aligned}
I_L^+(E,\alpha) &= \left\langle \Psi_\alpha^+(E) \left| I_{N+1\to N+2} \right| \Psi_\alpha^+(E) \right\rangle \\
&= \left\langle \Psi_{L,\alpha}^+(E) \left| I_{N+1\to N+2} \right| \Psi_{L,\alpha}^+(E) \right\rangle - e \sum_{\delta,\delta'} \left( r_{\delta'\alpha}^{R\leftarrow L} \right)^* r_{\delta\alpha}^{R\leftarrow L} \left\langle \Psi_{L,\delta'}^-(E) \left| I_{N+1\to N+2} \right| \Psi_{L,\delta}^-(E) \right\rangle \\
&= \left( v_{\alpha,L} - \sum_\delta v_{\delta,R} \left| r_{\delta\alpha}^{R\leftarrow L} \right|^2 \right).
\end{aligned}
\tag{B.23}
$$

The current flux conservation gives us

$$
I_L^+(E,\alpha) = I_R^+(E,\gamma)
$$

$$
\left( v_{\alpha,L} - \sum_\delta v_{\delta,R} \left| r_{\delta\alpha}^{R\leftarrow L} \right|^2 \right) = \sum_\gamma v_{\gamma,R} \left| t_{\gamma\alpha}^{R\leftarrow L} \right|^2
$$

$$
v_{\alpha,L} = \sum_\gamma \left| t_{\gamma\alpha}^{R\leftarrow L} \right|^2 v_{\gamma,R} + \sum_\delta \left| r_{\delta\alpha}^{R\leftarrow L} \right|^2 v_{\delta,L}.
\tag{B.24}
$$

Analogously we get, for left-propagating states,

$$
v_{\gamma,R} = \sum_\delta v_{\delta,L} \left| r_{\delta\gamma}^{L\leftarrow R} \right|^2 + \sum_\alpha v_{\alpha,R} \left| t_{\alpha\gamma}^{L\leftarrow R} \right|^2,
\tag{B.25}
$$

or, in its most generic form,

$$
\begin{bmatrix} \sqrt{\frac{v_{\alpha,L}}{v_{\beta,L}}} r_{\alpha\beta}^{R\leftarrow L} & \sqrt{\frac{v_{\alpha,L}}{v_{\delta,R}}} t_{\alpha\delta}^{L\leftarrow R} \\ \sqrt{\frac{v_{\gamma,R}}{v_{\beta,L}}} t_{\gamma\beta}^{R\leftarrow L} & \sqrt{\frac{v_{\gamma,R}}{v_{\delta,R}}} r_{\gamma\delta}^{L\leftarrow R} \end{bmatrix} \begin{bmatrix} \Psi_{L,\beta}^+(E) \\ \Psi_{R,\delta}^-(E) \end{bmatrix} = \begin{bmatrix} \Psi_{L,\alpha}^-(E) \\ \Psi_{R,\gamma}^+(E) \end{bmatrix}
\tag{B.26}
$$

is unitary.

## B.5. Landauer-Büttiker Formula

The current contribution from a given state propagating to the right $\left| \Psi_\alpha^+(E) \right\rangle$ is

$$
\begin{aligned}
I_{L\to R}^+(E,\alpha) &= \left\langle \Psi_\alpha^+(E) \left| I_{N+1\to N+2} \right| \Psi_\alpha^+(E) \right\rangle \\
&= \sum_{\gamma,\delta} \left( t_{\delta\alpha}^{R\leftarrow L} \right)^* t_{\gamma\alpha}^{R\leftarrow L} \left\langle \Psi_{R,\delta}^+(E) \left| I_{N+1\to N+2} \right| \Psi_{R,\gamma}^+(E) \right\rangle \\
&= \sum_{\gamma,\delta} \left( t_{\delta\alpha}^{R\leftarrow L} \right)^* t_{\gamma\alpha}^{R\leftarrow L} v_{\gamma,R} \delta_{\gamma,\delta} \\
&= \sum_\gamma v_{\gamma,R} \left| t_{\gamma\alpha}^{R\leftarrow L} \right|^2
\end{aligned}
\tag{B.27}
$$

To sum these current contributions over all propagating states, we write

$$I^+_{L \to R} = \sum_{k_y} \int \frac{dk_x(E)}{2\pi} f_L(E) I^+_{L \to R}(k_x, k_y), \tag{B.28}$$

at which point we perform a change of variable in the energy:

$$dk_x(E) = dE \frac{dk_x}{dE} = dE \frac{1}{\hbar v_{k_y,L}(E)}, \tag{B.29}$$

with $v_{k_y,L}(E)$ being the group velocity at a fixed $k_y$ and energy, giving us

$$I^+_{L \to R} = \sum_{k_y} \int \frac{dE}{2\pi} \frac{1}{\hbar v_{k_y,L}(E)} f_L(E) I^+_{L \to R}(E, k_y). \tag{B.30}$$

We are now in a position to realize that indexing the states at a given energy by $k_y$ or by $\alpha$ is the same, allowing us to revert to the previous notation:

$$I^+_{L \to R} = \sum_{\alpha} \int \frac{dE}{2\pi} \frac{1}{\hbar v_{\alpha,L}(E)} f_L(E) I^+_{L \to R}(E, \alpha) \tag{B.31}$$

$$= \frac{1}{\hbar} \sum_{\alpha,\gamma} \int \frac{dE}{2\pi} f_L(E) \frac{v_{\gamma,R}(E)}{v_{\alpha,L}(E)} \left| t^{R \leftarrow L}_{\gamma\alpha} \right|^2. \tag{B.32}$$

Conversely, for a state propagating to the left $|\Psi_{-,\gamma}\rangle$ the current is

$$I^-_{L \to R}(E, \gamma) = \left\langle \Psi^-_\gamma(E) \left| I_{N+1 \to N+2} \right| \Psi^-_\gamma(E) \right\rangle$$

$$= \left\langle \Psi^-_{R,\gamma}(E) \left| I_{N+1 \to N+2} \right| \Psi^-_{R,\gamma}(E) \right\rangle + \sum_{\delta,\delta'} \left( r^{L \leftarrow R}_{\delta'\gamma} \right)^* r^{L \leftarrow R}_{\delta\gamma} \left\langle \Psi^+_{R,\delta'}(E) \left| I_{N+1 \to N+2} \right| \Psi^+_{R,\delta}(E) \right\rangle$$

$$= \left( -v_{\gamma,R} + \sum_{\delta} v_{\delta,R} \left| r^{L \leftarrow R}_{\delta\gamma} \right|^2 \right). \tag{B.33}$$

Evoking equation [B.25](#) allows us to write

$$I^-_{L \to R}(E, \gamma) = \sum_{\alpha} v_{\alpha,L} \left| t^{L \leftarrow R}_{\alpha\gamma} \right|^2. \tag{B.34}$$

We thus obtain

$$I_{L \to R} = I^+_{L \to R} - I^-_{L \to R}$$

$$= \frac{1}{\hbar} \sum_{\alpha,\gamma} \int \frac{dE}{2\pi} \left( f_L(E) \frac{v_{\gamma,R}}{v_{\alpha,L}} \left| t^{R \leftarrow L}_{\gamma\alpha} \right|^2 - f_R(E) \frac{v_{\alpha,L}}{v_{\gamma,R}} \left| t^{L \leftarrow R}_{\alpha\gamma} \right|^2 \right). \tag{B.35}$$

The equation is now close to its final form, but by implying thermodynamic equilibrium we are able to further discern one last property of the the eigenstate problem: In thermodynamic equilibrium, and therefore a system with a uniformly defined chemical potential, the system must display a null net current, meaning

$$
\begin{aligned}
I_{L \to R} &= I_{L \to R}^+ - I_{L \to R}^- = 0 \\
&\Leftrightarrow \frac{1}{\hbar} \sum_{\alpha, \gamma} \int \frac{dE}{2\pi} f(E) \left( \frac{v_{\gamma,R}}{v_{\alpha,L}} \left| t_{\gamma\alpha}^{R \leftarrow L} \right|^2 - \frac{v_{\alpha,L}}{v_{\gamma,R}} \left| t_{\alpha\gamma}^{L \leftarrow R} \right|^2 \right) = 0,
\end{aligned}
\tag{B.36}
$$

the only difference from the previous equation being that now we have the same Fermi-Dirac distribution defined in all the system. This allows us to get a final relation which is independent of the thermodynamic state the system is:

$$
\frac{v_{\gamma,R}}{v_{\alpha,L}} \left| t_{\gamma\alpha}^{R \leftarrow L} \right|^2 - \frac{v_{\alpha,L}}{v_{\gamma,R}} \left| t_{\alpha\gamma}^{L \leftarrow R} \right|^2.
\tag{B.37}
$$

Substituting this into equation B.35 then finally gives us the Landauer-Büttiker formula for the nearest-neighbor tight-binding model:

$$
\frac{1}{\hbar} \sum_{\alpha, \gamma} \int \frac{dE}{2\pi} \left( f_L(E) - f_R(E) \right) \frac{v_{\gamma,R}}{v_{\alpha,L}} \left| t_{\gamma\alpha}^{R \leftarrow L} \right|^2.
\tag{B.38}
$$

Defining the transmission coefficient as

$$
T(E) = \sum_{\alpha, \gamma} \frac{v_{\gamma,R}}{v_{\alpha,L}} \left| t_{\gamma\alpha}^{R \leftarrow L} \right|^2
\tag{B.39}
$$

allows us to see that we have regained the Landauer Formula B.1 presented in section 3.1. The calculation of the coefficients $t_{\gamma\alpha}^{R \leftarrow L}$ may be done numerically through various methods. To achieve this computation, we have utilized the Kwant package, a python package optimized for such calculations using wave-function matching [55].

## B.6. Self Energy introduced by the Leads

In this short section, we will express the effect the leads have on the central sample as a self-energy introduced in the central sample's Green function. We will be tracing out the Wannier states of the leads and thus obtain a Green function $\mathbf{G}_{CC}$ written solely in the Wannier basis of the central sample. In doing so, we lose the hermiticity of this Green function: because it is coupled to an environment (in this case, the leads), $\mathbf{G}_{CC}$ will describe the dynamics of an open system.

The system in question has the Hamiltonian

$$\hat{\mathbf{H}} = \hat{\mathbf{H}}_L + \hat{\mathbf{H}}_R + \hat{\mathbf{H}}_C + \hat{\mathbf{V}}_{LC} + \hat{\mathbf{V}}_{CR}, \tag{B.40}$$

where

$$\begin{aligned}
\hat{\mathbf{H}}_L &= \hat{\mathbf{H}}_L - \text{Left Lead Hamiltonian}, \\
\hat{\mathbf{H}}_R &- \text{Right Lead Hamiltonian}, \\
\hat{\mathbf{H}}_C &- \text{Central Sample Hamiltonian}, \\
\hat{\mathbf{V}}_{LC} &- \text{Connecting term between left lead and sample}, \\
\hat{\mathbf{V}}_{CR} &- \text{Connecting term between right lead and sample}.
\end{aligned} \tag{B.41}$$

To make the subsequent calculations simpler and more compact, we will define $\hat{\mathbf{H}}_p \equiv \hat{\mathbf{H}}_L + \hat{\mathbf{H}}_R$ and $\hat{\mathbf{V}} \equiv \hat{\mathbf{V}}_{CR} + \hat{\mathbf{V}}_{LC}$. It is easier to understand what will follow if we expand this operators in terms of the Wannier basis of the system. It is therefore important to notice the operator $\hat{\mathbf{H}}_C$ is written solely in terms of the Wannier states of the central sample, $\hat{\mathbf{H}}_p$ is written in terms of the Wannier basis of the leads exclusively and $\hat{\mathbf{V}}$ is the only matrix that has Wannier states from both basis. Written more explicitly, we have

$$\hat{\mathbf{H}}_C = \sum_{i_C, i_C'} \left( \hat{\mathbf{H}}_C \right)_{i_C, i_C'} |i_C\rangle \langle i_C'|, \tag{B.42}$$

$$\hat{\mathbf{H}}_p = \sum_{i_p, i_p'} \left( \hat{\mathbf{H}}_p \right)_{i_p, i_p'} |i_p\rangle \langle i_p'|, \tag{B.43}$$

$$\hat{\mathbf{V}} = \sum_{i_C, i_p} \left( \hat{\mathbf{V}} \right)_{i_C, i_p} |i_C\rangle \langle i_p| + \text{h.c}, \tag{B.44}$$

where $i_C, i_C'$ index solely the Wannier states of the sample and $i_p, i_p'$ index those of the leads. The retarded Green function of such a system is expressed as

$$\mathbf{G}^R (\varepsilon) = [(\varepsilon + \mathrm{i}0^+)\mathbf{I} - \mathbf{H}]^{-1}. \tag{B.45}$$

Such equation may be explicitly written as

$$\begin{bmatrix} (\varepsilon + \mathrm{i}0^+)\mathbf{I} - \hat{\mathbf{H}}_p & \hat{\mathbf{V}} \\ \hat{\mathbf{V}}^\dagger & (\varepsilon + \mathrm{i}0^+)\mathbf{I} - \hat{\mathbf{H}}_C \end{bmatrix} \begin{bmatrix} \hat{\mathbf{G}}_{pp}^R (\varepsilon) & \hat{\mathbf{G}}_{Cp}^R (\varepsilon) \\ \left( \hat{\mathbf{G}}_{Cp}^R \right)^\dagger (\varepsilon) & \hat{\mathbf{G}}_{CC}^R (\varepsilon) \end{bmatrix} = I. \tag{B.46}$$

This allows us to get two different equations

$$\left( (\varepsilon + \mathrm{i}0^+)\mathbf{I} - \hat{\mathbf{H}}_p \right) \hat{\mathbf{G}}_{Cp}^R (\varepsilon) + \hat{\mathbf{V}} \hat{\mathbf{G}}_{CC}^R (\varepsilon) = 0, \tag{B.47}$$

$$\hat{\mathbf{V}}^\dagger \hat{\mathbf{G}}_{Cp}^R (\varepsilon) + \left( (\varepsilon + \mathrm{i}0^+)\mathbf{I} - \hat{\mathbf{H}}_C \right) \hat{\mathbf{G}}_{CC}^R (\varepsilon) = I. \tag{B.48}$$

We may identify the inverse of the free Green function of the leads in the first equation because of its definition

$$\hat{\mathbf{g}}_{pp}^{R}\left(\varepsilon\right) = \left((\varepsilon + \mathrm{i}0^{+})\mathbf{I} - \hat{\mathbf{H}}_{p}\right)^{-1} \tag{B.49}$$

and using such equation leaves us with

$$\hat{\mathbf{G}}_{Cp}^{R}\left(\varepsilon\right) = -\mathbf{g}_{pp}^{R}\hat{\mathbf{V}}\hat{\mathbf{G}}_{CC}^{R}\left(\varepsilon\right). \tag{B.50}$$

Substituting this into the first equation yields

$$\left((\varepsilon + \mathrm{i}0^{+})\mathbf{I} - \hat{\mathbf{H}}_{CC} - \hat{\mathbf{V}}^{\dagger}\mathbf{g}_{pp}^{R}\hat{\mathbf{V}}\right)\hat{\mathbf{G}}_{CC}^{R}\left(\varepsilon\right) = I. \tag{B.51}$$

This calculation unveils the added self-energy term arising from the coupling of the leads to the central sample, which we'll write as

$$\boldsymbol{\Sigma}^{R}\left(\varepsilon\right) = \hat{\mathbf{V}}^{\dagger}\mathbf{g}_{pp}^{R}\hat{\mathbf{V}}. \tag{B.52}$$

One may think we have gained little to no advantage since $\mathbf{g}_{pp}^{R}$ is obtained by inverting an infinite matrix, however, since it it the Green function associated with the unperturbed Hamiltonian, it can be usually be solved analytically. It's also worthy to notice that the self-energy is purely written in the Wannier basis of the central sample alone: because $\mathbf{g}_{pp}^{R}$ is composed only of the Wannier states of the leads, the matricial products in equation B.52 are equivalent to tracing out the leads' Wannier states. Put in mathematical terms,

$$\begin{aligned}
\boldsymbol{\Sigma}^{R}\left(\varepsilon\right) &= \sum_{i_{C},i_{C}'}\sum_{i_{p},i_{p}'} V_{i_{p},i_{C}}^{\dagger} \left|i_{C}\right\rangle \left\langle i_{p} \mid i_{p}\right\rangle \left(\mathbf{g}_{pp}^{R}\right)_{i_{p},i_{p}'} \left\langle i_{p}' \mid i_{p}'\right\rangle V_{i_{p}',i_{C}'} \left\langle i_{C}'\right| \\
&= \sum_{i_{C},i_{C}'} \mathcal{V}_{i_{C},i_{C}'} \left|i_{C}\right\rangle \left\langle i_{C}'\right|,
\end{aligned} \tag{B.53}$$

where $\mathcal{V}_{i_{C},i_{C}'} = \sum_{i_{p},i_{p}'} V_{i_{p},i_{C}}^{\dagger} \left(\mathbf{g}_{pp}^{R}\right)_{i_{p},i_{p}'} V_{i_{p}',i_{C}'}$. Operators that live in the Hilbert space spawned by the Wannier states of the central sample will now be denoted in bold (this means that operators such as $\boldsymbol{\Sigma}^{R}\left(\varepsilon\right)$, $\hat{\mathbf{G}}_{CC}^{R}$ and $\hat{\mathbf{H}}_{CC}$ are all written in the Wannier basis of the sample). The sample's Green function is then written as the solution of the equation

$$\left((\varepsilon + \mathrm{i}0^{+})\mathbf{I} - \hat{\mathbf{H}}_{CC} - \boldsymbol{\Sigma}^{R}\left(\varepsilon\right)\right)\hat{\mathbf{G}}_{CC}^{R}\left(\varepsilon\right) = I. \tag{B.54}$$

which lives purely in the hilbert space of the central sample. Analogously, for the advanced Green function we get

$$\left((\varepsilon + \mathrm{i}0^{+})\mathbf{I} - \hat{\mathbf{H}}_{CC} - \boldsymbol{\Sigma}^{A}\left(\varepsilon\right)\right)\hat{\mathbf{G}}_{CC}^{R}\left(\varepsilon\right) = I, \tag{B.55}$$

where $\boldsymbol{\Sigma}^A\left(\varepsilon\right) = \hat{\mathbf{V}}^\dagger \mathbf{g}_{pp}^A \hat{\mathbf{V}}$. It is important to notice that $\boldsymbol{\Sigma}^{R/A}\left(\varepsilon\right)$ is, in general, non-hermitian, therefore making $\hat{\mathbf{G}}_{CC}^{R/A}\left(\varepsilon\right)$ non-hermitian as well. This means that the time-evolution operator will no longer be unitary, because the states inside the sample are allowed to couple with those of the environment and "escape", leading for a decay of such states. Nevertheless, it is a useful tool to express the sample's green function in this way which served us well in section 3.3.2, since the Caroli Formula for the transmission coefficient [29] is written in terms of the matrices $\hat{\mathbf{G}}_{CC}^R(\varepsilon)$, $\hat{\mathbf{G}}_{CC}^A(\varepsilon)$, $\boldsymbol{\Gamma}_L(\varepsilon)$ and $\boldsymbol{\Gamma}_R(\varepsilon)$, which all live in the central sample's Hilbert space.

# C. Calculations

In this chapter, we calculate the expression for the evolution of a gaussian wave-packet in real space. We do so by Fourier transforming $\psi_l(t) = \frac{a}{2\pi} \int_{-\pi/a}^{\pi/a} dk \, \hat{\psi}(k,t) \exp ikla$

The expression for the wave-packet in the reciprocal space with the expansion of $\cos\left(ka + \frac{eaEt}{2\hbar}\right)$ around $k(t)$ yields

$$\hat{\psi}(k,t) \approx \left(\frac{8\pi\sigma^2}{a^2}\right)^{1/4} \exp\left[i\frac{4w}{eaE}\sin\left(\frac{eaEt}{2\hbar}\right)\left[\cos\left(a\left(k(t) + \frac{eEt}{2\hbar}\right)\right)\right.\right.$$
$$\left.\left. -a\sin\left(a\left(k(t) + \frac{eEt}{2\hbar}\right)\right)(k - k(t))\right]\right] \tag{C.1}$$
$$\times \exp\left(-2\sigma^2\left(k - k_0 + \frac{eEt}{\hbar}\right)^2\right). \tag{C.2}$$

Let us first work the first term in the first exponential who will not get transformed by the integral. This term is then

$$i\frac{4w}{eaE}\sin\left(\frac{eaEt}{2\hbar}\right)\cos\left(a\left(k_0 - \frac{eEt}{2\hbar}\right)\right) = i\frac{4w}{eaE}\left(\cos(ak_0)\sin\left(\frac{eaEt}{2\hbar}\right)\cos\left(-\frac{eaEt}{2\hbar}\right)\right.$$
$$\left. + \sin(ak_0)\sin^2\left(\frac{eaEt}{2\hbar}\right)\right)$$

By using $\sin(\alpha)\cos(\alpha) = \frac{1}{2}\sin(2\alpha)$ and $\sin^2\alpha = \frac{1-\cos 2\alpha}{2}$ on the first and second term respectively, we get

$$= i\frac{2w}{eaE}\left(\cos(ak_0)\sin\left(\frac{eaEt}{\hbar}\right) + \sin(ak_0) - \sin(ak_0)\cos a\frac{eEt}{\hbar}\right)$$
$$= i\frac{2w}{eaE}\left(\sin(ak_0) - \left(\cos(ak_0)\sin\left(-\frac{eaEt}{\hbar}\right) - \sin(ak_0)\cos\left(-\frac{eaEt}{\hbar}\right)\right)\right)$$
$$= i\frac{2w}{eaE}\left(\sin(ak_0) - \sin\left(ak_0 - \frac{eaEt}{\hbar}\right)\right). \tag{C.3}$$

The second term involves the Fourier Transform, which yields

$$\frac{a}{2\pi} \int_{-\pi/a}^{\pi/a} dk \, \exp\left(\beta(k - k\,(t))\right) \times \tag{C.4}$$

$$\frac{a}{2\pi} \int_{-\pi/a}^{\pi/a} dk \, \exp\left(\beta(k - k\,(t))\right) \times \exp\left(-2\sigma^2 \left(k - k\,(t)\right)^2\right) \exp\left(ikla\right)$$

$$= \sqrt{\frac{\pi}{2\sigma^2}} \exp\left(ikla - \frac{(al - i\beta)^2}{8\sigma^2}\right) \tag{C.5}$$

where $\beta$ is defined as

$$\beta \equiv -i\frac{4w}{eaE} \sin\left(\frac{eaEt}{2\hbar}\right) a \sin\left(a\left(k\,(t) + \frac{eEt}{2\hbar}\right)\right) \tag{C.6}$$

we then have

$$\begin{aligned}
i\beta &= \frac{4w}{eaE} \sin\left(\frac{eaEt}{2\hbar}\right) a \sin\left(a\left(k\,(t) + \frac{eEt}{2\hbar}\right)\right) \\
&= \frac{4w}{eE} \sin\left(\frac{eaEt}{2\hbar}\right) \left(\sin\left(ak_0\right) \cos\left(-\frac{eaEt}{2\hbar}\right) + \cos\left(ak_0\right) \sin\left(-\frac{eaEt}{2\hbar}\right)\right) \\
&= \frac{4w}{eE} \left(\sin\left(ak_0\right) \sin\left(\frac{eaEt}{2\hbar}\right) \cos\left(\frac{eaEt}{2\hbar}\right) - \cos\left(ak_0\right) \sin^2\left(\frac{eaEt}{2\hbar}\right)\right).
\end{aligned}$$

Using the same tricks as before gives us

$$\begin{aligned}
i\beta &= \frac{2w}{eE} \left(\sin\left(ak_0\right) \sin\left(\frac{eaEt}{\hbar}\right) - \cos\left(ak_0\right) + \cos\left(ak_0\right) \cos\left(\frac{eaEt}{\hbar}\right)\right) \\
&= \frac{2w}{eE} \left(\cos\left(ak_0\right) \cos\left(-\frac{eaEt}{\hbar}\right) - \sin\left(ak_0\right) \sin\left(-\frac{eaEt}{\hbar}\right) - \cos\left(ak_0\right)\right) \\
&= \frac{2w}{eE} \left(\cos\left(ak_0 - \frac{eaEt}{\hbar}\right) - \cos\left(ak_0\right)\right). \tag{C.7}
\end{aligned}$$

Putting equations C.3, C.5 and C.7 together finally gives us the wanted expression for the Fourier transform of $\hat{\psi}\,(k, t)$:

$$\psi_l(t) \approx \left(\frac{a^2}{2\pi\sigma^2}\right)^{1/4} \exp\left(i\left(k_0 - eE\frac{t}{\hbar}\right) la - i\Phi(t) - \frac{a^2}{4\sigma^2}(l - \bar{l}(t))^2\right), \tag{C.8}$$

with

$$\Phi(t) = \frac{2w}{eEa} \left[\sin\left(k_0 a - eEa\frac{t}{\hbar}\right) - \sin\left(k_0 a\right)\right], \tag{C.9}$$

and

$$\bar{l}(t) = \frac{2w}{eEa} \left[ \cos \left( k_0 a - eEa\frac{t}{\hbar} \right) - \cos \left( k_0 a \right) \right].$$

(C.10)

# D. Single Disorder Realization Curves

## D.1. 1 Dimension

Two different plots of current VS disorder parameter are presented in figures D.1a and D.1b, each corresponding to a unique disorder realization. The current curve is clearly very dependent on the disorder configuration at this scale due to it being so small. The current always ends up decaying to zero nonetheless.
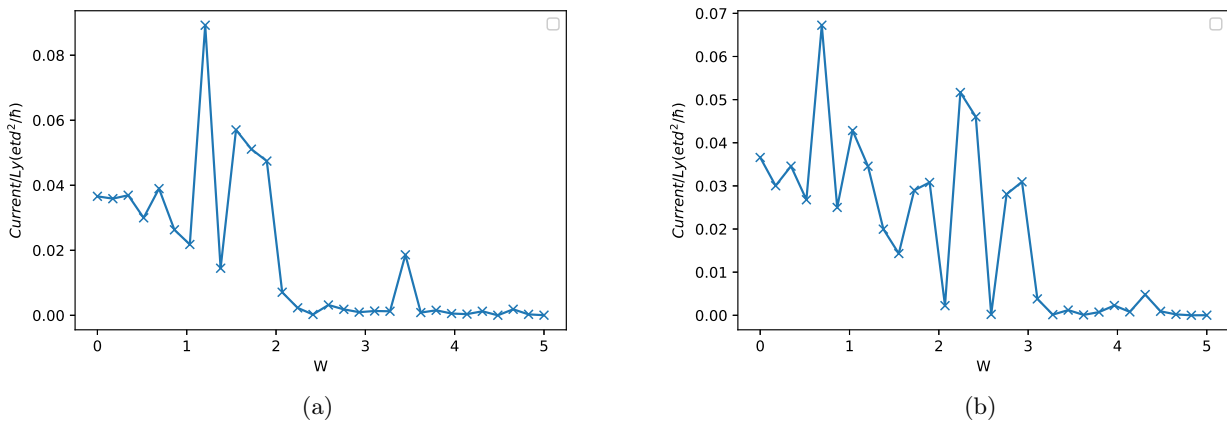


(a)



(b)

Figure D.1.: Total Landauer current through the 1D sample of size $L = 25a$ and $\Delta V = 6t$ as a function of the disorder parameter. Each graph is a different disorder realization.

## D.2. 2 Dimensions

The plots of current VS disorder parameter for a single realization of disorder are presented in figures D.2 a) and b), corresponding to the total and divided by width currents, for different system sizes. Contrary to the one-dimensional case, the current curves do not alter meaningfully with the disorder configuration and they preserve the essential behavior, it being, for example, the place where the maximal value is met. In figure b), we can see that the curve gets smoother with increasing width, a result of the self-averaging properties of the current with increasing sample size.
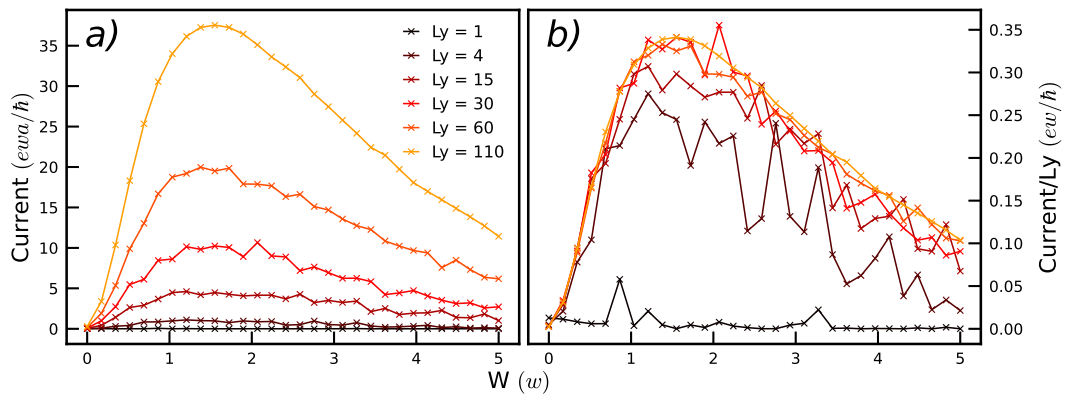


Figure D.2.: a) Total Landauer current through the sample and b) Landauer current through the sample divided by the width on a sample of length $L_x = 25a$ and $\Delta V = 6w$ as a function of the disorder parameter for different widths and a single disorder realization.

# Bibliography

[1] Carlo Jacoboni. *Theory of Electron Transport in Semiconductors: A Pathway from Elementary Physics to Nonequilibrium Green Functions*. Number 165 in Springer Series in Solid-State Sciences. Springer, Heidelberg ; New York, 2010.

[2] P. W. Anderson. Absence of Diffusion in Certain Random Lattices. *Physical Review*, 109(5):1492–1505, March 1958.

[3] M. Büttiker. Absence of backscattering in the quantum Hall effect in multiprobe conductors. *Physical Review B*, 38(14):9375–9389, November 1988.

[4] M. Büttiker. Chapter 4: The Quantum Hall Effect in Open Conductors. In *Semiconductors and Semimetals*, volume 35, pages 191–277. Elsevier, 1992.

[5] Bogdan Stefan Popescu and Alexander Croy. Emergence of Bloch oscillations in one-dimensional systems. *Physical Review B*, 95(23):235433, June 2017.

[6] Felix Bloch. Über die Quantenmechanik der Elektronen in Kristallgittern. *Zeitschrift für Physik*, 52(7-8):555–600, July 1929.

[7] N.F. Mott and W.D. Twose. The theory of impurity conduction. *Advances in Physics*, 10(38):107–163, April 1961.

[8] E. Abrahams, P. W. Anderson, D. C. Licciardello, and T. V. Ramakrishnan. Scaling Theory of Localization: Absence of Quantum Diffusion in Two Dimensions. *Physical Review Letters*, 42(10):673–676, March 1979.

[9] P. Wölfle and D. Vollhardt. Self-consistent theory of Anderson localization: General formalism and applications. *International Journal of Modern Physics B*, 24(12n13):1526–1554, May 2010.

[10] V.L Berezinskii. Kinetics of a quantum particle in a one-dimensional random potential. *JETP*, 38(3):620, 1974.

[11] D. J. Thouless. Maximum Metallic Resistance in Thin Wires. *Physical Review Letters*, 39(18):1167–1169, October 1977.

[12] K. B. Efetov and A. I. Larkin. Kinetics of a quantum particle in a long metallic wire. *Sov. Phys. JETP*, 58:444, 1983.

[13] K.-H. Hoffmann and Michael Schreiber. *Computational Statistical Physics: From Billards to Monte Carlo.* Springer, Berlin ; New York, 2002.

[14] B Kramer and A MacKinnon. Localization: Theory and experiment. *Reports on Progress in Physics*, 56(12):1469–1564, December 1993.

[15] Patrick A. Lee and T. V. Ramakrishnan. Disordered electronic systems. *Reviews of Modern Physics*, 57(2):287–337, April 1985.

[16] Ferdinand Evers and Alexander D. Mirlin. Anderson transitions. *Reviews of Modern Physics*, 80(4):1355–1417, October 2008.

[17] Rolf Landauer. Electrical resistance of disordered one-dimensional lattices. *The Philosophical Magazine: A Journal of Theoretical Experimental and Applied Physics*, 21(172):863–867, April 1970.

[18] M. Büttiker. Four-Terminal Phase-Coherent Conductance. *Physical Review Letters*, 57(14):1761–1764, October 1986.

[19] Aaron Szafer and A. Douglas Stone. Theory of Quantum Conduction through a Constriction. *Physical Review Letters*, 62(3):300–303, January 1989.

[20] B. J. van Wees, H. van Houten, C. W. J. Beenakker, J. G. Williamson, L. P. Kouwenhoven, D. van der Marel, and C. T. Foxon. Quantized conductance of point contacts in a two-dimensional electron gas. *Physical Review Letters*, 60(9):848–850, February 1988.

[21] Hideaki Ohnishi, Yukihito Kondo, and Kunio Takayanagi. Quantized conductance through individual rows of suspended gold atoms. *Nature*, 395(6704):780–783, October 1998.

[22] T. Ando. Quantum point contacts in magnetic fields. *Physical Review B*, 44(15):8017–8027, October 1991.

[23] Jean-Philippe Brantut, Charles Grenier, Jakob Meineke, David Stadler, Sebastian Krinner, Corinna Kollath, Tilman Esslinger, and Antoine Georges. A Thermoelectric Heat Engine with Ultracold Atoms. *Science*, 342(6159):713–715, November 2013.

[24] Chih-Chun Chien, Massimiliano Di Ventra, and Michael Zwolak. Landauer, Kubo, and microcanonical approaches to quantum transport and noise: A comparison and implications for cold-atom dynamics. *Physical Review A*, 90(2):023624, August 2014.

[25] D J Thouless and S Kirkpatrick. Conductivity of the disordered linear chain. *Journal of Physics C: Solid State Physics*, 14(3):235–245, January 1981.

[26] R. L. Schult, D. G. Ravenhall, and H. W. Wyld. Quantum bound states in a classically unbound system of crossed wires. *Physical Review B*, 39(8):5476–5479, March 1989.

[27] Fernando Sols. Recursive Tight-Binding Green's Function Method: Application to Ballistic and Dissipative Transport in Semiconductor Nanostructures. In David K. Ferry, Harold L. Grubin, Carlo Jacoboni, and Anti-Pekka Jauho, editors, *Quantum Transport in Ultrasmall Devices*, volume 342, pages 329–338. Springer US, Boston, MA, 1995.

[28] J L Pichard. The one-dimensional Anderson model: Scaling and resonances revisited. *Journal of Physics C: Solid State Physics*, 19(10):1519–1535, April 1986.

[29] C Caroli, R Combescot, P Nozieres, and D Saint-James. Direct calculation of the tunneling current. *Journal of Physics C: Solid State Physics*, 4(8):916–929, June 1971.

[30] Antti-Pekka Jauho, Ned S. Wingreen, and Yigal Meir. Time-dependent transport in interacting and noninteracting resonant-tunneling systems. *Physical Review B*, 50(8):5528–5544, August 1994.

[31] Gianluca Stefanucci and Carl-Olof Almbladh. Time-dependent partition-free approach in resonant tunneling systems. *Physical Review B*, 69(19):195318, May 2004.

[32] G Stefanucci and C.-O Almbladh. Time-dependent quantum transport: An exact formulation based on TDDFT. *Europhysics Letters (EPL)*, 67(1):14–20, July 2004.

[33] Riku Tuovinen, Robert van Leeuwen, Enrico Perfetto, and Gianluca Stefanucci. Time-dependent Landauer–Büttiker formula for transient dynamics. *Journal of Physics: Conference Series*, 427:012014, March 2013.

[34] Riku Tuovinen, Enrico Perfetto, Gianluca Stefanucci, and Robert van Leeuwen. Time-dependent Landauer-Büttiker formula: Application to transient dynamics in graphene nanoribbons. *Physical Review B*, 89(8):085131, February 2014.

[35] S. Latini, E. Perfetto, A.-M. Uimonen, R. van Leeuwen, and G. Stefanucci. Charge dynamics in molecular junctions: Nonequilibrium Green's function approach made fast. *Physical Review B*, 89(7):075306, February 2014.

[36] Bogdan Stefan Popescu and Alexander Croy. Efficient auxiliary-mode approach for time-dependent nanoelectronics. *New Journal of Physics*, 18(9):093044, September 2016.

[37] Alexander Croy and Ulf Saalmann. Propagation scheme for nonequilibrium dynamics of electron transport in nanoscale devices. *Physical Review B*, 80(24):245311, December 2009.

[38] Neil Bushong, Na Sai, and Massimiliano Di Ventra. Approach to Steady-State Transport in Nanoscale Conductors. *Nano Letters*, 5(12):2569–2572, December 2005.

[39] Chih-Chun Chien, Michael Zwolak, and Massimiliano Di Ventra. Bosonic and fermionic transport phenomena of ultracold atoms in one-dimensional optical lattices. *Physical Review A*, 85(4):041601, April 2012.

[40] M Di Ventra and T N Todorov. Transport in nanoscale systems: The microcanonical versus grand-canonical picture. *Journal of Physics: Condensed Matter*, 16(45):8025–8034, November 2004.

[41] J. P. Santos Pires, B. Amorim, and J. M. Viana Parente Lopes. Landauer transport as a quasisteady state on finite chains under unitary quantum dynamics. *Physical Review B*, 101(10):104203, March 2020.

[42] H. Tal-Ezer and R. Kosloff. An accurate and efficient scheme for propagating the time dependent Schrödinger equation. *The Journal of Chemical Physics*, 81(9):3967–3971, November 1984.

[43] A theory of the electrical breakdown of solid dielectrics. *Proceedings of the Royal Society of London. Series A, Containing Papers of a Mathematical and Physical Character*, 145(855):523–529, July 1934.

[44] Neil W. Ashcroft and N. David Mermin. *Solid State Physics*. Holt, Rinehart and Winston, New York, 1976.

[45] Vincenzo Grecchi and Andrea Sacchetti. Acceleration theorem for Bloch oscillators. *Physical Review B*, 63(21):212303, May 2001.

[46] R. Peierls. Zur Theorie des Diamagnetismus von Leitungselektronen. *Zeitschrift für Physik*, 80(11):763–791, November 1933.

[47] Milena Grifoni and Peter Hänggi. Driven quantum tunneling. *Physics Reports*, 304(5):229–354, October 1998.

[48] T. Hartmann, F. Keck, H. J. Korsch, and S. Mossmann. Dynamics of Bloch oscillations. *New Journal of Physics*, 6:2–2, January 2004.

[49] Martin Holthaus and Daniel W. Hone. Localization effects in ac-driven tight-binding lattices. *Philosophical Magazine B*, 74(2):105–137, August 1996.

[50] Milton Abramowitz and Irene A. Stegun. *Handbook of Mathematical Functions with Formulas, Graphs, and Mathematical Tables*. U.S. Government Printing Office, 1964.

[51] Hidetoshi Fukuyama, Robert A. Bari, and Hans C. Fogedby. Tightly Bound Electrons in a Uniform Electric Field. *Physical Review B*, 8(12):5579–5586, December 1973.

[52] G. C. Stey and G. Gusman. Wannier-Stark ladders and the energy spectrum of an electron in a finite one dimensional crystal. *Journal of Physics C: Solid State Physics*, 6(4):650–656, February 1973.

[53] Michele Cini. Time-dependent approach to electron transport through junctions: General theory and simple applications. *Physical Review B*, 22(12):5887–5899, December 1980.

[54] Horia D Cornean, Céline Gianesello, and Valentin Zagrebnov. A partition-free approach to transient and steady-state charge currents. *Journal of Physics A: Mathematical and Theoretical*, 43(47):474011, November 2010.

[55] Christoph W Groth, Michael Wimmer, Anton R Akhmerov, and Xavier Waintal. Kwant: A software package for quantum transport. *New Journal of Physics*, 16(6):063065, June 2014.

[56] Gianluca Stefanucci. Bound states in ab initio approaches to quantum transport: A time-dependent formulation. *Physical Review B*, 75(19):195115, May 2007.

[57] E. Khosravi, G. Stefanucci, S. Kurth, and E. K. U. Gross. Bound states in time-dependent quantum transport: Oscillations and memory effects in current and density. *Physical Chemistry Chemical Physics*, 11(22):4535–4538, May 2009.

[58] Supriyo Datta. *Electronic Transport in Mesoscopic Systems*. Number 3 in Cambridge Studies in Semiconductor Physics and Microelectronic Engineering. Cambridge University Press, Cambridge ; New York, 1995.

[59] Enrique Diez, Francisco Domínguez-Adame, and Angel Sánchez. Dephasing effects induced by weak disorder in superlattices. *Microelectronic Engineering*, 43–44:117–123, August 1998.

[60] Massimiliano Di Ventra. *Electrical Transport in Nanoscale Systems*. August 2008.

[61] M. Zwierzycki, P. A. Khomyakov, A. A. Starikov, K. Xia, M. Talanana, P. X. Xu, V. M. Karpan, I. Marushchenko, I. Turek, G. E. W. Bauer, G. Brocks, and P. J. Kelly. Calculating scattering matrices by wave function matching. *physica status solidi (b)*, 245(4):623–640, April 2008.

[62] Michael Wimmer. *Quantum Transport in Nanostructures: From Computational Concepts to Spintronics in Graphene and Magnetic Tunnel Junctions*. Number 5 in Dissertationsreihe Der Fakultät Für Physik Der Universität Regensburg. Univ.-Verl. Regensburg, Regensburg, 1. aufl edition, 2009.